

University of Kentucky

UKnowledge

Theses and Dissertations--Medical Sciences

Medical Sciences

2022

Mammalian Target of Rapamycin Cell Signaling Pathway in Phosphatase and Tensin Homolog Induced Kinase 1 Knockout Rat Model of Familial Parkinson's Disease

Martha Helena Mortell

University of Kentucky, mhmortell@gmail.com

Digital Object Identifier: <https://doi.org/10.13023.107>

[Right click to open a feedback form in a new tab to let us know how this document benefits you.](#)

Recommended Citation

Mortell, Martha Helena, "Mammalian Target of Rapamycin Cell Signaling Pathway in Phosphatase and Tensin Homolog Induced Kinase 1 Knockout Rat Model of Familial Parkinson's Disease" (2022). *Theses and Dissertations--Medical Sciences*. 19.

https://uknowledge.uky.edu/medsci_etds/19

This Master's Thesis is brought to you for free and open access by the Medical Sciences at UKnowledge. It has been accepted for inclusion in Theses and Dissertations--Medical Sciences by an authorized administrator of UKnowledge. For more information, please contact UKnowledge@lsv.uky.edu.

STUDENT AGREEMENT:

I represent that my thesis or dissertation and abstract are my original work. Proper attribution has been given to all outside sources. I understand that I am solely responsible for obtaining any needed copyright permissions. I have obtained needed written permission statement(s) from the owner(s) of each third-party copyrighted matter to be included in my work, allowing electronic distribution (if such use is not permitted by the fair use doctrine) which will be submitted to UKnowledge as Additional File.

I hereby grant to The University of Kentucky and its agents the irrevocable, non-exclusive, and royalty-free license to archive and make accessible my work in whole or in part in all forms of media, now or hereafter known. I agree that the document mentioned above may be made available immediately for worldwide access unless an embargo applies.

I retain all other ownership rights to the copyright of my work. I also retain the right to use in future works (such as articles or books) all or part of my work. I understand that I am free to register the copyright to my work.

REVIEW, APPROVAL AND ACCEPTANCE

The document mentioned above has been reviewed and accepted by the student's advisor, on behalf of the advisory committee, and by the Director of Graduate Studies (DGS), on behalf of the program; we verify that this is the final, approved version of the student's thesis including all changes required by the advisory committee. The undersigned agree to abide by the statements above.

Martha Helena Mortell, Student

Dr. D. Allan Butterfield, Major Professor

Dr. Melinda E. Wilson, Director of Graduate Studies

MAMMALIAN TARGET OF RAPAMYCIN CELL SIGNALING PATHWAY
IN PHOSPHATASE AND TENSIN HOMOLOG INDUCED KINASE 1
KNOCKOUT RAT MODEL OF FAMILIAL PARKINSON'S DISEASE

THESIS

A thesis submitted in partial fulfillment of the
requirements for the degree of
Master of Science in Medical Sciences in the
College of Medicine
at the University of Kentucky

By

Martha Mortell

Lexington, Kentucky

Director: Dr. D. Allan Butterfield, Professor of Biological Chemistry

Lexington, Kentucky

2022

Copyright © Martha Mortell 2022

ABSTRACT OF THESIS

MAMMALIAN TARGET OF RAPAMYCIN CELL SIGNALING PATHWAY IN PHOSPHATASE AND TENSIN HOMOLOG INDUCED KINASE 1 KNOCKOUT RAT MODEL OF FAMILIAL PARKINSON'S DISEASE

More than 10 million people are living with Parkinson's disease (PD), one million of which are people in the United States. PD is the second most common age-related neurodegenerative disorder, after Alzheimer's disease, and is characterized by the accumulation of α -synuclein aggregates and the degeneration of dopaminergic neurons. The loss of endogenous dopamine in PD brain accounts for the motor decline presented clinically in PD patients. Etiological factors of PD include oxidative damage and inflammation, although the detailed mechanisms remain unknown. Risk factors for PD include gender, age, environmental factors, and gene mutations.

The current thesis research employed phosphatase and tensin homolog (PTEN)-induced kinase 1 (PINK1) knockout (KO) rats because mutations in *PINK1* lead to familial PD. In normal brain, PINK1 serves to recruit Parkin, an E3 ubiquitin protein ligase, to the outer mitochondrial membrane of depolarized mitochondria to induce mitophagy, a mitochondrial quality control mechanism in which damaged mitochondria are degraded. In brain lacking PINK1, mitochondrial homeostasis cannot be maintained, resulting in mitochondrial dysfunction, oxidative damage, and neuronal cell death.

The PINK1 KO rat brain was studied in conjunction with the mammalian target of rapamycin (mTOR) cell signaling pathway due to the capability of mTOR to regulate autophagy, glucose metabolism, mitochondrial function, and neuronal development and function. A disturbance in mTOR signaling in the brain, thus disturbances to such pathways, have shown to be implicated in cancer, diabetes, and neurodegeneration.

This thesis project studied the expression and phosphorylation (resulting in the activation or inhibition dependent upon the phosphorylation site of the protein in question) of the key enzymes in the mTOR pathway of a PINK1 KO rat brain model of familial PD as a function of age. The proteins studied include phosphoinositide 3-kinase (PI3K), protein kinase B (Akt), mammalian target of rapamycin complex I (mTORC1), ribosomal protein S6 kinase (P70S6K), and insulin receptor substrate 1 (IRS-1). The control group (male and female wild type (WT) rat brain at 2 months of age) and the male and female PINK1 KO rat brain at 4 months, 6 months, and 8 months of age were analyzed with the *ProteinSimple* JessTM instrument, which employs capillary electrophoresis for automated Western blotting. Three rats per group (WT 2-month, KO 4-month,

KO 6-month, KO 8-month) were ran in duplicates for each protein (non-phosphorylated and phosphorylated form) with the JessTM instrument. The expression and phosphorylation levels of PI3K, Akt, mTOR, P70S6K, and IRS-1 in the male and female PINK1 KO rat brain were studied to gain further insight into autophagic function and insulin resistance in the rat brain lacking *PINK1* to advance understanding of familial PD caused by the loss-of-function mutation in *PINK1*.

KEYWORDS: Parkinson's Disease (PD), Mammalian Target of Rapamycin (mTOR), Phosphatase and Tensin Homolog Induced Kinase 1 (PINK1), Neurodegeneration, Oxidative Damage

Martha Mortell

4.19.2022

MAMMALIAN TARGET OF RAPAMYCIN CELL SIGNALING
PATHWAY IN PHOSPHATASE AND TENSIN HOMOLOG INDUCED
KINASE 1 KNOCKOUT RAT MODEL OF PARKINSON'S DISEASE

By
Martha Mortell

Dr. D. Allan Butterfield

Director of Thesis

Dr. Melinda E. Wilson

Director of Graduate Studies

4.19.2022

Date

ACKNOWLEDGEMENTS

I would first like to extend my deepest gratitude to Professor D. Allan Butterfield. Dr. Butterfield's knowledge, guidance, and support has had a profound impact on my life as a student, as a scientist and as a person. His unwavering commitment to science, research and mentorship has been an immense source of inspiration. The standard he sets for himself and those around him will continue to serve me in all endeavors moving forward. It has been an honor to be a student in his lab for the last four years. I would also like to thank Dr. Nada Porter and Dr. Samuel Franklin for constituting my thesis advisory committee. I am sincerely grateful for their time, patience, and insight. The opportunity to present my thesis research to accomplished members of the scientific and medical community such as Dr. Butterfield, Dr. Porter and Dr. Franklin is one I hold with great regard.

The completion of this thesis research would not have been possible without Dr. Butterfield's PhD student, Nicole Rummel, to whom I am tremendously grateful. Nicole's knowledge and patience while teaching, guiding, and supporting me has been crucial in my success with this project and I could not have done it without her. I would also like to thank other members of the Butterfield lab including Shekinah Alfaro who welcomed me four years ago as an undergraduate student and who has always been there to answer questions; and to past lab member Dr. Xiaojia Ren who provided significant insight into my project.

I would like to thank the St. Clair Laboratory in the Department of Toxicology and Cancer Biology. I could not have achieved my project without the willingness of Dr. Daret St. Clair and Dr. Luksana Chaiswing in allowing me to use their JessTM instrument to collect data.

Lastly, I would like to extend my heartfelt gratitude to my family and friends who have been of the utmost importance in my journey through their untiring support. To my parents, Paul and Helen, I cannot thank you enough for your support in all aspects of my life. The determination, hard work and bravery you both have portrayed has not only afforded me opportunities I never imagined but has also set the standard for the kind of person I want to be. To my sister, Abigail, thank you for being a light in my life. Your work ethic and strong will motivates me in every way. I am proud to be your big sister. I would also like to thank my uncle and aunt, Edward and Jennifer, for being models of strength and dignity in the face of adversity. Thank you to my grandmother, Rosemary, for always listening to me and helping me keep perspective. Thank you to my amazing friends who have believed in me and supported me beyond measure.

TABLE OF CONTENTS

ACKNOWLEDGEMENTS	iii
LIST OF FIGURES	v
CHAPTER 1. INTRODUCTION	1
CHAPTER 2. BACKGROUND	5
2.1 Neurodegeneration and Oxidative Damage	5
2.1.1 Lipid Peroxidation and HNE	7
2.2 Autophagy	8
2.2.1 Mammalian Target of Rapamycin Cell Signaling Pathway	9
2.2.2 Phosphatase and Tensin Homolog Induced Kinase 1	11
2.3 Parkinson's Disease.....	13
2.3.1 Alpha-synuclein Aggregation.....	15
2.3.2 Dopaminergic Neurons.....	15
2.3.3 Genetics in Parkinson's Disease.....	16
CHAPTER 3. MAMMALIAN TARGET OF RAPAMYCIN CELL SIGNALING PATHWAY IN PHOSPHATASE AND TENSIN HOMOLOG INDUCED KINASE 1 KNOCKOUT RAT MODEL OF PARKINSON'S DISEASE	18
3.1 Overview	18
3.2 Introduction	18

3.3 Materials and Methods	19
3.3.1 Chemicals	19
3.3.2 Animals.....	20
3.3.3 Sample Preparation.....	21
3.3.4 ProteinSimple Jess™	21
3.4 Results	26
3.4.1 Expression Levels.....	26
3.4.2 Phosphorylation Levels	37
3.5 Discussion of Results	51
3.5.1 Phosphoinositide 3-Kinase	51
3.5.2 Protein Kinase B.....	53
3.5.3 Mammalian Target of Rapamycin	56
3.5.4 Ribosomal Protein S6 Kinase	58
3.5.5 Insulin Receptor Substrate 1	62
3.5.6 PINK1 KO Rat at Age 6 Months.....	64
3.5.7 Oxidative Damage in PINK1 KO Rat Brain	66
CHAPTER 4. CONCLUSION AND FUTURE STUDIES	67
4.1 Conclusions	67
4.2 Future Studies.....	70

APPENDIX.....	73
Figure 3.2 – Figure 3.11	73
Figure 3.2, 3.7	73
Figure 3.3, Figure 3.8	84
Figure 3.4, 3.9	95
Figure 3.5, 3.10	105
Figure 3.6, 3.11	126
REFERENCES	138
VITA.....	146

LIST OF FIGURES

Figure 2.1 mTOR Cell Signaling Pathway.....	10
Figure 2.2 Mitophagy induced by PINK1/Parkin signaling.....	12
Figure 3.1 Capillary Electrophoresis with Jess™, RePlex™ steps with Jess™....	23
Figure 3.2 The expression levels of PI3K in male and female WT 2-month rat brain and PINK1 KO 4-month, KO 6-month and KO 8-month rat brain.....	27
Figure 3.3 The expression levels of Akt in male and female WT 2-month rat brain and PINK1 KO 4-month, KO 6-month and KO 8-month rat brain.....	30
Figure 3.4 The expression levels of mTOR in male and female WT 2-month rat brain and PINK1 KO 4-month, KO 6-month and KO 8-month rat brain.....	32
Figure 3.5 The expression levels of P70S6K in male and female WT 2-month rat brain and PINK1 KO 4-month, KO 6-month and KO 8-month rat brain.....	34
Figure 3.6 The expression levels of IRS-1 in male and female WT 2-month rat brain and PINK1 KO 4-month, KO 6-month and KO 8-month rat brain.....	36
Figure 3.7 The phosphorylation levels of PI3K at Tyr 458/Tyr 199 in male and female WT 2-month rat brain and PINK1 KO 4-month, KO 6-month and KO 8-month rat brain.....	39
Figure 3.8 The phosphorylation levels of Akt at Ser 473 in male and female WT 2-month rat brain and PINK1 KO 4-month, KO 6-month and KO 8-month rat brain.....	41
Figure 3.9 The phosphorylation levels of mTORC1 at Ser 2448 in male and female WT 2-month rat brain and PINK1 KO 4-month, KO 6-month and KO 8-month rat brain.....	43
Figure 3.10 The phosphorylation levels of P70S6K at Thr 389 in male and female WT 2-month rat brain and PINK1 KO 4-month, KO 6-month and KO 8-month rat brain.....	46
Figure 3.11 The phosphorylation of IRS-1 at Ser 307 in male and female WT 2-month rat brain and PINK1 KO 4-month, KO 6-month and KO 8-month rat brain.....	50

CHAPTER 1. INTRODUCTION

Parkinson's disease (PD) is the second most common age-related neurodegenerative disorder and is characterized by the accumulation of α -synuclein aggregates and the degeneration of dopaminergic (DA) neurons. More than 10 million people worldwide are living with the disease, one million of which are people in the United States. The incidence in the U.S. is more than the combined number of people diagnosed with multiple sclerosis, muscular dystrophy, and Lou Gehrig's disease (or Amyotrophic Lateral Sclerosis) and is expected to rise to 1.2 million by the year 2030. Approximately 60,000 Americans are diagnosed with PD every year, with incidence increasing with age. PD presents clinically with motor symptoms such as bradykinesia, postural instability, tremor, and non-motor symptoms such as REM sleep disruption and depression, which are said to be due to the loss of endogenous dopamine in PD brain. Etiological factors of PD include oxidative damage and inflammation. Risk factors for PD include gender, age, environmental factors, and gene mutations. Epidemiological studies have shown that men are 1.5 times more likely to develop PD than women.

Genetic research on PD has led to the identification of inheritable risk factors that increase the probability of its development. Between five and ten percent of PD cases are a result of a genetic mutation. The scientific research presented in this thesis investigates PTEN-induced kinase 1 (PINK1) knockout (KO) rats because mutations in *PINK1* lead to familial PD. PINK1 is an integrity surveillance protein of the mitochondria and is of particular importance to the long term survival of dopaminergic neurons. In normal brain, PINK1 serves to recruit Parkin, an E3 ubiquitin protein ligase, to the outer mitochondrial membrane of depolarized mitochondria to

induce mitophagy. In brain lacking PINK1, mitochondrial homeostasis cannot be maintained, resulting in mitochondrial dysfunction, increased oxidative damage, and neuronal cell death.

In this thesis research, the PINK1 KO rat brain was probed for the expression and phosphorylation of key enzymes involved in the mammalian target of rapamycin (mTOR) cell signaling pathway, a cell signaling pathway that has shown to be implicated in cancer, diabetes, and neurodegeneration. The mTOR cell signaling pathway impacts cellular function through autophagy and cellular metabolism; a disturbance of which negatively impacts pathways including glucose metabolism, energy production, mitochondrial function, cell growth and autophagy.

Mutations in PINK1 have shown to lead to familial PD, the ultimate mutation of which is the loss-of-function mutation. This thesis research probed the rat brain in the complete absence of PINK1 as a model of familial PD. The results indicate conceivable etiology of PD brain due to loss-of-function mutations in PINK1 with respect to the mTOR cell signaling pathway regarding mitochondrial dysfunction, autophagy, and insulin resistance. This investigation focused on the correlation between the mTOR cell signaling pathway and PINK1 KO brain in the rodent model of PD. The concurrent exploration of PD brain and the mTOR cell signaling pathway is indicative of their overlap in autophagy (for the degradation of α -synuclein, as well as, synaptic plasticity, memory formation, and retention of neuronal cells, specifically in this instance, DA neurons) and insulin resistance (due to the association between type 2 diabetes and PD and the correlation between glucose metabolism in brain and cognitive function).

The scientific inquiry contained in this thesis research on the mTOR pathway provided insight on the phosphorylation of phosphoinositide 3-kinase (PI3K), protein kinase B (Akt), mammalian target of rapamycin complex 1 (mTORC1), ribosomal protein S6 kinase (P70S6K),

and insulin receptor substrate 1 (IRS-1), in brain of PINK1 KO rats at 2-, 4-, 6-, and 8-months of age. This inquiry probed for the phosphorylation at the activation site of PI3K (Tyr 458/Tyr 199), Akt (Ser 473), mTORC1 (Ser 2448), and P70S6K (Thr 389), thus increased phosphorylation denotes increased activation and vice versa. The phosphorylation of IRS-1 was probed for at its inhibitory site (Ser 307), thus phosphorylation of IRS-1 in this thesis research signifies inhibition of IRS-1.

The overall hypothesis of this thesis research is (A) that the loss of PINK1 will lead to an increase in mTOR signaling pathway phosphorylation over time (increased inhibition of autophagy and leading to insulin resistance) and (B) such phosphorylation will occur at higher levels in the male rat brain than in the female rat brain (due to PD incidence being higher in men). To support the overall hypothesis, plausible answers to the following questions were investigated using the PINK1 KO rat model of PD:

(A)

1. Will phosphorylation (activation) of PI3K increase with age in the absence of PINK1 in the rodent model (thereby leading to increased phosphorylation (activation) of Akt)?
2. Will phosphorylation (activation) of Akt increase with age in the absence of PINK1 in the rodent model (leading to increased phosphorylation (activation) of mTORC1 at Ser 2448)?
3. Will phosphorylation (activation) of mTORC1 at Ser 2448 increase with age in the absence of PINK1 in the rodent model (leading to inhibition of autophagy, impaired neuronal survival)?

4. Will phosphorylation (activation) of P70S6K increase with age in the absence of PINK1 in the rodent model (leading to increased phosphorylation (inhibition) of IRS-1 at Ser 307)?
5. Will phosphorylation (inhibition) of IRS-1 at Ser 307 increase in the absence of PINK1 in the rodent model (leading to insulin resistance)?

(B)

1. Will the phosphorylation levels of PI3K, Akt, mTORC1, P70S6K, and IRS-1 be greater in the male brain than female brain of the rodent model?

CHAPTER 2. BACKGROUND

2.1 Neurodegeneration and Oxidative Damage

Neurodegeneration is a condition characterized by the dysfunction and deterioration of neurons as a consequence of selective structural and functional loss, presenting clinically in cognitive decline (Przedborski, Vila, & Jackson-Lewis, 2003). The synaptic loss due to structural and functional forfeiture of the neuron evokes the impairment of synaptic transmission and long-term potentiation (LTP) (Gorman, 2008); that of which is said to underlie learning and memory (Sumi & Harada, 2020). Additionally, LTP is controlled and modulated in part by dopaminergic transmission. The impairment of synaptic plasticity, specifically in the nucleus striatum when regarding PD brain, could account for the onset and the progression of both motor and cognitive symptoms presented clinically in patients with PD, keeping in mind the immense degeneration of dopaminergic (DA) neurons in the *substantia nigra pars compacta* (Picconi, Piccoli, & Calabresi, 2012). In the normal aging brain, there is little neuronal loss observed in comparison to the high levels seen in patients diagnosed with neurodegenerative diseases (Gorman, 2008). Hence, the research exploring the dysfunction and deterioration of neurons is pertinent to the investigation of root causes, in the effort to ascertain effective treatments.

Although the pathogenesis of neurodegenerative diseases is still being investigated, mitochondrial dysfunction has been found to play a significant role (Monzio Compagnoni et al., 2020). Oxidative damage, a process that occurs due to an imbalance between reactive oxygen species (ROS) and antioxidant defense, has shown to be an instigator of neurodegeneration (Calabrese et al., 2005). Mitochondria, the main function of which is the production of energy in the form of ATP, is a major intracellular source of ROS through the mitochondrial respiratory

chain and the substantial oxygen levels of the organelle (Uttara, Singh, Zamboni, & Mahajan, 2009).

ROS are produced in many enzymes within the mitochondria; however, the majority of mitochondrial ROS are produced in the electron transport chain (ETC) (Angelova & Abramov, 2018; MacMahon Copas, McComish, Fletcher, & Caldwell, 2021). The ETC catalyzes the oxidation of reducing equivalents, nicotinamide adenine dinucleotide (NADH) and flavin adenine dinucleotide (FADH₂), using O₂ (the terminal electron acceptor in the inner mitochondrial membrane). This electron transfer mediated by the respiratory chain leads to the generation of ATP via ATP synthase (Lemarie & Grimm, 2011). It is through this energy transduction pathway that electrons can “leak” to molecular oxygen (which is highly abundant in the brain because the brain consumes up to 30% of total oxygen consumption), resulting in oxygen free radicals (Nowak, 2013). A complication of this nature occurring in the mitochondria constitutes defective energy metabolism which compromises cell viability (Guo, Sun, Chen, & Zhang, 2013).

In the standard aging brain, antioxidants balance the presence of ROS (Calabrese et al., 2005), protecting against the accelerated progression of neurodegeneration; the antioxidative ability of the brain is imperative for neuronal protection (Gilgun-Sherki, Melamed, & Offen, 2001). Glutathione, one of many antioxidants the body relies on, is important in preventing damage caused by ROS. The production of glutathione, which occurs in the cytoplasm before being actively pumped into the mitochondria, is supported by antioxidant enzymes, such as superoxide dismutase, and work in tandem to inhibit the formation of ROS and remove them for the cell’s protection (Kurutas, 2016). An inadequate amount of antioxidant defenses allows ROS to cause damage to membrane lipids, proteins, and nucleic acids (Triplett et al., 2015). In

particular, polyunsaturated fatty acids (PUFAs), which are abundant in the central nervous system, are susceptible to oxidation and fragmentation during lipid peroxidation (oxidative degradation of lipids) which induces the formation of toxic species (Nowak, 2013).

Grievously, the brain is particularly susceptible to oxidative damage because of its high oxygen consumption and the large number of PUFAs present (Uttara et al., 2009). The amalgamation of oxygen and PUFAs in the brain paves the way for ROS to cause great harm (Juan, Perez de la Lastra, Plou, & Perez-Lebena, 2021) which, without sufficient defensive mechanisms, can lead to severe neurological complications because ROS activity materializes mostly in the brain and neuronal tissue (Triplett et al., 2015). Commonly defined ROS include superoxide radicals ($O_2^{\bullet -}$), hydroxyl radicals ($\bullet OH$), nitric monoxide ($NO\bullet$) and singlet oxygen (1O_2) (Pizzino et al., 2017).

Substantial research on neurodegenerative disorders has also supported the involvement of inflammation in the development of neurodegenerative diseases. Although the exact trigger for the inflammatory response is unclear, oxidative damage can take a toll on intracellular signaling which can lead to dysfunction of the inflammatory response (Solleiro-Villavicencio & Rivas-Arancibia, 2018). The role of inflammation in PD brain is speculated to be the consequence of α -synuclein aggregates and neuronal cell death (Pajares, A, Manda, Bosca, & Cuadrado, 2020).

2.1.1 Lipid Peroxidation and HNE

The brain is abundant in PUFA (Bazinet & Laye, 2014). The phospholipid bilayer is the basis for cell membrane structure. A phospholipid consists of a polar head, composed of a glycerol and a phosphate molecule, and two non-polar tails, composed of fatty acid

(hydrocarbon) chains (Bretscher, 1972). The presence of PUFAs, which are easily attacked by free radicals, explains why the brain is highly susceptible to oxidative damage (Uttara et al., 2009). The most common unsaturated fatty acids found in the brain are docosahexaenoic acid and arachidonic acid (Rapoport, 2008).

Lipid peroxidation involves the removal of an allylic hydrogen from the lipid acyl chain of the PUFA by free radicals. This results in the formation of a carbon centered radical ($R\cdot$) with the ability to react with oxygen molecules to produce a peroxy radical ($ROO\cdot$), the propagation of which would include the continuous removal of allylic hydrogens from the chain, causing lipid asymmetry to be lost. The consequence of this is neuronal apoptosis (Castegna, Lauderback, Mohammad-Abdul, & Butterfield, 2004). The occurrence of lipid peroxidation on arachidonic acid, one of the most common fatty acids found in the brain, leads to the formation of 4-hydroxy-2-nonenal (HNE). HNE can bind cysteine residues of proteins (by Michael's addition reaction) which structurally and functionally alters the proteins, inducing apoptosis and the disruption of cellular ion homeostasis (Castegna et al., 2004). Subsequently, HNE serves as a biomarker for oxidative damage (Butterfield, Bader Lange, & Sultana, 2010).

2.2 Autophagy

Autophagy is a critical regulatory function of the body that is responsible for the disposal of damaged cells and the generation of new cells. This process allows for the removal of aggregated proteins, damaged organelles (such as mitochondria (specifically termed mitophagy)), and intracellular pathogens (W. Xu et al., 2021). In addition to the elimination capability, autophagy promotes cellular senescence, the process of cell cycle arrest to protect against genome instability, and cell surface antigen presentation, preventing necrosis, an acute

form of cell death. For these reasons, pristine regulation and execution of autophagy is essential for the regulation and prevention of diseases such as cancer and neurodegeneration, among others (Glick, Barth, & Macleod, 2010). Specifically, aggregates associated with neurodegeneration (such as α -synuclein in PD) are degraded by autophagy (Sarkar, 2013).

The target of rapamycin kinase complex I (TORC1) plays a crucial role in the stimulation of autophagy. By way of oxidative damage, ROS can cause damage to macromolecules and autophagy is a crucial response to oxidative damage for maintaining cellular homeostasis. mTOR inhibition activates autophagy (Ciccarone, Castelli, & Ciriolo, 2019).

2.2.1 Mammalian Target of Rapamycin Cell Signaling Pathway

The Mammalian Target of Rapamycin (mTOR) cell signaling pathway regulates autophagy (Bartolome et al., 2017; Wang & Zhang, 2019; Zhu et al., 2019), glucose metabolism (Butterfield & Halliwell, 2019), mitochondrial function (Perluigi, Di Domenico, & Butterfield, 2015; Zhu et al., 2019), neuronal development and the function of mature neurons, including synaptic plasticity and memory formation (Switon, Kotulska, Janusz-Kaminska, Zmorzynska, & Jaworski, 2017). mTOR executes its role in neuronal growth by the suppression of autophagy. However, mTOR inhibition of autophagy has been implicated in the progression of disease, such as cancer, diabetes, and aging (Saxton & Sabatini, 2017). Thus, vigilant balance between activation of mTOR signaling (leading to the inhibition of autophagy) and the inhibition of mTOR (which allows for the proper functioning of autophagy) is imperative to the brain. Too much or too little mTOR activity can be fatal to the neuron (Zhu et al., 2019). The mTOR pathway is presented schematically in Figure 2.1.

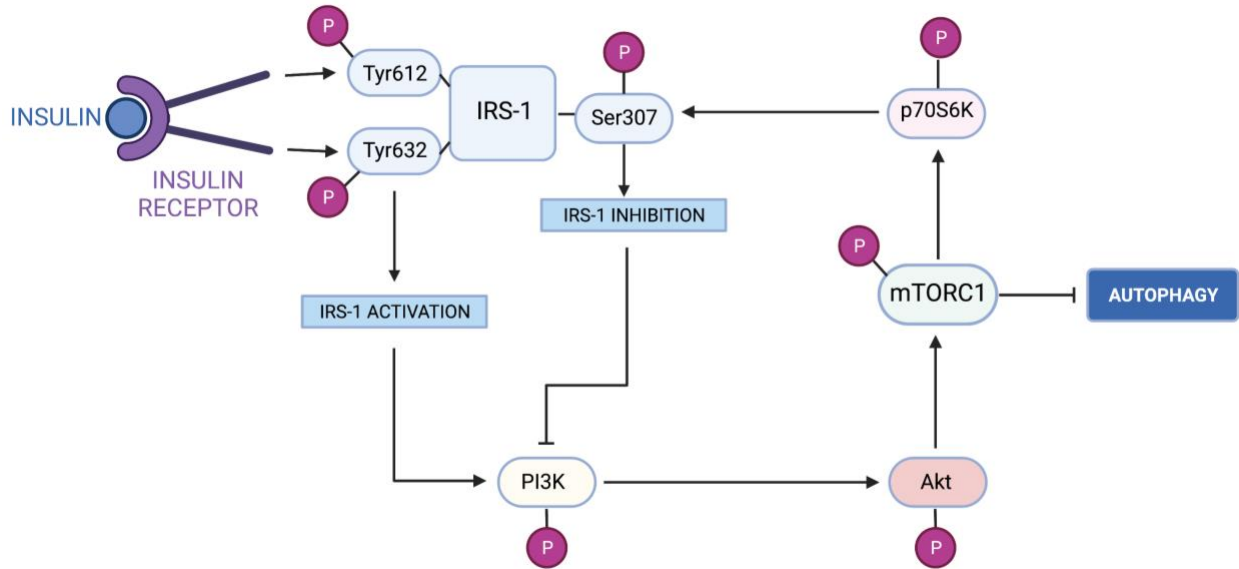


Figure 2.1 Schematic representation of the mTOR cell signaling pathway

The overall representation portrays mTOR activation leading to the inhibition of autophagy and the development of insulin resistance due to the binding of insulin to its receptor, leading to activation of mTORC1. Constructed based on the mTOR cell signaling pathway in accordance with the Nature paper “Oxidative stress, dysfunctional glucose metabolism and Alzheimer disease” (Butterfield & Halliwell, 2019), insulin binds to the insulin receptor (located on the neuronal membrane), which causes the insulin receptor to dimerize and the auto-phosphorylate on tyrosine residues. Insulin receptor substrate 1 (IRS-1) recognizes these phosphorylated tyrosine residues of the insulin receptor and is prompted to bind to the insulin receptor. This instigates the phosphorylation of IRS-1 on Tyr612 and Tyr632, which subsequently activates IRS-1. Activated IRS-1 leads to the phosphorylation and activation of an insulin signaling cascade, the PI3K/Akt pathway. The phosphorylation of PI3K induces the phosphorylation and activation of Akt, which phosphorylates the mechanistic target of rapamycin complex 1 (mTORC1) at Ser2448. Phosphorylated mTORC1 becomes activated as a kinase and has several key downstream effects which include the inhibition of autophagy (impairing neuronal survival) and phosphorylation of the protein P70S6K. When phosphorylated, P70S6K becomes a kinase, which phosphorylates Ser307 of IRS-1. Consequently, IRS-1 function is inhibited, signifying insulin resistance (Butterfield & Halliwell, 2019). [Schematic created with BioRender.com with Butterfield lab license].

2.2.2 Phosphatase and Tensin Homolog Induced Kinase 1

Phosphatase and tensin homolog induced kinase 1 (PINK1) is a mitochondrial serine/threonine-protein kinase encoded by the *PINK1* gene (Unoki & Nakamura, 2001). The presence of PINK1 is essential as it serves as an integrity surveillance protein, guarding the cell from stress-induced mitochondrial dysfunction. PINK1 presentation on the outer mitochondrial membrane of depolarized mitochondria instigates the translocation of Parkin, an E3 ubiquitin protein ligase, to such mitochondria which initiates mitophagy, thus preserving energy metabolism of the cell (Quinn, Moreira, Ambrosio, & Alves, 2020). The regulation of neuronal health and function is heavily dependent on the proper maintenance of mitochondria due to neurons' metabolic reliance on mitochondria (Lizama & Chu, 2021).

The majority of cellular ATP comes from the process of oxidative phosphorylation carried out in the mitochondria. Electron transfer from NADH and FADH₂ to O₂ creates a membrane potential because of the high concentration of protons in the intermembrane space and the low concentration in the mitochondrial matrix. This gradient leads to the subsequent return of the protons back into the mitochondrial matrix by way of ATP synthase, thus creating ATP. Damage and dysfunction of the mitochondria leads to a reduction in this membrane potential; hence, the mitochondria in this state are considered depolarized (Lemarie & Grimm, 2011).

Depolarized mitochondria trigger the accumulation of PINK1 on the outer mitochondrial membrane (OMM), the presence of which recruits Parkin from the cytosol to the OMM. PINK1 activates Parkin by phosphorylating the Ser 65 residue of Parkin. This phosphorylation elicits a conformational change that exposes the catalytic residues of Parkin, the E3 activity of which promotes mitophagy, through the ubiquitination of mitochondrial proteins, which elicits mitochondrial degradation (Lizama & Chu, 2021). This process is shown in Figure 2.2.

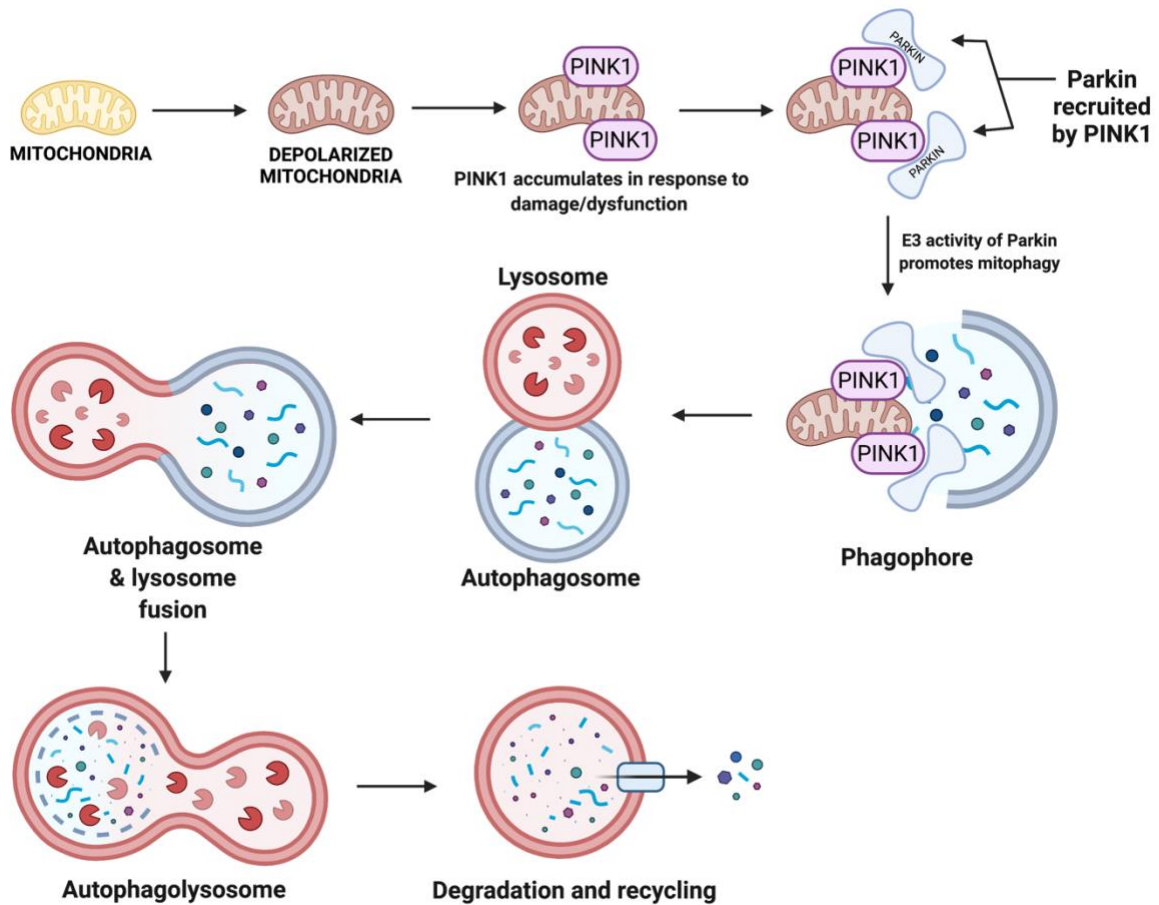


Figure 2.2 Schematic representation of mitophagy by PINK1/Parkin signaling. PINK1 presents on the outer mitochondrial membrane of the depolarized mitochondria which instigates the translocation of Parkin, an E3 ubiquitin ligase, to the depolarized mitochondria, thus promoting mitophagy. The damaged mitochondria are engulfed by the phagophore which leads to the production of the double-membraned autophagosome which is delivered to the lysosome. The autophagosome and lysosome fuse, creating an autophagolysosome leading to the degradation and recycling of damaged mitochondria, thus preserving energy metabolism of the cell. [Schematic created with BioRender.com with Butterfield lab license].

It is important to note that calcium-mediated excitotoxicity (Huang, Ren, Jiang, & Wang, 2016), complex I and II inhibitors (Okatsu et al., 2012; Shin et al., 2019), protein folding (Burman et al., 2017; Jin & Youle, 2013) and ROS (Frank et al., 2012) can also trigger the presence of PINK1 on the OMM of damaged mitochondria. Evidently, PINK1 presentation on the OMM is a crucial response to several problematic circumstances. Defective PINK1/Parkin signaling has been observed in neurodegenerative diseases (Quinn et al., 2020).

2.3 Parkinson's Disease

Parkinson's disease (PD) is an age-related neurodegenerative disorder characterized by the accumulation of Serine-129 phosphorylated α -synuclein aggregates within clumps, known as Lewy bodies, and the progressive degeneration of dopaminergic (DA) neurons (Sato et al., 2011). PD presents clinically in motor decline which includes tremor, bradykinesia, postural/gait instability, and rigidity (Hernandez, Reed, & Singleton, 2016). Non-motor symptoms of PD, which can present years before motor symptoms, include hallucinations, depression, and REM sleep behavior disorder (Chaudhuri, Healy, Schapira, & National Institute for Clinical, 2006; Tibar et al., 2018). Dementia has also been observed, mostly in severe cases of PD. Speculation of Parkinson's Disease Dementia (PDD) pathogenesis underlying insulin resistance (L. Yang, Wang, Liu, & Xie, 2018) and a link between diabetes mellitus and the incidence and progression of PD have become apparent in recent years (Hassan et al., 2020). Gender is a risk factor for PD; specifically, more men diagnosed with PD than women (Miller & Cronin-Golomb, 2010), however, women have a faster disease progression and worse prognosis than men with a higher mortality rate (Cerri, Mus, & Blandini, 2019). Age, environmental factors, and genetic mutations are also risk factors for the disease (H. Chen & Ritz, 2018; Reeve, Simcox, & Turnbull, 2014).

Inflammation, oxidative damage, and mitochondrial dysfunction are all significant contributing factors to the pathogenesis of PD (Triplet et al., 2015). The body's inflammatory response can be triggered by the abnormal accumulation of α -synuclein into aggregates, found in DA neurons of the substantia nigra (SN), which can result in further damage and disease progression (Codolo et al., 2013). The infiltration of α -synuclein aggregates in DA neurons specifically accounts for the detrimental impact on motor function, as dopamine is a neurotransmitter responsible for movement. Endogenous dopamine levels decrease dramatically by way of α -synuclein aggregate damage as well as the deterioration of dopaminergic neurons themselves. The inflammatory response in the brain, which in this case is provoked by the accumulation of α -synuclein aggregates, can injure cells and increase blood-brain barrier (BBB) permeability (L. Chen et al., 2018; Nelson, Soma, & Lavi, 2002). The loss of BBB integrity equates to not only a significant but also severely dangerous reduction in brain protection (Rhea & Banks, 2019). This, in addition to the ability of α -synuclein to propagate between neurons, demonstrates the implication of inflammation in PD brain.

Oxidative damage targets the mitochondria due to the decrease in the respiratory chain complex activities associated with the imbalance between ROS and antioxidant defense. Disproportionate outcomes of this nature can underlie defects in energy metabolism and induce cellular degeneration. The impairment of intramitochondrial metabolism is associated with increased free radical generation and oxidative damage. Mitochondrial dysfunction plays a big part in the pathogenesis of several neurodegenerative diseases (Calabrese et al., 2005).

2.3.1 Alpha-synuclein Aggregation

α -Synuclein, localized in the nerve terminal, is responsible for the normal function and integrity of the synapse (Bendor, Logan, & Edwards, 2013; Burre, 2015). Mitochondrial dysfunction and oxidative damage can induce protein modifications that facilitate the conversion of α -synuclein to aggregates (Hijaz & Volpicelli-Daley, 2020). This abundant neuronal protein has been linked to several disease states due to its aggregation that is toxic to the cell through the disruption of cellular homeostasis. This disturbance prompts neuronal death induced by cytotoxicity through damaging the mitochondria and disrupting microtubules, key players in the stability, structure, and function of the neuron (Ren, Hinchie, Swomley, Powell, & Butterfield, 2019).

Although not exclusive to this region of the brain, α -synuclein aggregates are found in dopaminergic (DA) neurons (Gomez-Benito et al., 2020). From there, the aggregates can propagate by cell-to-cell transmission (Fields, Bengoa-Vergniory, & Wade-Martins, 2019). This seeding of aggregation possibly contributes to disease propagation (Burre, 2015). The propagation of α -synuclein has been observed from the lower brainstem to the cortex (Braak et al., 2003). The presence of such aggregates contributes to the dysfunction of the neuron, which explains why, clinically, patients with PD present with cognitive and motor impairment (Gomez-Benito et al., 2020).

2.3.2 Dopaminergic Neurons

Dopaminergic (DA) neurons are the brain's main source of dopamine, the neurotransmitter that is key to the biochemical interaction responsible in part for movement (Chinta & Andersen, 2005). DA neurons originate in the midbrain floor plate and migrate to their

destination, one of which is the substantia nigra (SN). From the SN, the nigrostriatal pathway connects DA neurons to the dorsal striatum, the pathway responsible for voluntary movement (Volpicelli, Perrone-Capano, Bellenchi, Colucci-D'Amato, & di Porzio, 2020). The degeneration of these neurons, due to increased production of ROS, explains the clinical presentation of motor dysfunction in patients with PD (MacMahon Copas et al., 2021). It has also been suggested that insulin levels and glucose dysregulation can contribute to the degeneration of DA neurons (Song & Kim, 2016).

2.3.3 Genetics in Parkinson's Disease

Between five and ten percent of PD cases are a result of an inheritable mutation in one of several genes (Triplett et al., 2015). Many proteins encoded by PD-related genes are associated with the mitochondria, including the mitochondrial Serine/Threonine kinase phosphatase and tensin homolog-induced kinase 1 (PINK1) (Mouton-Liger, Jacoupy, Corvol, & Corti, 2017). The ultimate PINK1 gene mutation, the loss-of-function mutation, alters or eliminates the kinase domain (Exner et al., 2007). The loss-of-function mutation interrupts the ability of PINK1 to recruit Parkin for mitophagy. This inability to translocate Parkin to the outer mitochondrial membrane of depolarized mitochondria leads to an accumulation of damaged organelles because they are not being degraded and recycled (Pickrell & Youle, 2015). Mutations in PINK1 are associated with the familial form of PD (Quinn et al., 2020).

2.3.3.1 Animal Models in Parkinson's Disease

Genetically modified PD rodent animal models are a pragmatic means by which to study the mechanisms and potential therapeutic targets for PD with respect to the inheritable risk

factors (Ren & Butterfield, 2021). An animal model exhibiting age-associated motor decline, progressive degeneration of dopaminergic neurons, and aggregation of α -synuclein would be the ideal animal model representation of PD, optimal for studying the pathogenesis. However, many years of PD rodent models suggests there is not a mouse model that mimics all human PD characteristics (Dawson, Ko, & Dawson, 2010) and none of the models used to date present every characteristic of PD (Jiang & Dickson, 2018). The degeneration of dopaminergic neurons in the SN, the major hallmark for PD, was not observed in PINK1 KO mice (Glasl et al., 2012). The PINK1 KO rat was employed by the Butterfield Neurochemistry Lab in part to investigate the fidelity of the PINK1 KO rat brain as a model for PD. The use of a genetic rat model could be advantageous over a genetic mouse model because of the bigger brain size in rats. In this thesis research, familial PD was studied using PINK1 knockout (KO) rats. It is important to note that the PINK1 KO rat brain has not proven to be a perfect model because it did not present with α -synuclein aggregates or the death of dopaminergic neurons, however, the PINK1 KO rat brain did present with increased oxidative damage with age (Ren & Butterfield, 2021; Ren et al., 2019).

CHAPTER 3. MAMMALIAN TARGET OF RAPAMYCIN CELL SIGNALING PATHWAY IN PHOSPHATASE AND TENSIN HOMOLOG INDUCED KINASE 1 KNOCKOUT RAT MODEL OF PARKINSON'S DISEASE

3.1 Overview

Parkinson's disease (PD) is the second most common age-related neurodegenerative disease characterized by α -synuclein aggregation and dopaminergic neuronal degeneration. Etiological factors of PD include oxidative damage and inflammation. Risk factors for PD include age, gender, environmental factors, and gene mutations. Mutations in phosphatase and tensin homolog-induced kinase 1 (PINK1), including the ultimate mutation loss-of-function mutation, have been implicated in familial PD. The current study employed PINK1 knockout (KO) rats in accordance with the mammalian target of rapamycin (mTOR) cell signaling pathway due to this pathway's involvement in autophagic inhibition and insulin resistance, both of which have been observed in many neurodegenerative diseases. The mTOR cell signaling pathway was evaluated in the brain of PINK1 KO rats as a model for familial PD using the *ProteinSimple Jess*TM instrument which employs capillary electrophoresis for automated Western blotting. The brains of 2-month, 4-month, 6-month and 8-month-old male and female PINK1 KO rats were used. The control group was a 2-month-old wild type (WT) rat. Gender- and age-related changes were observed in PINK1 KO brain.

3.2 Introduction

PD is the second most common age-related neurodegenerative disorder, behind Alzheimer's disease, and is characterized by the accumulation of α -synuclein aggregates and the degeneration of dopaminergic neurons (Sato et al., 2011). Etiological factors of PD include

oxidative damage and inflammation (Beal, 2003). Risk factors for PD include gender, age, environmental factors, and gene mutations (Balestrino & Schapira, 2020).

Autophagy, the function of the body assigned to remove damaged cells (W. Xu et al., 2021), and more specifically mitophagy, which deals explicitly with removing damaged mitochondria (Malpartida, Williamson, Narendra, Wade-Martins, & Ryan, 2021) is implicated in those with the familial form of PD, associated with the loss-of-function mutation in PINK1 (Barodia, Creed, & Goldberg, 2017). PINK1 plays an important integrity surveillance role against mitochondrial dysfunction by phosphorylating and recruiting Parkin to facilitate the elimination of damaged mitochondria via mitophagy (Barodia et al., 2017). The loss of PINK1 leads to various mitochondrial impairments and oxidative stress, culminating in DA neuronal death. PINK1 has also shown to alleviate α -synuclein induced toxicity, therefore, a mutation in PINK1 would hinder this ability (Liu et al., 2017).

The mTOR cell signaling pathway, in which mTORC1 is activated, leads to the inhibition of autophagy and the development of insulin resistance (Butterfield & Halliwell, 2019). The mTOR cell signaling pathway is implicated in many nervous system disorders and is the center of this project on PINK1 and familial PD.

3.3 Materials and Methods

3.3.1 Chemicals

The Pierce Rapid Gold BCA Protein Assay Kit was purchased from Thermo Scientific (Waltham, MA, USA). Chemicals used in this study in conjunction with the Jess™ Simple Western automated nano-immunoassay instrument (ProteinSimple, San Jose, CA, USA, a Bio-Techne Brand) were purchased within the kits specified below.

Specific assay modules purchased from *ProteinSimple* included the Anti-Rabbit Detection Module (DM-001) which contained luminol-S, peroxide, antibody diluent 2, anti-rabbit secondary antibody, streptavidin-HRP; the 12-230 kDa separation module, 8 x 25 capillary cartridges (SMW-004) which contained the separation box with capillary cartridges, 12-230 kDa pre-filled plates (pre-filled with separation matrix 2, stacking matrix 2, split running buffer 2 and matrix removal buffer), sample buffer, wash buffer, plus standard pack 1 clamshell with DTT, FL standard master mix with 29 kDa System Control protein; RePlex™ Module (RP-001) which contained all the reagents needed to remove primary and secondary antibodies in a RePlex assay with two immunoassays or immunoassay with Total Protein assay in a single run (ProteinSimple, San Jose, CA, USA, a Bio-Techne Brand). The antibodies were purchased from Cell Signaling Technology (Danvers, MA); IRS-1 (Rabbit, Lot 10), pIRS-1 S307 (Rabbit, Lot 9), PI3K p85 (Rabbit, Lot 11), pPI3K p85 (Y458) / p55 (Y199) (Rabbit, Lot 6), Akt (Rabbit, Lot 28), pAkt S473 (Rabbit, Lot 15), mTOR (Rabbit, Lot 10), p-mTOR Ser2448 (Rabbit, Lot 12), P70S6K (Rabbit, Lot 20), p-P70S6K T389 (Rabbit, Lot 25).

3.3.2 Animals

The rat strain used in this thesis research was the Long-Evans rat. The animal studies were approved by the University of Kentucky Institutional Animal Care and Use Committee and followed NIH Guidelines for the Care and Use of Laboratory Animals. Male and female rats (WT and KO) were purchased from the Sage Research Labs (Horizon, Inc.) at 2 months of age. The rats were housed in the University of Kentucky Animal Facility under standard conditions and were sacrificed at 2-months, 4-months, 6-months, and 8-months old. The rats were anesthetized using CO₂ before they were sacrificed. The whole brain was excised immediately

after sacrifice and frozen in liquid nitrogen. The brain samples for this thesis research were sacrificed by past students in the Butterfield Neurochemistry Lab (Ren, 2019).

3.3.3 Sample Preparation

The rat brains were homogenized with a Wheaton glass homogenizer with cold isolation buffer [0.32 M sucrose, 2 mM EDTA, 2 mM EGTA, 20 mM HEPES, 0.2 µg/mL PMSF, 5 µg/mL aprotinin, 4 µg/mL leupeptin, 4 µg/mL pepstatin, and 10 µg/mL phosphatase inhibitor cocktail 2]. The homogenates were put on ice and sonicated for 10 seconds. This was carried out twice with 10 second rest periods between. The brain samples for this thesis research were prepared by past students in the Butterfield Neurochemistry Lab, therefore, the brain samples were already homogenized, sorted and ready to be used with the JessTM instrument. The protein concentration of the homogenates was determined using the Pierce Rapid Gold BCA Protein Assay Kit from Thermo Scientific (Waltham, MA, USA).

3.3.4 ProteinSimple JessTM

The JessTM Simple Western automated nano-immunoassay system, which employs capillary electrophoresis (ProteinSimple, San Jose, CA, USA, a Bio-Techne Brand), was used to evaluate the expression and phosphorylation levels of the key enzymes in the mTOR cell signaling pathway in the PINK1 WT and KO rat brain. The samples were handled according to the *ProteinSimple* standard method for the 12-230 kDa Jess Separation Module with 8 x 25 Capillary Cartridges (Ref: SM-W004-1) (ProteinSimple, San Jose, CA, USA, a Bio-Techne Brand). The Compass Simple Western Software (Version 5.0.1), which is the control and data analysis application for Simple Western Instruments, was used for the automatic calculation of

peak area (chemiluminescence intensity), the signal/noise ratio, and the digital image of the capillary chemiluminescence (Nguyen, Squaglia, Boge, & Fung, 2011). Expression levels (non-phosphorylated) and phosphorylated levels of the mTOR cell signaling pathway were measured which included: IRS-1, PI3K, Akt, mTOR, P70S6K.

3.3.4.1 Preparation for ProteinSimple Jess Instrument

The JessTM Simple Western automated nano-immunoassay system (ProteinSimple, San Jose, CA, USA, a Bio-Techne Brand) employs capillary electrophoresis, separating proteins by size (Edouard et al., 2021; Laidoudi et al., 2021). The instrument was utilized for this thesis research to measure phosphorylated and non-phosphorylated levels of the mTOR cell signaling pathway (including PI3K, Akt, mTOR, P70S6K, IRS-1) via REPLEXTM with JessTM. REPLEXTM with JessTM allows for the analysis of the phosphorylated and non-phosphorylated form of the protein on the same plate, in the same capillary. Three different rat brain samples (of same sex) for each group (WT 2-month, KO 4-month, KO 6-month, and KO 8-month) were ran with the phosphorylated and non-phosphorylated antibody on a plate in duplicates. The RePlexTM with JessTM steps are shown in demonstrated in Figure 3.1.

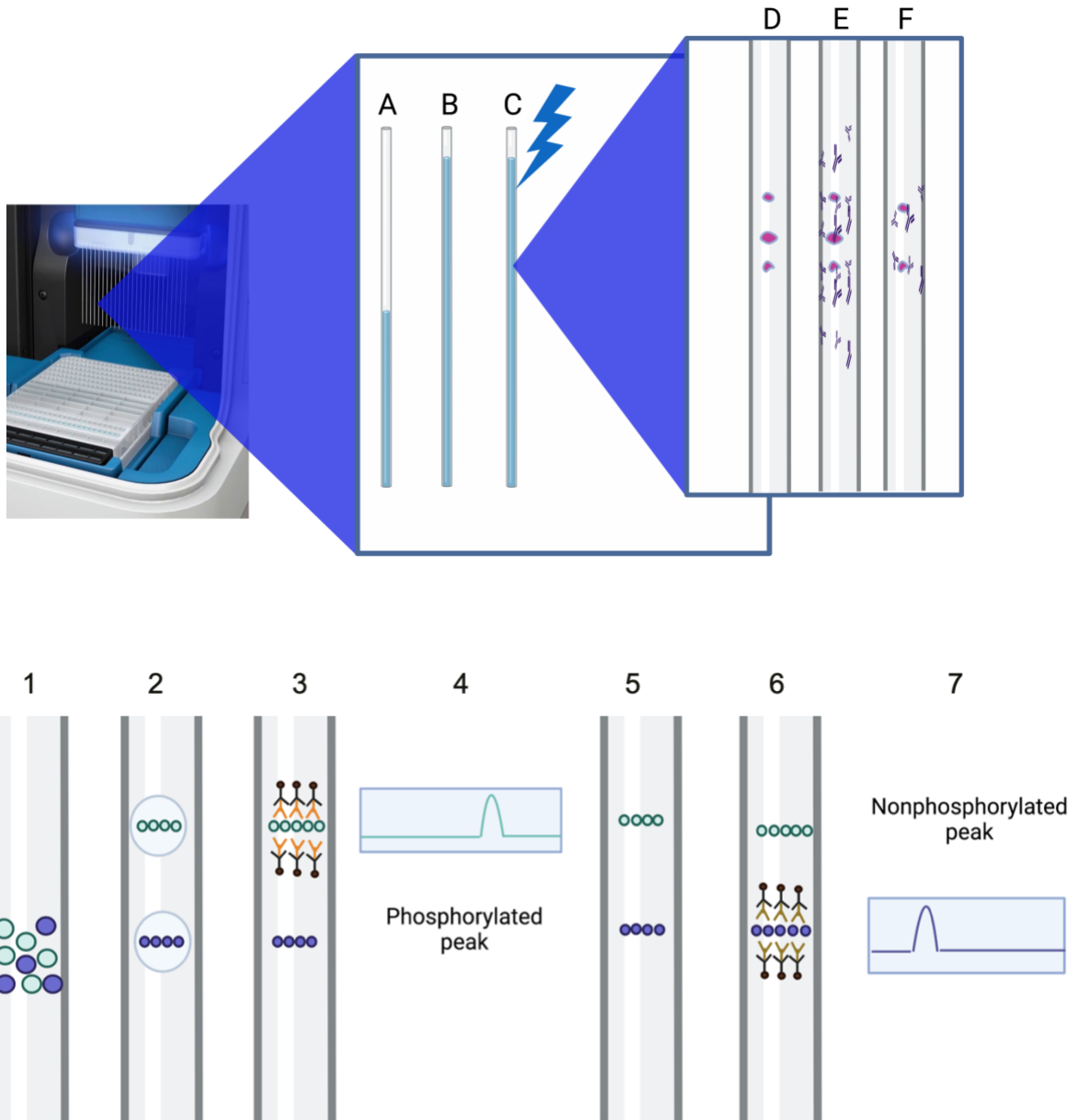


Figure 3.1 Capillary Electrophoresis with Jess™, RePlex™ steps with Jess™

Figure 3.1 (A-F: Capillary Electrophoresis); (A) The stacking and separation matrix are loaded. (B) The samples are loaded. (C) The capillary is introduced to the running buffer and a voltage is applied to separate the samples by molecular weight. (D) Once the separation is complete, UV light immobilizes the proteins to the capillary wall. (E) The matrix is cleared of the capillary and the Jess™ starts the immunoprobing process, first with incubation with the primary antibody, followed by a secondary HRP conjugate, and then the chemiluminescent substrate. (G) The chemiluminescent reaction is recorded by a CCD camera in a series of images over time which provides quantitative size-based data for analysis. (1-7: RePlex™ steps with Jess™); (1) Loading of stacking matrix, separation matrix, and samples. (2) Separation of samples by molecular

weight via voltage applied. (3) Immunoprobng process for phosphorylated version of the protein. (4) CCD images create size-based data peak of phosphorylated version of the protein. (5) Capillary is washed. (6) Immunoprobng process for non-phosphorylated version of the protein. (7) CCD images create size-based data peak of non-phosphorylated version of the protein. (ProteinSimple). [Schematic created with BioRender.com with Butterfield lab license].

Sample dilutions were prepared using 0.1X Sample Buffer (SMW-004, ProteinSimple) in accordance with the protein concentration obtained using Pierce Rapid Gold BCA Protein Assay Kit from Thermo Scientific (Waltham, MA, USA). The optimal protein concentration used for the JessTM depends on the expression level of the protein based on the values obtained from the BCA. The JessTM instrument provides an excel spreadsheet for these calculations. Antibody dilutions were prepared at 1:20 with antibody diluent 2 (DM-001, ProteinSimple). EZ Standard Pack 1 (12-230 kDa, SMW-004, ProteinSimple) included DTT and Fluorescent 5X Master Mix (1-part 5X Fluorescent Master Mix with 4-parts diluted lysate, final concentration 0.4 mg/mL for chemiluminescence) and the Biotinylated Ladder. The samples were denatured at 95°C for 5 minutes in the Boekel Scientific (Feasterville-Trevose, PA) Digital Dry Bath Incubator, spun down in the Benchmark (Sayreville, NJ) MyFuge Mini Centrifuge, and vortexed using the Fisher Scientific (Hampton, NH) Vortex Genie 2. Streptavidin-HRP (DM-001, ProteinSimple), anti-rabbit secondary antibody (DM-001, ProteinSimple), antibody diluent 2 (DM-001) were added to plate. The plate was spun down in the ThermoFisher (Waltham, MA) Scientific Sorvall X Pro Series Centrifuge at 2500rpm and 21°C for five minutes. The Wash Buffer (SMW-004, ProteinSimple), 1:1 Luminol-Peroxide Mix (DM-001, ProteinSimple) (450µL Luminol-S and 450µL Peroxide) and RePlexTM reagent mix (RP-011) (1.4mL of RePlexTM Reagent 1 and 0.35 mL RePlexTM Reagent 2) were added to the plate.

3.3.4.2 Data Acquisition with ProteinSimple Jess Instrument

SimpleWesternTM by ProteinSimpleTM allows for the accelerated probing of protein sizing and quantitative immunodetection with higher throughput and reproducibility than

traditional Western blot analysis (Nguyen et al., 2011). The RePlex™ with Jess™ allows for the analysis of phosphorylated and non-phosphorylated form of protein to be quantified on the same plate (and in the same capillary), eliminating variability between plates, thus increasing confidence in the results. The migration of the proteins through the separation matrix was performed for the samples and Ladder (12-230 kDa). The separated proteins were immobilized using the *ProteinSimple* Jess™ photoactivated capture chemistry capability. RePlex™ occurs after the detection and quantification of antibody 1 (phosphorylated form) to remove the 1st antibody so that the 2nd antibody (non-phosphorylated form) can be run. The luminol-peroxide mix was used for the chemiluminescent step. The Compass Simple Western software (Version 5.0.1, ProteinSimple) was used for analysis (Laidoudi et al., 2021).

3.4 Results

3.4.1 Expression Levels

The expression levels (non-phosphorylated form) of each protein of the mTOR cell signaling pathway including PI3K, Akt, mTOR, P70S6K and IRS-1 are presented below for the male and female PINK1 KO rat brain compared to the control (wild type (WT) 2-month-old rat). The male and female rats were sacrificed at age 2-month, 4-month, 6-month, and 8-month. Homogenates of the rat brain were analyzed using *ProteinSimple* Jess™ to measure the expression (non-phosphorylated) levels of each protein.

3.4.1.1 Phosphoinositide 3-Kinase Expression Levels Decrease in Male and Female PINK1 KO Rat Brain with Age

The expression levels of phosphoinositide 3-kinase (PI3K) in both the male and female PINK1 KO rat brain decreased with age. The male PINK1 KO rat brain presented with a more severe decrease in PI3K expression at KO 6-month and KO 8-month (compared to male WT 2-month PI3K expression level) in comparison to the female PINK1 KO rat brain at those respective ages. In the absence of PINK1, the male rat brain showed a significant decrease of phosphoinositide 3-kinase (PI3K) expression between WT 2-month and KO 6-month (42% reduction in PI3K expression) and between WT 2-month and KO 8-month (48% reduction in PI3K expression). The male PINK1 KO rat brain also showed a significant decrease in PI3K expression between KO 4-month and KO 6-month (42% reduction in PI3K expression) and between KO 4-month and KO 8-month (49% reduction in PI3K expression). There was no significant change in PI3K expression from WT 2-month and KO 4-month in the male or female PINK1 KO rat brain.

In the female rat brain, the PINK1 KO model showed a significant decrease of PI3K expression between WT 2-month and KO 6-month (15% reduction in PI3K expression) and between WT 2-month and KO 8-month (18% reduction in PI3K expression). There was also a significant decrease in PI3K expression in the female rat brain between KO 4-month and KO 6-month (16% reduction in PI3K expression) and between KO 4-month and KO 8-month (19% reduction in PI3K expression). The female PINK1 KO rat brain did not present with a significant difference between that of WT 2-month and KO 4-month PI3K expression levels. The trend for PINK1 KO female rat brain showed a decrease in PI3K expression with age, however, the decrease was not as dramatic as that of the PINK1 KO male rat brain.

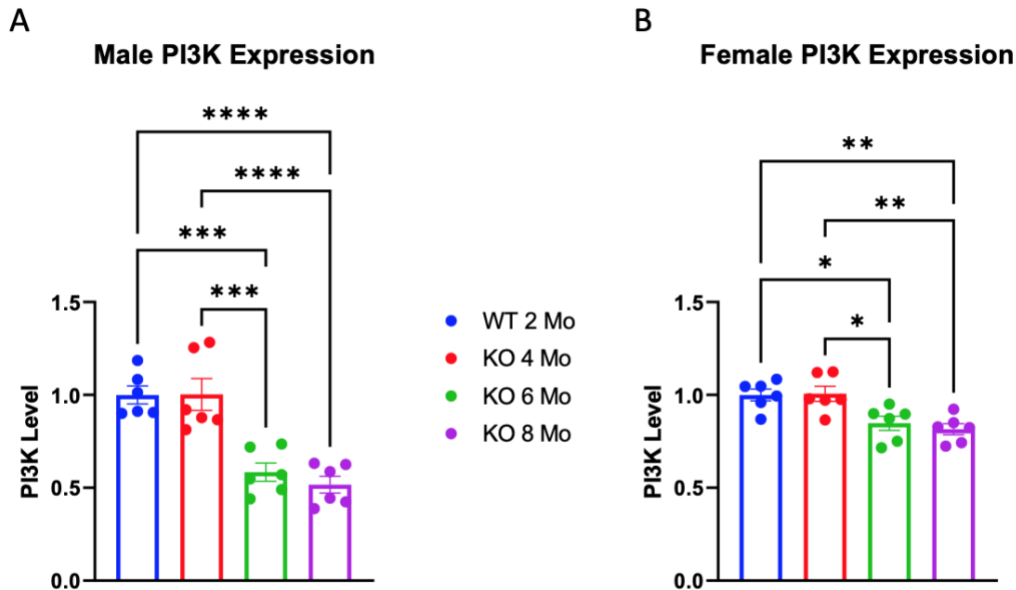


Figure 3.2 The expression levels of PI3K in male (A) and female (B) WT 2-month rat brain and PINK1 KO 4-month, KO 6-month and KO 8-month rat brain.

Figure 3.2 A and B show the levels of PI3K expression in WT and PINK1 KO rat brain collected using *ProteinSimple Jess*TM instrument capable of automated traditional Western blotting. PI3K expression levels were normalized to beta-actin. The plate ran with 3 rats for each group (WT 2-month, KO 4-month, KO 6-month, KO 8-month) in duplicates. Each value (6 values per group) was normalized to WT 2-month. The male PINK1 KO rat brain (A) showed a statistically significant decrease in PI3K expression between WT 2-month and KO 6-month ($***p=0.0002$), between WT 2-month and KO 8-month ($****p<0.0001$), between KO 4-month and KO 6-month ($***p=0.0002$) and between KO 4-month and KO 8-month ($****p<0.0001$). The female PINK1 KO rat brain (B) showed a statistically significant decrease in PI3K expression between WT 2-month and KO 6-month ($*p=0.0351$), between WT 2-month and KO 8-month ($**p=0.0099$), between KO 4-month and KO 6-month ($*p=0.0275$) and between WT 4-month and KO 8-month ($**p=0.0077$). Raw data for the male and female beta-actin plate, PI3K plate and calculations can be found in Appendix A.

3.4.1.2 Protein Kinase B Expression Levels Decrease in Male and Female PINK1 KO Rat Brain with Age

Protein Kinase B (Akt) expression levels decreased in male and female PINK1 KO rat brain with age. In the absence of PINK1, the male rat brain showed a significant decrease in Akt expression when comparing WT 2-month to that of KO 4-month (20% reduction), KO 6-month (30% reduction), and KO 8-month (21% reduction). It is important to note that, although not statistically significant, the PINK1 KO male rat brain showed a larger decrease in Akt expression at 6 months of age than that of 8 months of age.

In the female PINK1 KO rat brain, there was a significant decrease of Akt expression between WT 2-month and KO 6-month (23% reduction) and between WT 2-month and KO 8-month (16% reduction). There was also a significant decrease in Akt expression between KO 4-month and KO 6-month (23% reduction) and between KO 4-month and KO 8-month (17% reduction). As seen in the male PINK1 KO rat model, the female PINK1 KO rat brain showed a larger decrease in Akt expression at 6 months of age than that of 8 months of age.

The trend of Akt expression level in male and female PINK1 KO rat brain was similar, with an overall decrease in Akt expression level with age. Both the male and female PINK1 KO rat brain showed the largest decrease in Akt expression at 6 months of age. The female PINK1 KO rat brain did not initially decline at KO 4-month (male rat brain showed 20% decrease in Akt expression from WT 2-month to KO 4-month), however, the decreasing trend is similar between male and female PINK1 KO rat 6 months of age.

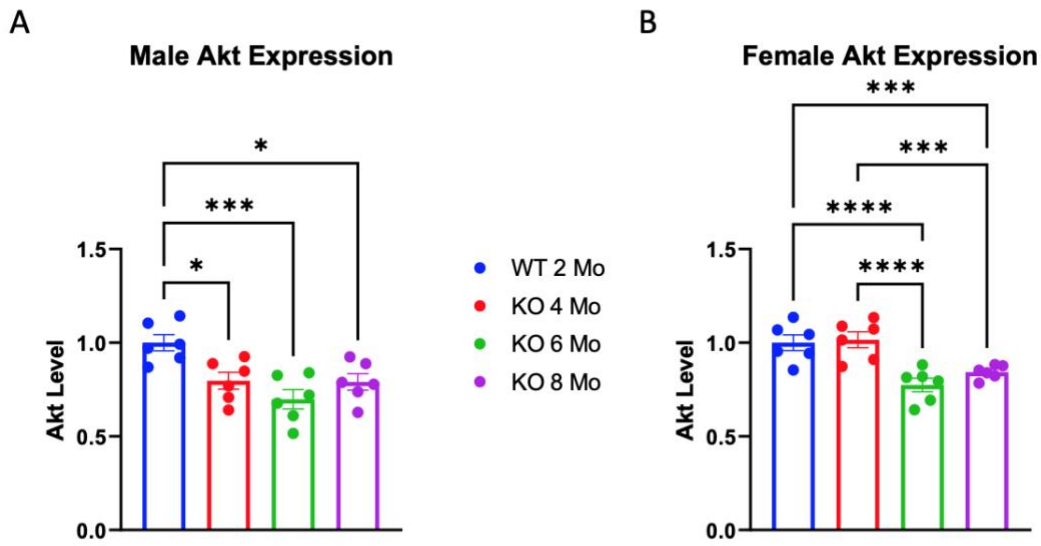


Figure 3.3 The expression levels of Akt in male (A) and female (B) WT 2-month rat brain and PINK1 KO 4-month, KO 6-month and KO 8-month rat brain.

Figure 3.3 A and B show the levels of Akt expression in WT and PINK1 KO rat brain collected using *ProteinSimple Jess*TM instrument capable of automated traditional Western blotting. Akt expression levels were normalized to beta-actin. The plate ran with 3 rats for each group (WT 2-month, KO 4-month, KO 6-month, KO 8-month) in duplicates. Each value (6 values per group) was normalized to WT 2-month. The male PINK1 KO rat brain (A) showed a statistically significant decrease in Akt expression between WT 2-month and KO 4-month (* $p=0.0218$), between WT 2-month and KO 6-month (*** $p=0.001$) and between WT 2-month and KO 8-month (* $p=0.0183$). The female PINK1 KO rat brain (B) showed a statistically significant decrease in Akt expression between WT 2-month and KO 6-month (**** $p<0.0001$), between WT 2-month and KO 8-month (*** $p=0.0007$), between KO 4-month and KO 6-month (**** $p<0.00001$) and between KO 4-month and KO 8-month (*** $p=0.0003$). Raw data for the male and female beta-actin plate, Akt plate and calculations can be found in Appendix A.

3.4.1.3 Mammalian Target of Rapamycin Expression Levels Decrease in Male and Female PINK1 KO Rat Brain with Age

The expression levels of mammalian target of rapamycin (mTOR) decreased in both the male and female PINK1 KO rat brain with age. In the absence of PINK1, the male rat brain showed a significant decrease of mTOR expression between WT 2-month and KO 6-month (67% reduction) and between WT 2-month and KO 8-month (75% reduction). A significant decrease in mTOR expression was also observed in the male PINK1 KO rat brain between KO 4-month and KO 6-month (66% reduction) and between KO 4-month and KO 8-month (74% reduction). The mTOR expression levels declined in the PINK1 KO male rat brain starting at 6 months of age. There was no significant decrease in mTOR expression between WT 2-month and KO 4-month.

In the female rat brain, there was a significant decrease of mTOR expression between WT 2-month and KO 6-month (65% reduction) and between WT 2-month and KO 8-month (62% reduction). There was also a significant decrease in mTOR expression between KO 4-month and KO 6-month (60% reduction) and between KO 4-month and KO 8-month (56% reduction). The female rat brain expressed lower levels of mTOR expression at KO 4-month than the male rat brain at KO 4-month (compared to WT 2-month), although the decrease in mTOR expression from WT 2-month to KO 4-month was not statistically significant for either sex.

Overall, the mTOR expression trend was similar between the male and female PINK1 KO rat brain with a decrease in expression with age beginning at 6 months old. In the female PINK1 KO rat brain, the lowest levels of mTOR expression occurred at 6 months. In the male PINK1 KO rat brain, the lowest levels of mTOR expression occurred at 8 months.

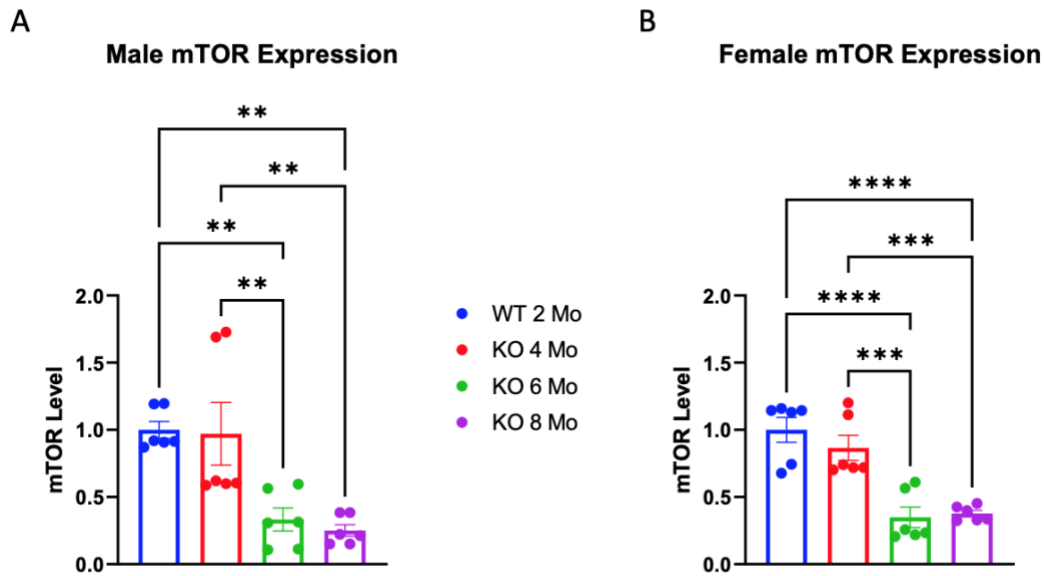


Figure 3.4 The expression levels of mTOR in male (A) and female (B) WT 2-month rat brain and PINK1 KO 4-month, KO 6-month and KO 8-month rat brain.

Figure 3.4 A and B show the levels of mTOR expression in WT and PINK1 KO rat brain collected using *ProteinSimple Jess*TM instrument capable of automated traditional Western blotting. mTOR expression levels were normalized to beta-actin. The plate ran with 3 rats for each group (WT 2-month, KO 4-month, KO 6-month, KO 8-month) in duplicates. Each value (6 values per group) was normalized to WT 2-month. The male PINK1 KO rat brain (A) showed a statistically significant decrease in mTOR expression between WT 2-month and KO 6-month (** $p=0.0071$), between WT 2-month and KO 8-month (** $p=0.0027$), between KO 4-month and KO 6-month (** $p=0.0098$) and between KO 4-month and KO 8-month (** $p=0.0038$). The female PINK1 KO rat brain (B) showed a statistically significant decrease in mTOR expression between WT 2-month and KO 6-month (**** $p<0.0001$), between WT 2-month and KO 8-month (**** $p<0.0001$), between KO 4-month and KO 6-month (*** $p=0.0002$) and between KO 4-month and KO 8-month (*** $p=0.0003$). Raw data for the male and female beta-actin plate, mTOR plate and calculations can be found in Appendix A.

3.4.1.4 Ribosomal Protein S6 Kinase Expression Levels Decrease in Male and Female PINK1 KO Rat Brain with Age

The ribosomal protein S6 kinase (P70S6K) expression levels decreased in the male and female PINK1 KO rat brain with age. The male PINK1 KO rat brain showed a significant decrease of P70S6K expression between WT 2-month and that of KO 4-month (38% reduction), KO 6-month (59% reduction), and KO 8-month (68% reduction).

In the female PINK1 KO rat brain, there was a significant decrease of P70S6K expression between WT 2-month and KO 6-month (64% reduction) and between WT 2-month and KO 8-month (51% reduction). There was also a significant decrease in P70S6K expression between KO 4-month and KO 6-month (55% reduction) and between KO 4-month and KO 8-month (40% reduction).

The trend in P70S6K expression levels between the male and female PINK1 KO rat brain was similar. The lowest levels of P70S6K expression for the male PINK1 KO rat brain occurred at 8 months old, however, the lowest levels of P70S6K expression in the female PINK1 KO rat brain occurred at 6 months old. The male PINK1 KO rat brain experienced a statistically significant decrease in P70S6K expression between WT 2-month and KO 4-month but the female PINK1 KO rat brain did not.

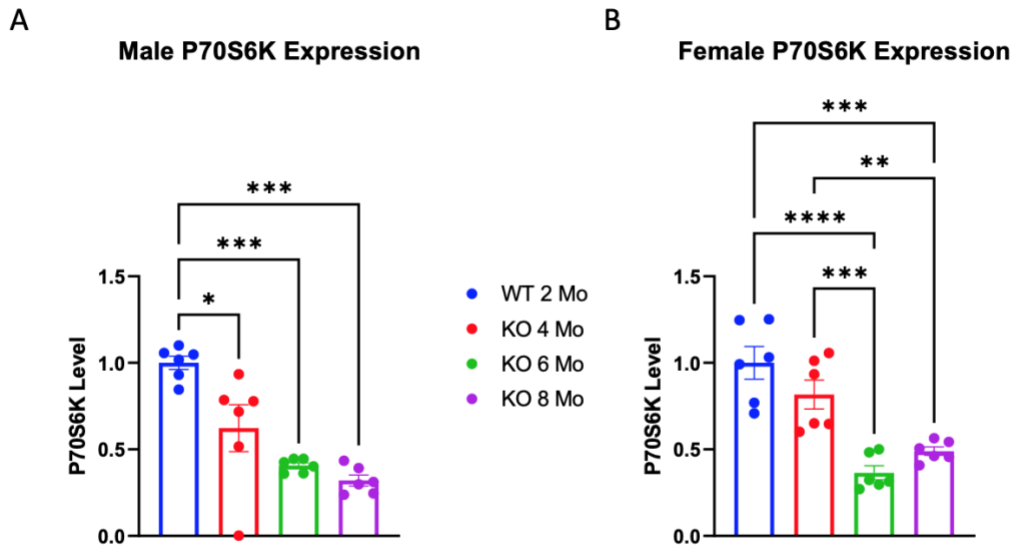


Figure 3.5 The expression levels of P70S6K in male (A) and female (B) WT 2-month rat brain and PINK1 KO 4-month, KO 6-month and KO 8-month rat brain.

Figure 3.5 A and B show the levels of P70S6K expression in WT and PINK1 KO rat brain collected using *ProteinSimple Jess*TM instrument capable of automated traditional Western blotting. P70S6K expression levels were normalized to beta-actin. The plate ran with 3 rats for each group (WT 2-month, KO 4-month, KO 6-month, KO 8-month) in duplicates. Each value (6 values per group) was normalized to WT 2-month. The male PINK1 KO rat brain (A) showed a statistically significant decrease in P70S6K expression between WT 2-month and KO 4-month (* $p=0.0186$), between WT 2-month and KO 6-month (*** $p=0.0004$) and between WT 2-month and KO 8-month (*** $p=0.0001$). The female PINK1 KO rat brain (B) showed a statistically significant decrease in P70S6K expression between WT 2-month and KO 6-month (**** $p<0.0001$), between WT 2-month and KO 8-month (*** $p=0.0002$), between KO 4-month and KO 6-month (*** $p=0.0006$) and between KO 4-month and KO 8-month (** $p=0.0093$). Raw data for the male and female beta-actin plate, P70S6K plate and calculations can be found in Appendix A.

3.4.1.5 Insulin Receptor Substrate 1 Expression Levels Decrease in Male and Female PINK1 KO Rat Brain with Age

Insulin Receptor Substrate 1 (IRS-1) expression levels decreased in both male and female PINK1 KO rat brain with age, although to differing degrees. In the absence of PINK1, the male rat brain showed a significant decrease of IRS-1 expression between WT 2-month and KO 6-month (79% reduction) and between WT 2-month and KO 8-month (62% reduction). Although not statistically significant, it is important to note that IRS-1 expression levels were lower at KO 6-month than at KO 8-month in the male PINK1 KO rat brain.

In the female rat brain, there was an overall decrease in IRS-1 expression with age. There was a significant decrease of IRS-1 expression between WT 2-month and KO 6-month (52% reduction) and between WT 2-month and KO 8-month (47% reduction). There was also a significant decrease in IRS-1 expression between KO 4-month and KO 6-month (39% reduction) and between KO 4-month and KO 8-month (32% reduction). Like the male PINK1 KO rat brain, the female PINK1 KO brain had a lower expression of IRS-1 at KO 6-month than that at KO 8-month.

In comparing the male PINK1 KO rat brain to that of the female, the trend for IRS-1 expression was the same with a decrease in IRS-1 expression with age. The levels of IRS-1 expression were lower across the board (KO 4-month, KO 6-month, KO 8-month) in the male PINK1 KO rat brain than that of the female PINK1 KO rat brain at those age points. Specifically, the male PINK1 KO rat experienced a 62% reduction in IRS-1 expression comparing WT 2-month to KO 8 month compared to the 47% reduction seen in the female PINK1 KO rat brain.

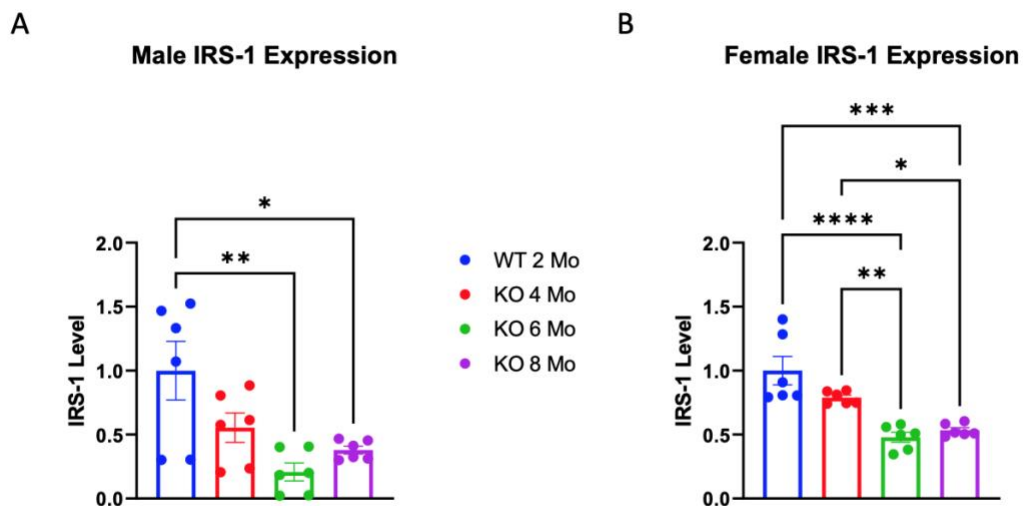


Figure 3.6 The expression levels of IRS-1 in male (A) and female (B) WT 2-month rat brain and PINK1 KO 4-month, KO 6-month and KO 8-month rat brain.

Figure 3.6 A and B show the levels of IRS-1 expression in WT and PINK1 KO rat brain collected using *ProteinSimple Jess*TM instrument capable of automated traditional Western blotting. IRS-1 expression levels were normalized to beta-actin. The plate ran with 3 rats for each group (WT 2-month, KO 4-month, KO 6-month, KO 8-month) in duplicates. Each value (6 values per group) was normalized to WT 2-month. The male PINK1 KO rat brain (A) showed a statistically significant decrease in IRS-1 expression between WT 2-month and KO 6-month (** $p=0.0038$) and between WT 2-month and KO 8-month (* $p=0.0224$). The female PINK1 KO rat brain (B) showed a statistically significant decrease in IRS-1 expression between WT 2-month and KO 6-month (**** $p<0.0001$), between WT 2-month and KO 8-month (*** $p=0.0002$), between KO 4-month and KO 6-month (** $p=0.0068$) and between KO 4-month and KO 8-month (* $p=0.026$). Raw data for the male and female beta-actin plate, IRS-1 plate, and calculations can be found in Appendix A.

3.4.2 Phosphorylation Levels

The level of phosphorylation for each protein from the mTOR cell signaling pathway including PI3K, Akt, mTORC1, P70S6K and IRS-1 are presented below for the male and female PINK1 KO rat brain. The male and female rats were sacrificed at age 2-month, 4-month, 6-month, and 8-month compared to the control (WT 2-month). Homogenates of the rat brain were analyzed using *ProteinSimple Jess*TM to measure the phosphorylation levels of each protein. The phosphorylation quantity for each protein was divided by the expression level of total protein to signify how much of the total protein was phosphorylated.

It is important to note that the phosphorylation of PI3K (at Tyr 458/Tyr199), Akt (at Ser 473), mTORC1 (at Ser 2448) and P70S6K (at Thr 389) indicate activation because the phosphorylation occurred at their respective activation sites. The phosphorylation of IRS-1 (at Ser 307) indicates inhibition of IRS-1 because Ser 307 is an inhibitory site for IRS-1.

3.4.2.1 Phosphoinositide 3-Kinase Phosphorylation Levels Decrease in Male and Female PINK1 KO Rat Brain with Age

Phosphorylated phosphoinositide 3-kinase (PI3K) indicates activated PI3K. Hence, phosphorylation levels of PI3K in this section symbolize PI3K activation.

The levels of PI3K activation, although decreasing with age, did not show statistically significant changes in either male PINK1 KO rat brain or female PINK1 KO rat brain. The male rat brain presented with a decrease in PI3K activation at KO 4-month and at KO 8-month when compared to the control. The activation of PI3K in the male PINK1 KO rat was largest at 6 months of age, even when compared to that of the control, WT 2-month rat brain.

In the female rat brain, there was a slight decrease in PI3K activation at KO 4-month, KO 6-month and KO 8-month in comparison to the control. The slight increase in PI3K activation observed in the male PINK1 KO rat brain at 6 months of age was not observed in the female PINK1 KO rat brain. The decrease in PI3K activation seen at KO 4-month and KO 8-month in the male PINK1 KO rat brain was larger than that of the decrease seen at any age of the female PINK1 KO rat brain.

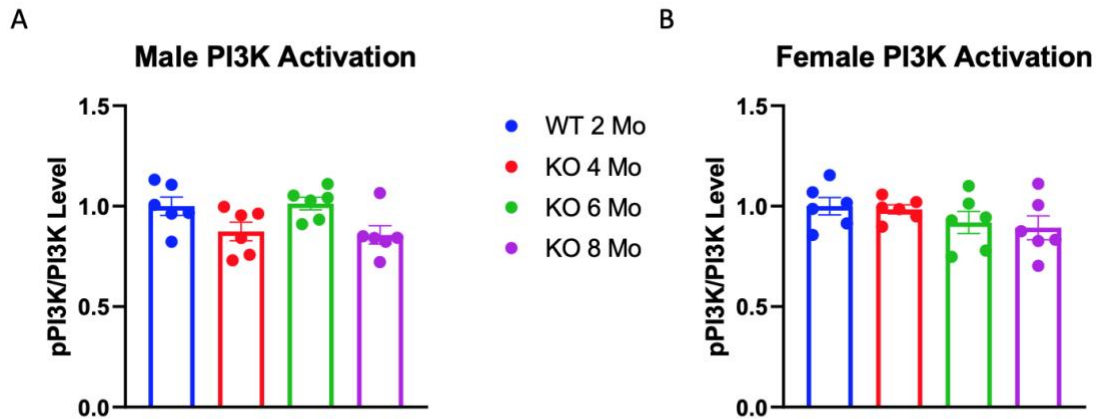


Figure 3.7 The phosphorylation levels of PI3K at Tyr 458/Tyr 199 (phosphorylated PI3K = pPI3K) in male (A) and female (B) WT 2-month rat brain and PINK1 KO 4-month, KO 6-month and KO 8-month rat brain. Phosphorylated PI3K leads to activated PI3K. Hence, phosphorylation levels of PI3K portrayed here symbolize PI3K activation.

Figure 3.7 A and B show the levels of PI3K activation at Tyr 458/Tyr 199 in WT and PINK1 KO rat brain collected using *ProteinSimple Jess*TM instrument capable of automated traditional Western blotting. PI3K activation levels were normalized to beta-actin and then divided by the corresponding normalized PI3K expression to represent the amount phosphorylated of the total protein expressed. The plate ran with 3 rats for each group (WT 2-month, KO 4-month, KO 6-month, KO 8-month) in duplicates. Each value (6 values per group) was normalized to WT 2-month. The male (A) and female (B) PINK1 KO rat brain did not show a statistically significant change in PI3K activation. The levels of PI3K activation decreased slightly but not significantly in both male and female PINK1 KO rat brain. Raw data for the male and female beta-actin plate, PI3K plate and the calculations can be found in Appendix A.

3.4.2.2 Protein Kinase B Phosphorylation Levels Increase in Male and Female PINK1 KO Rat Brain with Age

Phosphorylated protein kinase B (Akt) at Ser 473 presented here indicates activated Akt. Hence, phosphorylation levels of Akt in this section symbolize Akt activation.

The trend for Akt activation levels was similar between the male and female PINK1 KO rat brain, however, the males did not show statistically significant levels of activation. In the male rat brain, Akt activation increased only barely when comparing the KO 8-month to the control (WT 2-month) (<1% increase). However, there is a spike in Akt activation in the male PINK1 KO rat brain at 6 months old (69% increase) when compared to the control.

In the female rat brain, there was a trend of increasing Akt activation with age that was statistically significant. Specifically, there was a significant increase in Akt activation between WT 2-month and KO 6-month (153% increase) and between WT 2-month and KO 8-month (111% increase). There was also a statistically significant increase in Akt activation in the female rat brain between KO 4-month and KO 6-month (138%) and between KO 4-month and KO 8-month (98% increase).

It is of importance to note the increase in Akt activation observed at KO 6-month, which occurs in both male and female PINK1 KO rat brain. The increase at 6 months of age was the largest level of Akt activation between all ages; 69% increase in male PINK1 KO rat brain and 153% increase in female PINK1 KO rat compared when compared to male and female WT 2-month, respectively. Although the female PINK1 KO rat brain was observed to have larger levels of Akt activation than the male PINK1 KO rat brain, they had a similar trend of increased activation with age.

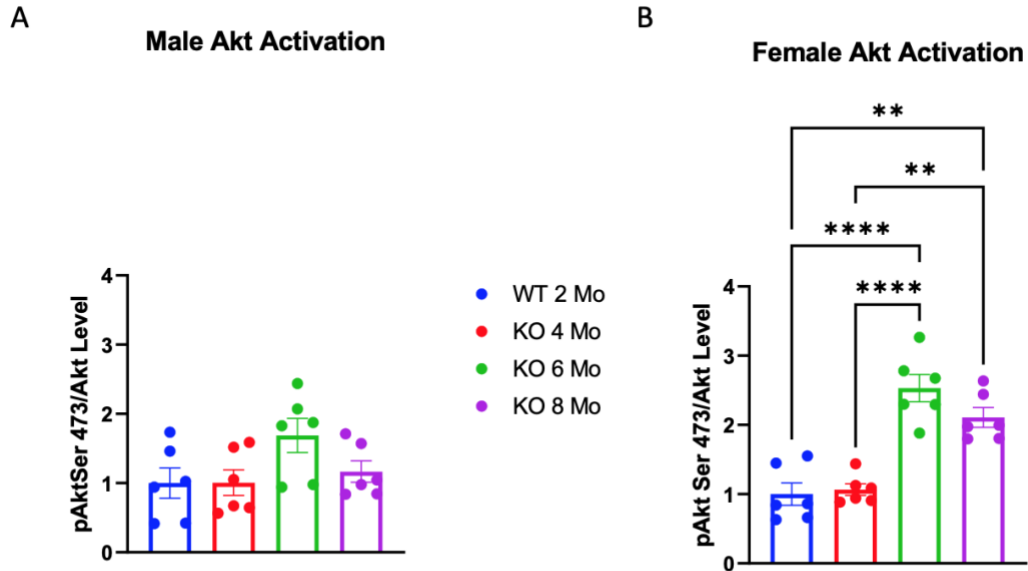


Figure 3.8 The phosphorylation levels of Akt at Ser 473 (phosphorylated Akt = pAkt) in male (A) and female (B) WT 2-month rat brain and PINK1 KO 4-month, KO 6-month and KO 8-month rat brain. Phosphorylated Akt at Ser 473 leads to activated Akt. Hence, phosphorylation levels of Akt portrayed here symbolize Akt activation.

Figure 3.8 A and B show the levels of Akt activation at Ser 473 in WT and PINK1 KO rat brain collected using *ProteinSimple Jess*TM instrument capable of automated traditional Western blotting. Akt activation levels were normalized to beta-actin and then divided by the corresponding normalized Akt expression to represent the amount phosphorylated of the total protein expressed. The plate ran with 3 rats for each group (WT 2-month, KO 4-month, KO 6-month, KO 8-month) in duplicates. Each value (6 values per group) was normalized to WT 2-month. The male (A) PINK1 KO rat brain did not show a statistically significant change in Akt activation. The levels of Akt activation increased slightly but not significantly. The female (B) PINK1 KO rat brain increased significantly in Akt activation between WT 2-month and KO 6-month (**** $p < 0.0001$), between WT 2-month and KO 8-month (** $p = 0.0014$), between KO 4-month and KO 6-month (**** $p < 0.0001$) and between KO 4-month and KO 8-month (** $p = 0.0023$). Raw data for the male and female beta-actin plate, Akt plate and the calculations can be found in Appendix A.

3.4.2.3 Mammalian Target of Rapamycin Complex I Phosphorylation Levels Decrease in Male and Increase in Female PINK1 KO Rat Brain with Age

Phosphorylated mammalian target of rapamycin complex I (mTORC1) at Ser 2448 presented here indicates activated mTORC1. Hence, phosphorylation levels of mTORC1 in this section symbolize mTORC1 activation.

The trend for activation levels of mammalian target of rapamycin complex I (mTORC1) at Ser 2448 was not consistent between the PINK1 KO male rat brain and the female PINK1 KO rat brain. The male rat brain showed a decrease (although minuscule) in activation of mTORC1, with no statistical significance. The largest decrease in mTORC1 activation observed in the male PINK1 KO rat brain was between WT 2-month and KO 4-month (22% reduction). The decrease from WT 2-month and KO 8-month in the male PINK1 KO rat brain was only 10%.

In the female PINK1 KO rat brain, there was a statistically significant increase in mTORC1 activation. Between WT 2-month and KO 6-month, mTOR activation increased by 213%. Between WT 2-month and KO 8-month, the increase in mTORC1 activation was 132%. There was also a statistically significant increase in mTORC1 activation between KO 4-month and KO 6-month (147% increase) and between KO 4-month and KO 8-month (83% increase). The largest levels of mTORC1 activation for the female PINK1 KO rat brain occurred at 6 months old. There was a statistically significant decrease in mTORC1 activation between KO 6-month and KO 8-month (26% reduction).

Overall, the male PINK1 KO rat brain showed a very slight decrease in mTORC1 activation with age and the female PINK1 KO rat brain showed a statistically significant increase in mTOR activation with age.

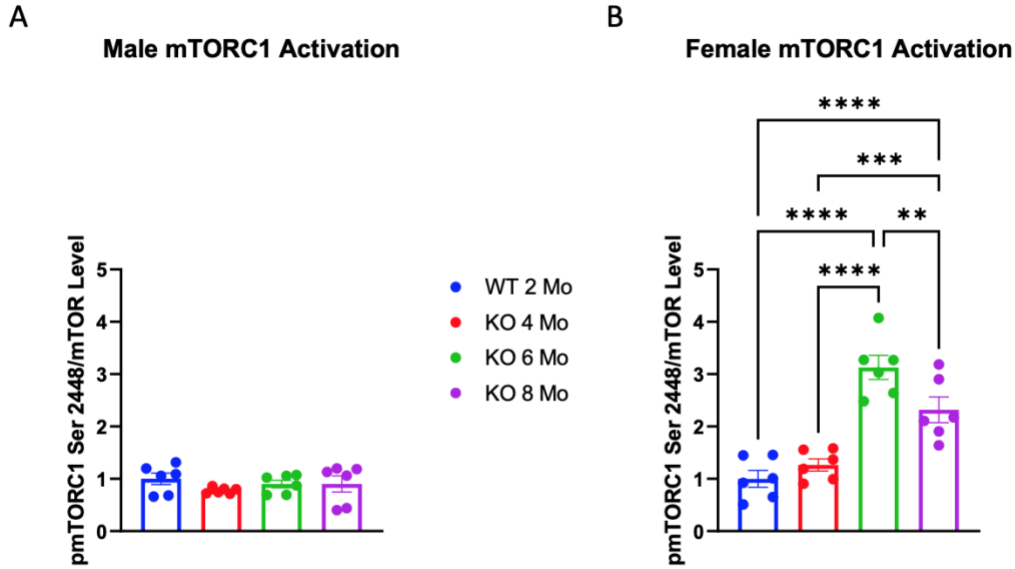


Figure 3.9 The phosphorylation levels of mTORC1 at Ser 2448 (phosphorylated mTORC1 = pmTOR) in male (A) and female (B) WT 2-month rat brain and PINK1 KO 4-month, KO 6-month and KO 8-month rat brain. Phosphorylated mTORC1 at Ser 2448 leads to activated mTORC1. Hence, phosphorylation levels of mTORC1 portrayed here symbolize mTORC1 activation.

Figure 3.9 A and B show the levels of mTORC1 activation at Ser 2448 in WT and PINK1 KO rat brain collected using *ProteinSimple Jess*TM instrument capable of automated traditional Western blotting. mTORC1 activation levels were normalized to beta-actin and then divided by the corresponding normalized mTOR expression to represent the amount phosphorylated of the total protein expressed. The plate ran with 3 rats for each group (WT 2-month, KO 4-month, KO 6-month, KO 8-month) in duplicates. Each value (6 values per group) was normalized to WT 2-month. The male (A) PINK1 KO rat brain did not show a statistically significant change in mTORC1 activation. The levels of mTORC1 activation decreased slightly but not significantly. The female (B) PINK1 KO rat brain increased significantly in mTORC1 activation between WT 2-month and KO 6-month (**** $p < 0.0001$), between WT 2-month and KO 8-month (**** $p < 0.0001$), between KO 4-month and KO 6-month (**** $p < 0.0001$), between KO 4-month and KO 8-month (*** $p = 0.0009$) and between KO 6-month and KO 8-month (** $p = 0.0085$). Raw data for the male and female beta-actin plate, mTOR plate and calculations can be found in Appendix A.

3.4.2.4 Ribosomal Protein S6 Kinase Phosphorylation Levels Increase in Male and Female PINK1 KO Rat Brain with Age

Phosphorylated ribosomal protein S6 kinase (P70S6K) presented here indicates activated P70S6K. Hence, phosphorylation levels of P70S6K in this section symbolize P70S6K activation.

The ribosomal protein S6 kinase (P70S6K) activation levels increased in the male and female PINK1 KO rat brain with age. However, there is caveat. The male rat brain presented with two peaks for P70S6K activation, a peak at 64 kDa and a peak at 88 kDa. The P70S6K activations levels in the male PINK1 KO rat brain at 64 kDa showed a decrease with age, while the P70S6K activations levels in the male PINK1 KO rat brain at 88 kDa showed an increase with age.

For the 64 kDa peak in the male rat brain, there was a significant decrease in P70S6K activation between WT 2-month and KO 6-month (77% reduction) and between WT 2-month and KO 8-month (73% reduction). There was also a significant decrease in P70S6K activation between KO 4-month and KO 6-month (73% reduction) and between KO 4-month and KO 8-month (68% reduction).

For the 88 kDa peak (only observed in male rat brain), there was a 760% increase in P70S6K activation at 6 months compared to the WT 2-month. The P70S6K activation levels in the male PINK1 KO rat brain at 6 months is the highest, given the 657% increase in P70S6K activation at 8 months. For both peaks, the change in P70S6K activation levels do not begin to significantly change until 6 months of age.

The female rat brain only presented with a peak at 64 kDa. The female PINK1 KO rat brain showed a statistically significant 836% increase in P70S6K activation evident at KO 6-month and tapered back down at KO 8-month (312% increase compared to WT 2-month). The

increase in P70S6K activation in the female rat brain was also statistically significant between KO 4-month and KO 6-month (904% increase).

The male and female PINK1 KO brain did not have similar trends regarding P70S6K activation at the 64 kDa peak. The males showed a statistically significant decrease in P70S6K activation with age at the 64 kDa peak, and the females show a statistically significant increase in P70S6K activation with age at the 64 kDa peak. The trend for P70S6K activation between the male PINK1 KO rat brain at the 88 kDa peak is similar to the P70S6K activation of the female PINK1 KO rat brain at the 64 kDa peak. The low levels of P70S6K activation at 4 months in the PINK1 KO male rat brain at the 88 kDa peak was also seen in the female KO 4-month at its 64 kDa peak. The large increase in activation at 6 months in the PINK1 KO male rat brain at the 88 kDa peak was also seen in the female KO 6-month at its 64 kDa peak, as was the decline in P70S6K activation from 6 months of age to 8 months of age.

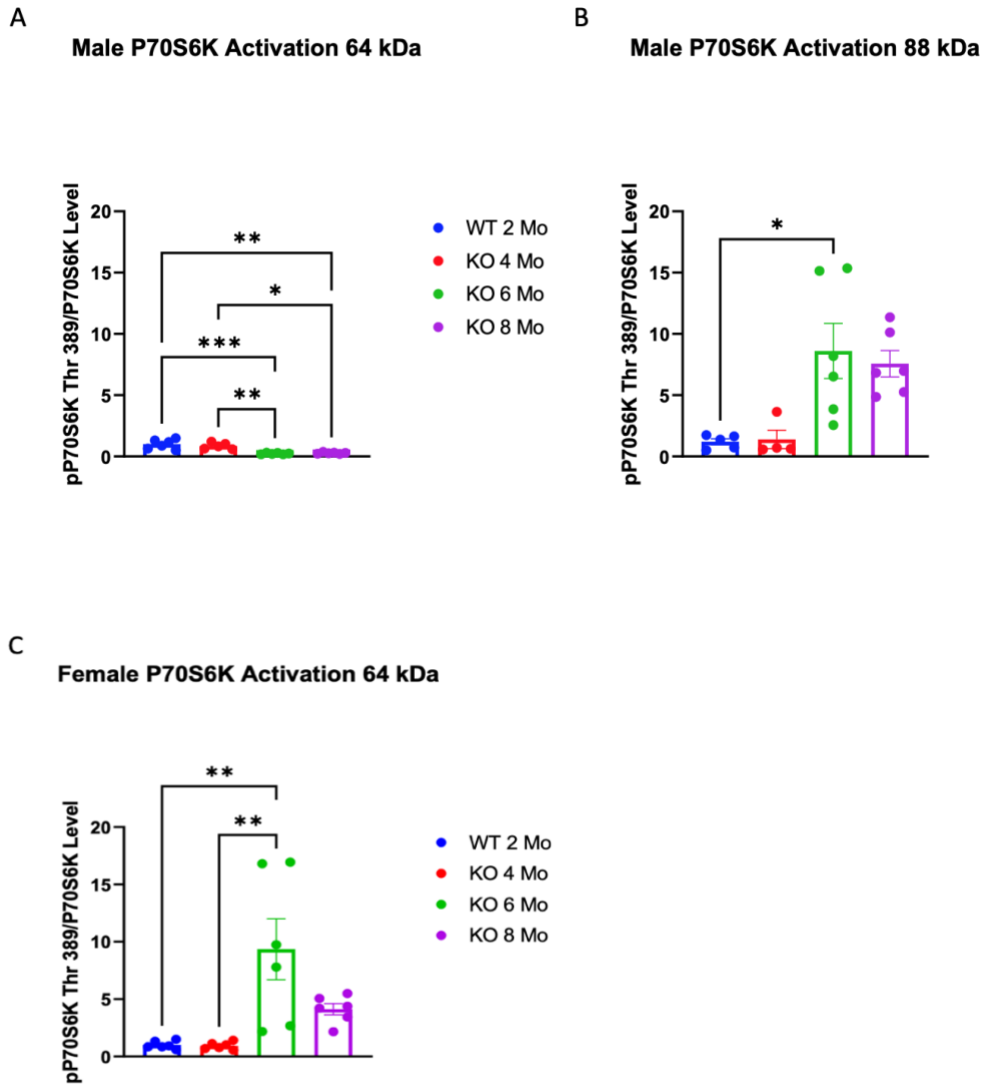


Figure 3.10 The phosphorylation levels of P70S6K at Thr 389 (phosphorylated P70S6K = pP70S6K) in male (A (64 kDa peak), B (88 kDa peak)) and female (C) WT 2-month rat brain and PINK1 KO 4-month, KO 6-month and KO 8-month rat brain. Phosphorylated P70S6K at Thr 389 leads to activated P70S6K. Hence, phosphorylation levels of P70S6K portrayed here symbolize P70S6K activation.

Figure 3.10 A, B, C show the levels of P70S6K activation at Thr 389 in WT and PINK1 KO rat brain collected using *ProteinSimple Jess*TM instrument capable of automated traditional Western blotting. P70S6K activation levels were normalized to beta-actin and then divided by the corresponding normalized P70S6K expression to represent the amount phosphorylated of the

total protein expressed. The plate ran with 3 rats for each group (WT 2-month, KO 4-month, KO 6-month, KO 8-month) in duplicates. Each value (6 values per group) was normalized to WT 2-month. The male PINK1 KO rat brain showed a statistically significant decrease in P70S6K activation at the 64 kDa peak (A) between WT 2-month and KO 6-month (**p=0.0007), between WT 2-month and KO 8-month (**p=0.0011), between KO 4-month and KO 6-month (**p=0.0071) and between KO 4-month and KO 8-month (*p=0.0116). The male PINK1 KO rat brain showed a statistically significant increase in P70S6K activation at the 88 kDa peak (B) between WT 2-month and KO 6-month (*p=0.0423). The female (C) PINK1 KO rat brain increased significantly in P70S6K activation between WT 2-month and KO 6-month (**p=0.0032) and between KO 4-month and KO 6-month (**p=0.003). Raw data for the male and female beta-actin plate, P70S6K plate and the calculations can be found in Appendix A.

3.4.2.5 Insulin Receptor Substrate 1 at Ser 307 Phosphorylation Levels Increase in Male and Decrease in Female PINK1 KO Rat Brain with Age

Phosphorylated insulin receptor substrate 1 (IRS-1) at Ser 307 presented here indicates inhibited IRS-1 function. Hence, phosphorylation levels of IRS-1 in this section symbolize IRS-1 inhibition.

The trend for IRS-1 inhibition at Ser 307 in the male and female rat brain appeared to be opposite in the PINK1 KO model. The male PINK1 KO rat brain increased in IRS-1 Ser 307 inhibition with age and the female PINK1 KO rat brain decreased in IRS-1 Ser 307 inhibition with age.

In the male rat brain, IRS-1 inhibition at Ser 307, although not statistically significant, increased with age. There was an increase in IRS-1 inhibition at 4 months of age (54% increase when compared to WT 2-month) and at 6 months of age (247% increase when compared to WT 2-month). IRS-1 inhibition at Ser 307 decreased by 8 months compared to the levels at 6 months of age (26% decrease) but did consistently increase in comparison to WT 2-month (155% increase comparing WT 2-month to KO 8-month).

In the female rat brain, IRS-1 inhibition decreased steadily with age. There was a statistically significant decrease in IRS-1 inhibition at Ser 307 in the female PINK1 KO rat brain between WT 2-month and KO 6-month (40% reduction) and between WT 2-month and KO 8-month (61% reduction). There was also a statistically significant decrease in IRS-1 Ser 307 inhibition in the female PINK1 KO rat brain between KO 4-month and KO 6-month (39% reduction) and between KO 4-month and KO 8-month (60% reduction).

Overall, the trend between the male and female PINK1 KO rat brain in IRS-1 Ser 307 inhibition was opposite, with an increase in IRS-1 Ser 307 inhibition seen in the male PINK1 KO

rat brain and a decrease seen in the female PINK1 KO rat brain. It is worth noting that the increased levels of IRS-1 Ser 307 seen in the male PINK1 KO rat brain were remarkably larger in quantity than that of the decreased levels of IRS-1 Ser 307 in the female PINK1 KO rat brain.

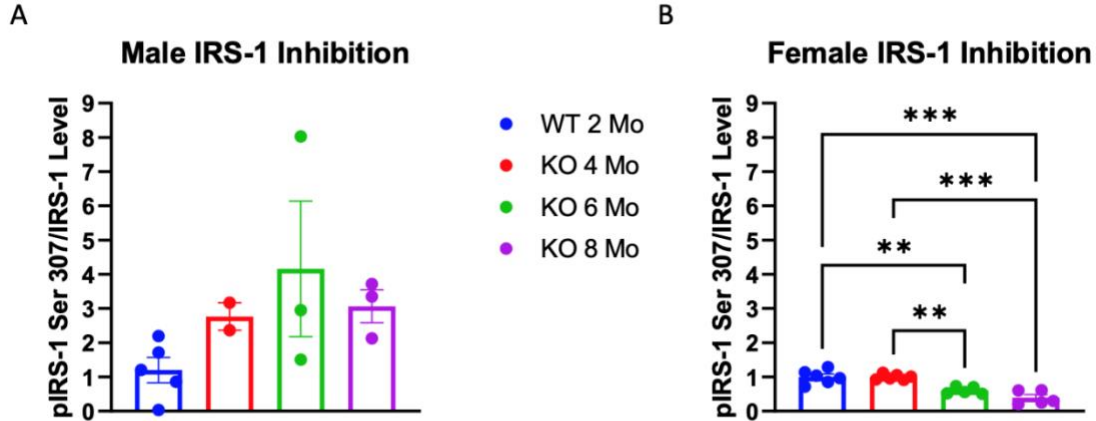


Figure 3.11 The phosphorylation levels of IRS-1 at Ser 307 (phosphorylated IRS-1 = pIRS-1) in male (A) and female (B) WT 2-month rat brain and PINK1 KO 4-month, KO 6-month and KO 8-month rat brain. Phosphorylated IRS-1 at Ser 307 leads to inhibited IRS-1 function. Hence, phosphorylation levels of IRS-1 portrayed here symbolize IRS-1 inhibition.

Figure 3.11 A and B show the levels of IRS-1 inhibition at Ser 307 in WT and PINK1 KO rat brain collected using *ProteinSimple Jess*TM instrument capable of automated traditional Western blotting with capillary electrophoresis. IRS-1 inhibition levels were normalized to beta-actin and then divided by the corresponding normalized IRS-1 expression to represent the amount phosphorylated of the total protein expressed. The plate ran with 3 rats for each group (WT 2-month, KO 4-month, KO 6-month, KO 8-month) in duplicates. Each value (6 values per group) was normalized to WT 2-month. The male (A) PINK1 KO rat brain did not show a statistically significant change in IRS-1 inhibition. The levels of IRS-1 inhibition increased but not significantly. The female (B) PINK1 KO rat brain increased significantly in IRS-1 inhibition between WT 2-month and KO 6-month (** $p=0.0037$), between WT 2-month and KO 8-month (** $p=0.0001$), between KO 4-month and KO 6-month (** $p=0.0041$) and between KO 4-month and KO 8-month (** $p=0.0001$). Raw data for the male and female beta-actin plate, IRS-1 plate, and calculations can be found in Appendix A.

3.5 Discussion of Results

3.5.1 Phosphoinositide 3-Kinase

Phosphoinositide 3-Kinase (PI3K) is an intracellular lipid kinase (J. Yang et al., 2019) that activates intracellular signaling pathways involved in functions such as growth, proliferation, differentiation, transcription, and translation (Zhao et al., 2021). Reduced PI3K signaling downstream of the insulin receptor has presented in type 2 diabetes mellitus (T2DM), while increased PI3K signaling has been observed in human cancer. The mTOR cell signaling pathway is one negative feedback loop that acts to balance PI3K signaling by interrupting insulin receptor substrate (IRS)-mediated PI3K activation (Engelman, Luo, & Cantley, 2006).

The binding of insulin to the insulin receptor instigates the dimerization of the receptor and the auto-phosphorylation of tyrosine residues. The phosphorylated tyrosine residues are recognized by IRS-1 which then binds to the insulin receptor which leads to the phosphorylation of Tyr 612 and Tyr 632 of IRS-1. This leads to the activation of IRS-1 (because Tyr 612 and Tyr 632 are activation sites for IRS-1) which subsequently leads to the phosphorylation and activation of the PI3K. The regulation of PI3K through the negative feedback loop of the mTOR cell signaling pathway includes the phosphorylation of Ser 307 of IRS-1, leading to IRS-1 inhibition (because Ser 307 is an inhibition site for IRS-1) which in turn inhibits PI3K activation (Butterfield & Halliwell, 2019). The phosphorylation of Ser 307 of IRS-1 is discussed below, in section 3.5.8. Activated PI3K, as a result of IRS-1 activation (IRS-1 phosphorylated on Tyr 612 and Tyr 632), leads to the phosphorylation and activation of Akt (Hemmings & Restuccia, 2012) constituting the PI3K/Akt signaling pathway, one that has been researched extensively. Neurodegenerative diseases have presented with implicated PI3K/Akt signaling, indicative of its role in cell proliferation, apoptosis inhibition and oxidative stress (F. Xu, Na, Li, & Chen, 2020).

Research for Parkinson's disease has focused, in part, on PI3K and Akt due to the neuroprotective abilities in preventing apoptosis and neuro-inflammation of the signaling pathway (Nakano et al., 2017).

In the male and female PINK1 KO rat brain, expression levels of PI3K decreased with age. The male PINK1 KO rat brain presented with a sharper decrease in PI3K expression at KO 6-month and KO 8-month in comparison to the female PINK1 KO rat brain at those respective ages. In the male rat brain, the expression level of PI3K was almost identical between the control and the PINK1 KO rat brain at 4 months of age. However, by 6 months of age, PI3K expression in the male rat brain dropped by 42% and decreased an additional 6% by 8 months of age.

In the female rat brain, the PI3K expression levels were almost identical between the control and the PINK1 KO rat brain at 4 months of age, as seen in the male. The female PINK1 KO rat brain presented with a decrease in PI3K expression by 6 months of age, similarly to the male, however, only by 15%, with an additional 3% decrease in by 8 months of age (compared to control). The decrease in PI3K expression with age in the male PINK1 KO rat brain was more than double (close to triple) that of the female PINK1 KO rat brain.

The phosphorylation (activation) levels of PI3K in male and female PINK1 KO rats, although lacking statistical significance, presented with a slight decrease with increasing age. The male and female rat brain presented with a similar overall decrease in PI3K activation when comparing the 8-month-old rat to the control (14% decrease in PI3K activation in male, 11% decrease in PI3K activation in female). The decrease in PI3K activation in the female PINK1 KO rat brain was small and continual with age. Conversely, the male PINK1 KO rat brain decreased in PI3K activation by 4-months-old when compared to the control (13% decrease) but then increased in PI3K activation by 6-months-old, the quantity of activation above that of the control

group. From 6 months of age to 8 months of age, the male rat brain again decreased in PI3K activation. This spike in PI3K activation at 6-months-old was not observed in the female PINK1 KO rat brain.

It has been previously hypothesized that PI3K/mTOR signaling is sexually dimorphic, as shown in a murine model of glioblastoma (Sponagel, Yu, Ippolito, Deneen, & Rubin, 2018) and in a *PTEN* mutant mouse model for metastatic follicular carcinomas (Antico-Arciuch, Dima, Liao, Refetoff, & Di Cristofano, 2010). The data from this thesis research on the PINK1 KO rat model for PD suggests that PI3K/mTOR signaling is sexually dimorphic. Regarding neurodegeneration, decreased levels of activated PI3K have been observed in Alzheimer's disease brain (Gabbouj et al., 2019). The trend in the PI3K data for the PD model aligns with such findings based on the decrease in PI3K expression and activation presented. It is conceivable that the low levels of PI3K activation with age are due to increased inhibition of IRS-1 at Ser 307. Lastly, the increase in phosphorylation at 6 months of age observed in PINK1 KO rat is an important trend seen again.

3.5.2 Protein Kinase B

Protein Kinase B (Akt) is a serine/threonine kinase that regulates the function of cellular proteins that are involved in metabolism, apoptosis, proliferation and cell survival (Nicholson & Anderson, 2002) and modulates signals from neurotransmitters, cytokines and growth factors (Chadha & Meador-Woodruff, 2020). As previously mentioned, phosphorylated PI3K leads to the phosphorylation and activation of Akt (Hemmings & Restuccia, 2012). Activated Akt (by phosphorylation) leads to activation of downstream targets, including mammalian target of rapamycin complex I (mTORC1) (Khan, Yap, Yan, & Cunningham, 2013). The

PI3K/Akt/mTOR signaling pathway is vital in the regulation of signal transduction and biological processes, such as apoptosis and metabolism, and has been compromised in neurodegenerative diseases and cancer (F. Xu et al., 2020).

The expression levels of Akt decreased in the male and female PINK1 KO rat brain with age. In the male PINK1 KO rat brain, there was a statistically significant decrease in Akt expression levels at 4-months, 6-months, and 8-months of age compared to the control. The decrease in Akt expression observed at 2-months-old compared to control and at 8-month-old compared to control were very similar at 20% and 21% decrease in Akt expression, respectively. The largest decrease in Akt expression seen in the male PINK1 KO rat brain was the 30% reduction in expression observed at 6 months of age. The PINK1 KO male rat brain was lowest in Akt expression at 6 months of age and then rose again by 8 months of age to almost the same expression level of that of the 4-month-old PINK1 KO rat brain.

In the female PINK1 KO rat brain, a similar trend was observed. A 22% decrease was observed in Akt expression in the female PINK1 KO rat brain at 6 months of age (compared to control). A 16% decrease in Akt expression was observed for the 8-month-old female PINK1 KO rat brain. Both male and female PINK1 KO rat brain decreased in Akt expression with age, and both observed the lowest levels of Akt expression at 6 months of age. The male PINK1 KO rat brain began to show a decline in Akt expression by 4 months of age, however, the female PINK1 KO rat brain did not decline in Akt expression until 6 months of age.

The phosphorylation (activation) of Akt increased in male and female PINK1 KO rat brain with age. However, in the male PINK1 KO rat brain, the change in Akt activation with age was not statistically significant. The levels of Akt activation in the male rat brain were relatively consistent until 6 months of age when an increase of 69% in Akt activation was observed.

Nevertheless, by 8 months of age, the male rat brain decreased in Akt activation by 31% (compared to 6 months of age). Overall, the Akt activation level at 6-months-old seemed to be the only legitimate change seen in the male PINK1 KO rat brain and even then, it was not statistically significant. The limited change seen activated Akt levels in the male PINK1 KO rat brain align with the limited change in activated PI3K levels. The limited change seen in activated PI3K levels would lead to the expectation that Akt would also not be largely activated, as was seen.

In the female PINK1 KO rat brain, the trend was like that of the male (increase Akt activation with age) though the Akt activation levels were higher in the female PINK1 KO rat brain compared to the male PINK1 KO rat brain with statistical significance. The change in activation by 4-months-old compared to the control were minor, comparable to the male PINK1 KO rat brain. However, there was an increase of 153% in Akt activation in the female rat brain by 6 months of age compared to the control and an 111% increase by 8 months of age compared to the control.

Overall, both male and female PINK1 KO rat brain saw an increase in Akt activation. The female PINK1 KO rat presented with higher levels of Akt activation at 6 months and 8 months of age compared to the male PINK1 KO rat brain at those respective ages. Both male and female PINK1 KO rat saw the highest levels of Akt activation at 6 months of age. Due to the small change in PI3K activation seen in the male PINK1 KO rat brain, it was to be expected that the Akt activation would not increase. The same expectation held for the female PINK1 KO rat brain based on its limited levels of PI3K activation, however, this was not observed.

The female PINK1 KO rat brain did not show significant changes in PI3K activation but did show significant increase in Akt activation. PI3K/Akt signaling can be activated in many

ways, so it is possible the female PINK1 KO rat brain is being activated by something other than PI3K activation. Research on Akt cell signaling across subregions of the hippocampus has been researched in models of estrogen activation of signaling cascades based on sex in which the female rodents had higher levels of phosphorylated Akt compared to the male rodents (Sheppard, Puri, & Galea, 2021). Although this thesis research and the research of the estrogen activation differ in brain area, the higher levels of phosphorylated Akt in the female compared to male aligns. It is possible that the female PINK1 KO rat brain observed higher levels of Akt activation due to estrogen levels, regardless of PI3K activation.

3.5.3 Mammalian Target of Rapamycin

Mammalian Target of Rapamycin (mTOR) is a protein serine/threonine kinase (Zarogoulidis et al., 2014) tasked with the regulation of cell proliferation, autophagy, and apoptosis through its role in numerous signaling pathways (Zou, Tao, Li, & Zhu, 2020). The activation of mTOR signaling is important for normal neuronal growth by promoting differentiation, elongation and branching of the neuron, synaptic formation during development through the enhancement of protein synthesis and the inhibition of autophagy. The disruption of this signaling pathway is associated with neuronal degeneration and abnormal neural development (both characteristics of neurodegeneration), and excessive activation of mTOR signaling can cause abnormal development of neurons, leading to brain malformation. The careful balance of mTOR signaling is imperative to the health of the cell and the brain as a whole (Takei & Nawa, 2014).

The expression levels of mTOR decreased in both the male and female PINK1 KO rat brain with age. This decrease occurred significantly by 6 months of age in the male PINK1 KO

rat with a 67% decrease in expression levels when compared to the control. The male PINK1 KO rat brain decreased in mTOR expression even more so by 8 months of age with a total of 75% reduction in mTOR expression in the male PINK1 KO rat brain when compared to the control.

In the female PINK1 KO rat brain, a decrease of 65% in mTOR expression was seen by 6 months of age when compared to the control. mTOR expression increased by about 3% by 8 months of age. The 6-month expression level was the lowest level of mTOR expression seen in the female rat brain. The female had a total reduction of 62% in mTOR expression by 8 months of age when compared to control, lower than that of the male PINK1 KO rat brain.

The phosphorylation (activation) levels of mTORC1 in the male PINK1 KO rat brain showed a minor decrease as the rat got older and was not statistically significant. Notwithstanding the activation levels at 6-months-old, the change in activation of Akt was also minor and not statistically significant for the male PINK1 KO rat brain. Activated Akt leads to activated mTORC1, therefore, it would not be expected for the male PINK1 KO rat brain to present with much activated mTORC1 based on its low levels of activated Akt.

Conversely, the female PINK1 KO rat brain showed an increase in mTORC1 activation. A 213% increase (the largest increase in mTORC1 activation seen in the female) occurred at 6 months of age when compared to the control. A 132% increase was observed at 8 months of age compared to the control. There was also a significant increase of 147% between 4 months and 6 months of age and 83% between 4 months and 8 months of age. The high levels of mTORC1 activation in the female PINK1 KO rat brain at 6 months and 8 months of age are consistent with the high levels of Akt activation at those ages. Phosphorylated Akt leads to the phosphorylation of mTORC1, so this observation is compatible with the pathway.

In this thesis research, the phosphorylation site probed for mTOR was Ser 2448. It is understood that phosphorylated PI3K leads to phosphorylation and activation of Akt, which leads to phosphorylation of Ser 2448 of the mechanistic target of rapamycin complex 1 (mTORC1). Activated mTORC1 kinase can lead to the impairment of neuronal survival by way of autophagic inhibition and the phosphorylation of P70S6K, which phosphorylates IRS-1 on Ser 307, halting IRS-1 function (marker for insulin resistance) (Butterfield & Halliwell, 2019). This would suggest that those with higher levels of activated mTORC1 would undergo increased inhibition of autophagy and have increased markers for insulin resistance.

Based on the results from this thesis research, the female PINK1 KO rat brain presented with increased levels of phosphorylated mTORC1 at Ser 2448, which is indicative of increased inhibition of autophagy. This could be supportive of the faster disease progression and worst prognosis seen in females with PD compared to males. The male PINK1 KO rat brain did not present with increased inhibition of autophagy based on its unchanging levels of phosphorylated mTORC1.

mTOR is phosphorylated differently depending on its association with mTORC1 and mTORC2. mTORC1 contains mTOR phosphorylated predominantly on Ser 2448 whereas mTORC2 contains mTOR phosphorylated predominantly on Ser 2481 (Copp, Manning, & Hunter, 2009). This thesis research studied the phosphorylation of mTOR at Ser 2448 which is why the activation levels are associated with mTORC1.

3.5.4 Ribosomal Protein S6 Kinase

Ribosomal protein S6 kinase (P70S6K) modulates cell-cycle progression, cell size, and cell survival. The activation of P70S6K can up-regulate ribosomal biosynthesis and translation of

the cell (An et al., 2003). P70S6K is phosphorylated by activated mTORC1. Activated mTORC1 not only leads to the phosphorylation of P70S6K, but also leads to the inhibition of autophagy, both of which threaten neuronal survival, and is consequently relevant to PD. The phosphorylation of P70S6K leads to its fulfilment as a kinase, one of the substrates of which is Ser 307 of IRS-1. Once IRS-1 is phosphorylated on Ser 307, IRS-1 function discontinues (a marker for insulin resistance) (Butterfield & Halliwell, 2019). The negative feedback loop for regulating PI3K in the mTOR cell signaling pathway includes the phosphorylation of Ser 307 of IRS-1 (IRS-1 inhibition) which inhibits PI3K activation (Engelman et al., 2006).

The expression levels of P70S6K decreased in the male and female PINK1 KO rat brain with age. The male PINK1 KO rat brain showed a significant 38% decrease of P70S6K expression by 4 months of age, a 59% decrease by 6 months of age, and a 68% decrease by 8 months of age (all in comparison to control). In the female PINK1 KO rat brain, there was a significant 64% decrease in P70S6K expression by 6 months of age compared to the control and a 51% decrease in expression by 8 months in age compared to the control.

The trend in P70S6K expression levels between the male and female PINK1 KO rat brain was similar. However, the lowest levels of P70S6K expression for the male PINK1 KO rat brain occurred at 8 months, while the lowest levels of P70S6K expression in the female PINK1 KO rat brain occurred at 6 months. Furthermore, the male PINK1 KO rat brain experienced a statistically significant decrease in P70S6K expression between the control group and PINK1 KO at 4 months but the female PINK1 KO rat brain did not.

The phosphorylation (activation) levels of P70S6K increased in the male and female PINK1 KO rat brain with age. The male rat brain presented with a peak for P70S6K activation at 64 kDa and at 88 kDa. The P70S6K activations levels in the male PINK1 KO rat brain at 64 kDa

showed a statistically significant decrease with age, while the P70S6K activations levels at 88 kDa showed an increase with age.

The 64 kDa peak in the male rat brain presented with a significant 77% decrease in P70S6K activation when comparing the 6-month-old KO rat brain to the control and a 73% decrease when comparing the 8-month-old to the control. There was also a significant decrease in P70S6K activation between KO 4-month and KO 6-month (73% reduction) and between KO 4-month and KO 8-month (68% reduction).

For the 88 kDa peak (a peak only observed in the male rat brain), there was a 760% increase in P70S6K activation at 6 months of age compared to the control. The P70S6K activation levels by 8 months had increased by 657% compared to the control. For both the 64 kDa peak and the 88 kDa peak, the change in P70S6K activation level began at 6 months of age.

The female rat brain only presented with a peak at 64 kDa - that of which showed a statistically significant 836% increase in P70S6K activation by 6 months of age compared to the control. This tapered back down by 8 months of age (312% increase compared to control). The increase in P70S6K activation in the female rat brain was also statistically significant between KO 4-month and KO 6-month (904% increase). Both the male P70S6K activation (at its 88 kDa peak) and the female P70S6K activation were highest at 6 months of age.

There are multiple phosphorylation sites associated with the activation of P70S6K. The phosphorylation sites Ser 411, Ser 418, Thr 421, Ser 424 (within the autoinhibitory domain), Thr 229 (in the catalytic domain), and Thr 389 and Ser 404 (in the linker region). In 1997, three new phosphorylation sites (Thr 367, Ser 371, and Thr 447) were identified, which have a recognition motif similar to Ser 411, Ser 418, Thr 421, and Ser 424 (Moser et al., 1997). This thesis research studied the P70S6K phosphorylation site at Thr 389. However, two P70S6K peaks (at 64 kDa

and 88 kDa) were observed for the male PINK1 KO rat brain. It is possible that the peak at 88 kDa represents phosphorylation at multiple phosphorylation sites. If this speculation is correct, the presence of the two peaks could represent higher quantities of activated P70S6K in the male PINK1 KO rat. However, other phosphorylation sites should not have appeared because the primary antibody was only for phosphorylated P70S6K at the Thr 389 site. Further research would need to be carried out to elucidate further on the reason for two P70S6K phosphorylation peaks in the male PINK1 KO rat brain.

The male and female PINK1 KO brain did not have similar trends regarding P70S6K activation at the 64 kDa peak. The males showed a statistically significant decrease in P70S6K activation with age at the 64 kDa peak, and the females show a statistically significant increase in P70S6K activation with age at the 64 kDa peak. Interestingly, however, the trend between the male PINK1 KO rat brain in P70S6K activation levels at the 88 kDa peak is comparable to the female PINK1 KO rat brain in P70S6K activation levels at its 64 kDa peak. The low levels of P70S6K activation at 4 months in the PINK1 KO male rat brain at the 88 kDa peak was seen in the female KO 6-month at its 64 kDa peak. The large spike in activation at 6 months in the PINK1 KO male rat brain at the 88 kDa peak was also seen in the female KO 6-month at its 64 kDa peak, as was the decline in P70S6K activation from 6 months of age to 8 months of age. If it is correct to speculate that two peaks are indicative of more activation, then the male PINK1 KO rat brain experienced a much larger degree of activation than the female PINK1 KO rat brain. Even if this speculation is incorrect, the similarity between the trend for the male 88 kDa peak and the female 64 kDa peak should be noted.

It cannot go without saying that the male PINK1 KO rat brain did not present significant change in mTORC1 activation which, based on the pathway, would mean that the activation

levels of P70S6K would also be low (seen in 64 kDa peak data). However, the activation of P70S6K requires phosphorylation at two stages; the first of which is independent of insulin stimulation (by an unknown kinase). The second phosphorylation is mediated by mTOR in an insulin dependent manner. The phosphorylation stage mediated by mTOR occurs at Thr 389, the site used in this study. It is possible P70S6K may be phosphorylated at the first stage by the unknown kinase and could account for the second peak in the male PINK1 KO rat brain.

Nevertheless, the trend of P70S6K activation presented in the female PINK1 KO rat brain was consistent with its trend of mTORC1 activation. The highest level of activation for both mTORC1 and P70S6K occurred at 6 months of age which decreased again by 8 months of age. While the male PINK1 KO rat brain data remains somewhat mysterious, the female PINK1 KO rat brain activation levels are consistent with the pathway.

3.5.5 Insulin Receptor Substrate 1

The insulin receptor substrate (IRS) are ligand proteins tasked with insulin signaling functions. Insulin resistance (which involves IRS, PI3K, and Akt) in the brain can eventually lead to apoptosis and neurodegeneration (Akhtar & Sah, 2020). Increased inhibition of IRS-1 at serine residues has presented in AD brain as well as in animal models of AD induced by T2DM. Elevated phosphorylation of IRS-1 at serine sites has been seen in brain plagued by neurodegeneration (Tanokashira, Fukuokaya, & Taguchi, 2019). IRS-1 is an important player in the mTOR signaling pathway with regard to neurodegeneration based on its ability to activate mTORC1 in a negative feedback loop (Yoneyama et al., 2018) and based on it becoming a marker for insulin resistance when phosphorylated on Ser 307 by activated P70S6K (Pearce et al., 2010). Diabetes is being increasingly associated with the development of PD, having shown

to promote the development and progression of the neurodegenerative disorder through mitochondrial dysfunction and increased ROS production (Hong et al., 2020).

IRS-1 expression levels decreased in both male and female PINK1 KO rat brain with age, although to differing degrees. In the absence of PINK1, the male rat brain presented with a statistically significant 79% decrease in IRS-1 expression by 6 months of age compared to the control and a 62% decrease by 8 months of old when compared to the control. IRS-1 expression levels were lower at 6 months of age than at 8 months of age in the male PINK1 KO rat brain (that of which was also seen in the female PINK1 KO rat brain).

In the female PINK1 KO rat brain, there was an overall decrease in IRS-1 expression with age. There was a statistically significant 52% decrease in IRS-1 expression by 6 months of age when compared to the control and a 47% decrease by 8 months of age when compared to the control. There was also a significant decrease in IRS-1 expression between KO 4-month and KO 6-month (39%) and between KO 4-month and KO 8-month (32%). Like the male PINK1 KO rat brain, the female PINK1 KO brain had a lower expression of IRS-1 at KO 6-month than that of KO 8-month. In comparing the male PINK1 KO rat brain to that of the female, although the trend was the same, the levels of IRS-1 expression were lower at all ages in the male PINK1 KO rat brain than that of female.

The trend for IRS-1 inhibition at Ser 307 in the male and female rat brain were opposite in the PINK1 KO model. The male PINK1 KO rat brain increased in IRS-1 inhibition with age and the female PINK1 KO rat brain decreased in IRS-1 inhibition with age. In the male rat brain, inhibition of IRS-1 at Ser 307, although not statistically significant, increased with age. There was a 54% increase in IRS-1 inhibition at 4 months of age when compared to the control and a 247% increase by 6 months of age when compared to the control. IRS-1 inhibition increased by

155% by 8 months of age when compared to the control. The highest level of IRS-1 inhibition in the male rat brain occurred at 6 months of age.

The interpretation of phosphorylation of IRS-1 at Ser 307 when analyzing the mTOR pathway overall for the male is obstructed by the differing levels of P70S6K activation. The increase in IRS-1 inhibition would lead to the expectation that P70S6K activation had increased as well. This is the case regarding the 88 kDa peak, but not for the 64 kDa peak in the male PINK1 KO rat brain. Either way, the increase in IRS-1 inhibition at Ser 307 indicates increased insulin resistance in the male PINK1 KO rat brain with age, which could be supportive of the increased risk of T2DM in males compared to females.

In the female rat brain, IRS-1 inhibition decreased steadily with age. There was a statistically significant 40% decrease in IRS-1 inhibition in the female PINK1 KO rat brain by 6 months of age compared to the control and a 61% decrease by 8 months of age compared to the control. There was also a statistically significant decrease in IRS-1 inhibition in the female PINK1 KO rat brain when comparing to KO 4-month to KO 6-month (39% reduction) and to KO 8-month (60% reduction). The decrease seen in the female PINK1 KO rat brain with age suggests that the female rat brain lacking PINK1 experienced less IRS-1 inhibition and therefore less insulin resistance.

3.5.6 PINK1 KO Rat at Age 6 Months

A clear trend has been observed at 6 months of age in the PINK1 KO rat brain. The level of phosphorylation and expression expected (based on the trend seen with each protein) has shown staggering inconsistency at 6 months of age in the PINK1 KO rat brain in every protein. Specifically, the expression levels have been lower than expected at 6 months of age and the

phosphorylation levels have been higher at 6 months of age. The male PINK1 KO rat brain experienced a lower level of expression in Akt and IRS-1, and a higher level of phosphorylation in PI3K, Akt, P70S6K (88 kDA peak) and IRS-1. Similarly, the female PINK1 KO rat brain experienced a lower level of expression in Akt, mTOR, P70S6K, and IRS-1, and a higher level of phosphorylation in Akt, mTOR, and P70S6K.

A rat brain at 6 months of age would be comparable to an 18 year old human (Sengupta, 2013). The chronic brain disorder schizophrenia has a typical age of onset in late adolescence or early twenties (Gogtay, Vyas, Testa, Wood, & Pantelis, 2011). In 2007, the University of Lübeck in Germany studied a possible association of mutations in PINK1 with psychiatric disorders and found predominantly affective and schizophrenia spectrum disorders in 61% of the PINK1 mutation carriers. They concluded that affective and psychotic symptoms may be due entirely to manifestation of PINK1 mutations (Steinlechner et al., 2007). Although PD and schizophrenia have completely opposite pathophysiology (hypodopaminergic transmission in the SN of PD brain and hyperdopaminergic transmission in the mesolimbic pathway of the brain in schizophrenia) comorbidity of the two have occurred (Grover, Sahoo, & Goyal, 2017). It is curious that the age of onset for schizophrenia (late adolescence/early twenties - comparable to the rat at 6 months of age), which has been seen to be implicated by PINK1 mutations, shows the highest level of phosphorylation and the lowest level of expression of the proteins in the mTOR pathway. This trend seen at 6 months of age of the PINK1 KO rat data presented in this thesis research was also observed in previous PINK1 KO data in the Butterfield Neurochemistry Lab (Ren & Butterfield, 2021; Ren et al., 2019).

3.5.7 Oxidative Damage in PINK1 KO Rat Brain

4-hydroxy-2-nonenal (HNE) serves as a biomarker for oxidative damage associated with lipid peroxidation. The brain is susceptible to oxidative damage due to its high consumption of oxygen and the high levels of polyunsaturated fatty acids (PUFAs). Lipid peroxidation on arachidonic acid (one of the most abundant PUFAs in the brain) leads to the formation of HNE. This alters the structure and function of proteins and leads to decreased cellular ion homeostasis and increased apoptosis (Butterfield et al., 2010). The first study on oxidative damage in the PINK1 KO rat as a function of age and gender was conducted in the Butterfield laboratory. The research investigating the pathobiology of familial PD was carried out and published by Dr. Ren and other lab members. The publication included biomarkers for oxidative damage including HNE, 3-nitrotyrosine, and protein carbonyls (Ren et al., 2019). HNE is the only biomarker discussed in this thesis research for example of the results but the trend for all three biomarkers were the same.

Protein-bound HNE levels increased with age in the male and female PINK1 KO rat brain compared to the control. The rat at 4 months of age showed a significantly higher level of HNE compared to the other groups. The increased levels of HNE with age in the male and female PINK1 KO rat indicate increased oxidative damage. The elevated level of oxidative damage in the PINK1 KO rat brain was consistent with mitochondrial implications seen in PD. It was proposed in the published work by Dr. Ren that mutations in PINK1, which lead to familial PD, likely result in increased superoxide leak from damaged mitochondria and is possibly related to the increased oxidative damage in the PINK1 KO rat brain (since the mutation in PINK1 is loss-of-function) (Ren et al., 2019).

CHAPTER 4. CONCLUSION AND FUTURE STUDIES

4.1 Conclusions

Parkinson's disease is unrelenting. Accordingly, the commitment to PD research must be relentless in equal magnitude to achieve a deeper understanding of the disease that millions of people live with so that their quality of life can be improved upon.

Between five and ten percent of PD cases are a result of an inheritable mutation. The current thesis research employed PTEN-induced kinase 1 (PINK1) knockout (KO) rats because mutations in PINK1 lead to familial PD. In brain lacking this mitochondrial integrity surveillance protein, there is significant mitochondrial dysfunction, oxidative damage, and neuronal cell death, which accounts for the motor and cognitive decline seen in PD brain.

The key proteins in the mammalian target of rapamycin (mTOR) cell signaling pathway were analyzed in the PINK1 KO rat brain due to the role the mTOR cell signaling pathway plays in cellular function through autophagy and cellular metabolism. Dysfunctional mTOR signaling in the brain can impact glucose metabolism, energy production, mitochondrial function, cell growth and autophagy.

The male PINK1 KO rat brain presented with a decrease in PI3K phosphorylation (meaning a decrease in PI3K activation) with age. PI3K phosphorylates and thereby activates Akt, therefore, a decrease in Akt phosphorylation was expected in the male PINK1 KO rat brain based on the decrease observed in PI3K phosphorylation levels. However, Akt phosphorylation presented with little change as age increased (only a slight increase at 6 months of age). Conceivably, this is due to the pleiotropic pathways for PI3K signaling. Activated Akt phosphorylates and thereby activates mTORC1 at Ser 2448. The male PINK1 KO rat brain showed little change in phosphorylation levels of mTORC1 at Ser 2448, which was to be

expected based on the low levels of Akt phosphorylation. The male PINK1 KO rat brain presented with a decrease in P70S6K phosphorylation with age at the 64 kDa peak, yet it presented with an increase in P70S6K phosphorylation with age at the 88 kDa peak. If the speculation that phosphorylation of P70S6K at the 88 kDa peak symbolizes increased phosphorylation of P70S6K, then the male PINK1 KO rat brain showed significant increase in P70S6K activation. Phosphorylated P70S6K leads to the phosphorylation of IRS-1 at Ser 307, its inhibitory site. The male PINK1 KO rat brain presented with an increase in phosphorylated IRS-1 at Ser 307 with age which is indicative of increased IRS-1 inhibition (a marker for insulin resistance). Overall, the male PINK1 KO rat brain showed increased markers for insulin resistance with age based on its increase in inhibition of IRS-1 at Ser 307. This could be supportive of the link between PD and T2DM and the increased risk of both of these diseases in males compared to females.

The female PINK1 KO rat brain presented with a decrease in PI3K phosphorylation (meaning a decrease in PI3K activation) with age. However, Akt phosphorylation increased - the opposite of that expected based on the decreased PI3K phosphorylation. mTORC1 phosphorylation (activated mTORC1) was increased in the female PINK1 KO rat brain with age which indicates increased inhibition of autophagy and impairment of neuronal survival. This would be expected based on increased phosphorylation and thereby activation of Akt. The phosphorylation of P70S6K also increased in the female PINK1 KO rat brain with age which aligns with the increase in mTORC1 phosphorylation. However, the phosphorylation level of IRS-1 at Ser 307 decreased in the female PINK1 KO rat brain with age, which indicates the female PINK1 KO rat brain did not present with markers for insulin resistance.

Overall, the male PINK1 KO rat brain presented with no significant change in mTORC1 activation at Ser 2448 with age, consequently the inhibition of autophagy was not denoted in the male. The male PINK1 KO rat did, however, present with increased inhibition of IRS-1 at Ser 307 with age, which is indicative of increased insulin resistance. According to the literature, men are more likely to develop PD and T2DM than women. The data from the male PINK1 KO rat brain did not suggest increased inhibition of autophagy. However, the data did suggest that the male PINK1 KO rat brain is increasingly susceptible to insulin resistance. This could be indicative of the higher incidence of T2DM in men, the association between clinical symptoms of PD and insulin resistance, and the link between T2DM and PD.

The female PINK1 KO rat brain presented with a statistically significant increase in mTORC1 activation with age, suggesting increased inhibition of autophagy and thus neuronal survival impairment. Although men are more likely to develop PD compared to women, women who do develop PD have high mortality rates and faster disease progression compared to men. The increase in inhibition of autophagic function seen in the female PINK1 KO rat brain could elucidate the worst prognosis seen in females with PD compared to males. The female PINK1 KO rat brain presented with a decrease in IRS-1 inhibition at Ser 307, thus not presenting with insulin resistance markers.

The current thesis research presented was aimed at investigating a possible correlation among the mTOR cell signaling pathway, mutations in PINK1, and PD. The original hypothesis expected an increase in mTOR cell signaling pathway phosphorylation with age. This was observed for P70S6K at 88kDa and IRS-1 in the male PINK1 KO rat brain and for Akt, mTORC1 and P70S6K in the female PINK1 KO rat brain. The hypothesis also stated that the phosphorylation of the mTOR cell signaling pathway would occur at a faster rate in the male

PINK1 KO rat brain compared to the female PINK1 KO rat brain. This part of the hypothesis was based on the knowledge that men are more likely to develop PD than women. However, with further investigation it became clear that although men are more likely to develop the disease, women who develop the disease progress much worse. With this in mind, it is conceivable that the female PINK1 KO rat brain experienced higher levels of autophagy inhibition. Based on the knowledge of T2DM and its link to PD, it is also conceivable as to why the male PINK1 KO rat brain increased in IRS-1 inhibition and the female PINK1 KO rat brain did not. The male rats lacking PINK1 presented with increased IRS-1 inhibition (marker for insulin resistance) which aligns with the evidence that men are more likely to develop T2DM and T2DM has shown to increase the risk of developing PD. Furthermore, the consistent decreased expression and increased phosphorylation of the key enzymes in the mTOR cell signaling pathway at 6 months of age could be indicative of the link between PINK1 mutations and psychiatric disorders.

4.2 Future Studies

If this research were extended, the project should include an increased age range beyond 8 months of age. It is important that the analysis of mTOR cell signaling in PINK1 KO rat brain is observed with increasing age, as age is a risk factor for PD. Observing the rodent model past 8 months of age would be relevant to understanding the progression of the disease. As stated previously, a rat brain at 8 months of age correlates to that of a human in their late adolescent to early twenties. The current model was useful in observing the trend as the rat got older, however, a timeline beyond 8 months old would be increasingly indicative of mTOR signaling in human PD brain lacking PINK1 because the model would correlate more so with human age of onset.

Future studies into P70S6K phosphorylation sites could be beneficial in understanding the increased inhibition of IRS-1 at Ser 307, particularly seen in the male PINK1 KO rat brain. Further investigation of this could accept or refute the speculation that the peaks seen at 64 kDa and 88 kDa symbolize increased phosphorylation at multiple sites. This would not only contribute to the investigation into the inhibition of IRS-1 at Ser 307, but also phosphorylation of P70S6K as a result of phosphorylation of mTORC1.

The decreased levels of expression and the increased levels of phosphorylation at 6 months of age in the PINK1 KO rat brain could be appropriate for research on psychiatric disorders, specifically schizophrenia. It is particularly interesting that affective and schizophrenia spectrum disorders were found in 61% of PINK1 mutations carriers in the study in Germany, as mentioned above.

Expansive research on IRS-1 inhibition at Ser 307 and insulin resistance could not only accommodate T2DM research but also the link between T2DM and PD. Reduced glucose tolerance is a potential risk factor for PD and insulin resistance has been linked to the pathology of neurodegeneration. T2DM is associated with an increased risk of PD development and faster symptom progression. The link between PD and T2DM could be of great importance to the understanding of these two chronic diseases.

It is possible that the PINK1 KO rat brain could be a good model for familial PD in females. The unexpected increase in Akt activation in the female could be investigated regarding estrogen levels and the increase in inhibited autophagy could be valuable to the understanding of faster progression and higher mortality rates seen in female PD patients.

Lastly, further research on this project should include a co-immunoprecipitation to investigate whether the phosphorylated proteins of the mTOR pathway are adducted by HNE to

further elucidate the work done by Dr. Ren on biomarkers for oxidative damage in the PINK1 KO rat model and this work done on the mTOR pathway in the PINK1 KO rat model.

APPENDIX

DATA TO SUPPLEMENT FIGURES

Figure 3.2 – Figure 3.11

B-actin Plate					
Sample	Primary	Secondary	Capillary	CHEMI Total Area	B-actin
A5	B-actin	RTU	2	8767429.9	2982523.6
A6	B-actin	RTU	3	9224446.6	3105503.4
A7	B-actin	RTU	4	7153936.4	3111404.9
C1	B-actin	RTU	5	8885097.7	3163847.8
C2	B-actin	RTU	6	5906572.9	2643163.2
C3	B-actin	RTU	7	8103878.6	3848582.3
D1	B-actin	RTU	8	8913506	3553814.7
D7	B-actin	RTU	9	7939934.2	3688641.3
D4	B-actin	RTU	10	8411278.5	3217870.5
E3	B-actin	RTU	11	8878986.9	3392842.1
E5	B-actin	RTU	12	8156999	3588640.6
E7	B-actin	RTU	13	8273215.9	4049769
A2	B-actin	RTU	14	8697773.5	3673525.2
A3	B-actin	RTU	15	6854328.5	3384400.5
A4	B-actin	RTU	16	7956712.5	3605922.1
C10	B-actin	RTU	17	9884896.8	3606932.8
C12	B-actin	RTU	18	10813738	3757463.4
C14	B-actin	RTU	19	8801072	3248877.6
D10	B-actin	RTU	20	8090688.5	4019829.1
D11	B-actin	RTU	21	7557310.9	3245539.9
D12	B-actin	RTU	22	7264085.3	3685760.4
E8	B-actin	RTU	23	8003294.4	3698866.2
E11	B-actin	RTU	24	9381397.8	3963397.8
E13	B-actin	RTU	25	8069768.2	3766117.9

Figure 3.2, 3.7

Male PI3K Plate							
Sample	Primary	Secondary	Capillary	P1 CHEMI Total Area	P2 CHEMI Total Area	pPI3K	PI3K

A5	P-PI3K	RTU	P1:2	129894.3		73790.7	
A5	P-PI3K	RTU	P1:3	134495.1		68879	
A6	P-PI3K	RTU	P1:4	92443.4		51384	
A6	P-PI3K	RTU	P1:5	90626.4		48842.4	
A7	P-PI3K	RTU	P1:6	132880.6		51057.8	
A7	P-PI3K	RTU	P1:7	94235.2		53505.6	
C1	P-PI3K	RTU	P1:8	115490.7		43524.6	
C1	P-PI3K	RTU	P1:9	110615		54682.8	
C2	P-PI3K	RTU	P1:10	106116.4		47356.8	
C2	P-PI3K	RTU	P1:11	123596		46733	
C3	P-PI3K	RTU	P1:12	126878.5		56788.4	
C3	P-PI3K	RTU	P1:13	77328.4		60709.9	
D1	P-PI3K	RTU	P1:14	81187.1		35643.5	
D1	P-PI3K	RTU	P1:15	89020		33453.8	
D7	P-PI3K	RTU	P1:16	122920.4		52588.1	
D7	P-PI3K	RTU	P1:17	78034.2		52087	
D4	P-PI3K	RTU	P1:18	55108.3		29689.6	
D4	P-PI3K	RTU	P1:19	97774.5		31367.4	
E3	P-PI3K	RTU	P1:20	75337.2		31586.3	
E3	P-PI3K	RTU	P1:21	73566.6		28850.7	
E5	P-PI3K	RTU	P1:22	70079		36340	
E5	P-PI3K	RTU	P1:23	45011		23610	

E7	P-PI3K	RTU	P1:24	77081.9		28548	
E7	P-PI3K	RTU	P1:25	92180.7		31538	
A5	PI3K	RTU	P2:2		1474388.7		632910.2
A5	PI3K	RTU	P2:3		1176654.1		577910.6
A6	PI3K	RTU	P2:4		1509286		506558.6
A6	PI3K	RTU	P2:5		981913.9		563224.4
A7	PI3K	RTU	P2:6		1173492.4		501230
A7	PI3K	RTU	P2:7		1427804.3		504553.2
C1	PI3K	RTU	P2:8		1408481.7		490954.7
C1	PI3K	RTU	P2:9		1754174.2		521110.7
C2	PI3K	RTU	P2:10		1661622.2		593057.8
C2	PI3K	RTU	P2:11		1592527.5		606957.6
C3	PI3K	RTU	P2:12		972785.5		559973.3
C3	PI3K	RTU	P2:13		1682224.4		604455.1
D1	PI3K	RTU	P2:14		1023335.2		362847.2
D1	PI3K	RTU	P2:15		1182451		348735.9
D7	PI3K	RTU	P2:16		1214754.7		485842.5
D7	PI3K	RTU	P2:17		982883.9		474473
D4	PI3K	RTU	P2:18		1164215.3		253944.3
D4	PI3K	RTU	P2:19		1040321.8		282849.2
E3	PI3K	RTU	P2:20		1301620.1		355992.6
E3	PI3K	RTU	P2:21		801761.3		379712.8
E5	PI3K	RTU	P2:22		1328202.1		405909.8

E5	PI3K	RTU	P2:23		897325.5		272412.3
E7	PI3K	RTU	P2:24		1066897.5		322062.8
E7	PI3K	RTU	P2:25		1202336.9		281019.6

Male PI3K Plate Calculations							
Sample	pPI3K Normalized	PI3K Normalized		pPI3K/PI3K	Average	StdDev	Std Error
A5	0.024741028			0.11658953	0.10530716	0.01177115	
A5	0.023094201			0.11918625			
A6	0.01654611			0.10143743			
A6	0.015727692			0.08671925			
A7	0.016409886			0.10186501			
A7	0.017196605			0.10604551			0.00679608
C1	0.013756856			0.08865299	0.0920476	0.01192481	
C1	0.017283638			0.10493509			
C2	0.017916714			0.07985191			
C2	0.017680709			0.07699549			
C3	0.014755667			0.10141269			
C3	0.015774614			0.1004374			0.00688479
D1	0.010029645			0.09823281	0.10666551	0.00801878	
D1	0.00941349			0.09592875			
D7	0.014256767			0.10824105			
D7	0.014120918			0.10977864			
D4	0.009226474			0.11691383			
D4	0.009747875			0.11089796			0.00462964
E3	0.009309688			0.08872741	0.09029554	0.01187305	
E3	0.008503402			0.07598032			
E5	0.010126397			0.08952728			
E5	0.006579093			0.0866701			
E7	0.007049291			0.0886411			
E7	0.007787605			0.11222705			0.00685491
A5		0.212206267			0.17895143	0.0208933	0.01206275
A5		0.193765642					
A6		0.163116421					
A6		0.181363318					

A7		0.16109443					
A7		0.162162501					
C1		0.155176459			0.17940867	0.03740835	0.02159772
C1		0.164707891					
C2		0.224374265					
C2		0.22963304					
C3		0.145501189					
C3		0.157059159					
D1		0.102100765			0.10456519	0.02144403	0.01238072
D1		0.098130018					
D7		0.131713132					
D7		0.128630832					
D4		0.07891688					
D4		0.087899498					
E3		0.1049246			0.0924629	0.01966549	0.01135387
E3		0.111915848					
E5		0.113109627					
E5		0.075909608					
E7		0.079526215					
E7		0.069391513					

Male PI3K Plate Standardized to WT				
Sample	Normalized/ Average WT	Average	Std Dev	Std Error
A5	1.10713765	1	0.11177918	0.06453574
A5	1.13179627			
A6	0.96325285			
A6	0.82348866			
A7	0.96731323			
A7	1.00701134			
C1	0.84185143			
C1	0.99646681			
C2	0.75827618			
C2	0.73115153			
C3	0.96301799			
C3	0.9537566			

D1	0.93282173	1.01289887	0.07614655	0.04396323
D1	0.91094233			
D7	1.02786023			
D7	1.04246127			
D4	1.11021723			
D4	1.0530904			
E3	0.84255813	0.85744918	0.11274686	0.06509443
E3	0.72151141			
E5	0.85015375			
E5	0.82302184			
E7	0.84173854			
E7	1.06571143			
A5	1.18583164	1	0.11675404	0.06740798
A5	1.08278342			
A6	0.91151225			
A6	1.01347789			
A7	0.90021315			
A7	0.90618164			
C1	0.86714289	1.00255509	0.20904191	0.1206904
C1	0.92040556			
C2	1.25382773			
C2	1.28321433			
C3	0.81307642			
C3	0.87766362			
D1	0.57055015	0.58432161	0.11983156	0.06918478
D1	0.54836118			
D7	0.73602727			
D7	0.71880304			
D4	0.44099608			
D4	0.49119193			
E3	0.58633005	0.51669272	0.10989287	0.06344668
E3	0.6253979			
E5	0.63206886			
E5	0.42419112			
E7	0.44440111			
E7	0.3877673			

Female PI3K Plate							
Sample	Primary	Secondary	Capillary	P1 CHEMI Total Area	P2 CHEMI Total Area	pPI3K	PI3K
A2	pPI3K	RTU	P1:2	105703.8		81850. 5	
A2	pPI3K	RTU	P1:3	153504.4		81519. 9	
A3	pPI3K	RTU	P1:4	61010.8		61010. 8	
A3	pPI3K	RTU	P1:5	155439.1		72453. 2	
A4	pPI3K	RTU	P1:6	66040.1		57735. 7	
A4	pPI3K	RTU	P1:7	152543.7		74851. 5	
C10	pPI3K	RTU	P1:8	157788		67432. 9	
C10	pPI3K	RTU	P1:9	94223.2		72284. 1	
C14	pPI3K	RTU	P1:10	83787		72464. 4	
C14	pPI3K	RTU	P1:11	96323.5		65717. 4	
C12	pPI3K	RTU	P1:12	105666.1		69289. 8	
C12	pPI3K	RTU	P1:13	124774.2		72963. 1	
D10	pPI3K	RTU	P1:14	109320.6		66787. 9	
D10	pPI3K	RTU	P1:15	85318.5		53856. 3	
D11	pPI3K	RTU	P1:16	66643.8		58650. 8	
D11	pPI3K	RTU	P1:17	182259.5		59301. 4	
D12	pPI3K	RTU	P1:18	102895.8		49891. 9	
D12	pPI3K	RTU	P1:19	140597.5		50446. 6	
E8	pPI3K	RTU	P1:20	92796.4		48252. 5	
E8	pPI3K	RTU	P1:21	80872.9		53675. 2	

E11	pPI3K	RTU	P1:22	143670.5		56047.5	
E11	pPI3K	RTU	P1:23	116251		49383.1	
E13	pPI3K	RTU	P1:24	133312.5		63074	
E13	pPI3K	RTU	P1:25	139734.1		61030.2	
A2	PI3K	RTU	P2:2		1084944.3		578728.8
A2	PI3K	RTU	P2:3		1264111.7		654473.1
A3	PI3K	RTU	P2:4		1229714.4		581792.4
A3	PI3K	RTU	P2:5		1409546.1		552978.3
A4	PI3K	RTU	P2:6		1334455.3		515257.4
A4	PI3K	RTU	P2:7		1562388.5		619328.1
C10	PI3K	RTU	P2:8		1400560.2		579953.5
C10	PI3K	RTU	P2:9		1552213.4		578402.3
C14	PI3K	RTU	P2:10		1456656		600361.9
C14	PI3K	RTU	P2:11		1453954.2		597756.4
C12	PI3K	RTU	P2:12		1388072.7		534505.4
C12	PI3K	RTU	P2:13		1339294.1		600146.4
D10	PI3K	RTU	P2:14		1328211.1		495599.2
D10	PI3K	RTU	P2:15		995059.2		472878.9
D11	PI3K	RTU	P2:16		1389324.3		507130.6
D11	PI3K	RTU	P2:17		1356689		478133.2
D12	PI3K	RTU	P2:18		1160380.4		544358.5
D12	PI3K	RTU	P2:19		1678747		528300
E8	PI3K	RTU	P2:20		1541039.8		560714.1

E8	PI3K	RTU	P2:21		1231566.5		500842.2
E11	PI3K	RTU	P2:22		1115266.2		553712
E11	PI3K	RTU	P2:23		1089516.6		483778.6
E13	PI3K	RTU	P2:24		1820459.7		512140.5
E13	PI3K	RTU	P2:25		1807462.9		448355.7

Female PI3K Calculations						
Sample	pPI3K Normalized	PI3K Normalized	pPI3K/PI3K	Average	StdDev	Std Error
A2	0.022281186		0.14143153	0.12246525	0.01310005	0.00756332
A2	0.022191191		0.12455806			
A3	0.018027063		0.10486696			
A3	0.021407986		0.13102359			
A4	0.016011355		0.11205215			
A4	0.020757936		0.1208592			
C10	0.018695358		0.11627294	0.12051587	0.00684097	0.00394964
C10	0.020040323		0.12497201			
C14	0.022304441		0.1207012			
C14	0.020227724		0.1099401			
C12	0.018440579		0.12963349			
C12	0.01941818		0.1215755			
D10	0.016614612		0.13476192	0.11257876	0.01651846	0.00953694
D10	0.013397659		0.11389026			
D11	0.0180712		0.11565226			
D11	0.01827166		0.12402694			

D12	0.013536393		0.0916526 5			
D12	0.013686891		0.0954885 5			
E8	0.013045214		0.0860554 4	0.1093003 8	0.0177404 5	0.0102424 5
E8	0.014511258		0.1071698 8			
E11	0.014141275		0.1012213 9			
E11	0.012459789		0.1020778 9			
E13	0.01674775		0.1231576 1			
E13	0.016205069		0.1361200 5			
A2		0.15754044 6		0.1642732 2	0.0127300 5	0.0073497
A2		0.17815941 5				
A3		0.17190412 3				
A3		0.16339032 6				
A4		0.14289199 4				
A4		0.17175304 5				
C10		0.16078855 1		0.1653165	0.0163478 7	0.0094384 5
C10		0.16035849 1				
C14		0.18479055 7				
C14		0.18398858 7				
C12		0.14225165 8				
C12		0.15972115 7				
D10		0.12328862 4		0.1392546	0.0152587 8	0.0088096 6
D10		0.11763656 8				

D11		0.15625461 9				
D11		0.14732008 1				
D12		0.14769231 9				
D12		0.14333541 6				
E8		0.15159080 4		0.1339665 3	0.0119494 2	0.006899
E8		0.13540424 9				
E11		0.13970639				
E11		0.12206158 1				
E13		0.13598631 6				
E13		0.11904983 1				

Female PI3K Standardized to WT				
Sample	Normalized/ Average WT	Average	Std Dev	Std Error
A2	1.15487073	1	0.10696953	0.06175889
A2	1.01708903			
A3	0.85629973			
A3	1.06988381			
A4	0.914971			
A4	0.9868857			
C10	0.94943622	0.98408223	0.05586054	0.0322511
C10	1.0204692			
C14	0.9855955			
C14	0.8977249			
C12	1.05853286			
C12	0.99273471			
D10	1.10040948	0.9192711	0.13488282	0.07787463
D10	0.92998022			
D11	0.94436799			
D11	1.01275216			

D12	0.74839722			
D12	0.77971955			
E8	0.70269275	0.89250118	0.1448611	0.0836356
E8	0.87510444			
E11	0.82653156			
E11	0.83352538			
E13	1.00565354			
E13	1.11149939			
A2	0.95901475	1	0.07749318	0.04474071
A2	1.08453106			
A3	1.04645248			
A3	0.99462542			
A4	0.86984348			
A4	1.0455328			
C10	0.97878733	1.00635085	0.09951635	0.05745579
C10	0.97616937			
C14	1.1248976			
C14	1.12001568			
C12	0.86594549			
C12	0.97228965			
D10	0.75050955	0.84770117	0.09288662	0.05362811
D10	0.71610312			
D11	0.95118738			
D11	0.8967991			
D12	0.89906507			
D12	0.87254278			
E8	0.92279678	0.81551043	0.07274114	0.04199711
E8	0.82426244			
E11	0.85045138			
E11	0.74304002			
E13	0.82780573			
E13	0.72470624			

Figure 3.3, Figure 3.8

Male Akt Plate							
Sample	Primary	Secondary	Capillary	P1 CHEMI Total Area	P2 CHEMI Total Area	pAkt	Akt

A5	P-AKT	RTU	P1:2	30913.8		8896.1	
A5	P-AKT	RTU	P1:3	20685.8		7808.7	
A6	P-AKT	RTU	P1:4	35022.4		31370.5	
A6	P-AKT	RTU	P1:5	50102.4		32766	
A7	P-AKT	RTU	P1:6	19168		15929.4	
A7	P-AKT	RTU	P1:7	24532.4		18347	
C1	P-AKT	RTU	P1:8	19816.4		17636.4	
C1	P-AKT	RTU	P1:9	13977.6		11379.4	
C2	P-AKT	RTU	P1:10	7864		7864	
C2	P-AKT	RTU	P1:11	6091		5981.7	
C3	P-AKT	RTU	P1:12	29576.9		29400.9	
C3	P-AKT	RTU	P1:13	36052.4		33872.2	
D1	P-AKT	RTU	P1:14	30339.4		29304.3	
D1	P-AKT	RTU	P1:15	34585.8		28229.1	
D7	P-AKT	RTU	P1:16	20403.1		18961.4	
D7	P-AKT	RTU	P1:17	20139.7		17935.6	
D4	P-AKT	RTU	P1:18	25803.7		25370.6	
D4	P-AKT	RTU	P1:19	25504.3		25504.3	
E3	P-AKT	RTU	P1:20	21993.6		17276.7	
E3	P-AKT	RTU	P1:21	17168.1		16359.8	
E5	P-AKT	RTU	P1:22	33129.1		32654.7	
E5	P-AKT	RTU	P1:23	35339.4		34154.2	
E7	P-AKT	RTU	P1:24	22346.3		15707.6	
E7	P-AKT	RTU	P1:25	16143.1		13469.8	

A5	AKT	RTU	P2:2		1912122. 1		1801140. 7
A5	AKT	RTU	P2:3		1819717. 9		1562108. 7
A6	AKT	RTU	P2:4		1829749		1811480. 6
A6	AKT	RTU	P2:5		1738198. 3		1591743. 1
A7	AKT	RTU	P2:6		1456652. 1		1428978. 2
A7	AKT	RTU	P2:7		1536719. 2		1511072. 6
C1	AKT	RTU	P2:8		1449180. 5		1416426. 5
C1	AKT	RTU	P2:9		1502264. 7		1484689. 2
C2	AKT	RTU	P2:10		988983.3		987560.1
C2	AKT	RTU	P2:11		894197.8		894197.8
C3	AKT	RTU	P2:12		1585226. 8		1562815. 2
C3	AKT	RTU	P2:13		1894016. 5		1880175. 8
D1	AKT	RTU	P2:14		1465948. 1		1352537. 8
D1	AKT	RTU	P2:15		1380305. 6		1270952. 5
D7	AKT	RTU	P2:16		1658231. 5		1634946. 6
D7	AKT	RTU	P2:17		1838269. 3		1609032. 9
D4	AKT	RTU	P2:18		877171.9		877171.9
D4	AKT	RTU	P2:19		1044993. 3		1038181. 5
E3	AKT	RTU	P2:20		1411363. 4		1393878
E3	AKT	RTU	P2:21		1423417. 3		1412170. 9
E5	AKT	RTU	P2:22		1765527. 3		1752357. 9
E5	AKT	RTU	P2:23		1687488. 3		1683512
E7	AKT	RTU	P2:24		1606781		1577517. 3

E7	AKT	RTU	P2:25		1355587. 8		1343740
----	-----	-----	-------	--	---------------	--	---------

Male Akt Plate Calculations						
Sample	pAkt Normalized	Akt Normalized	pAkt/Akt	Average	StdDev	Std Error
A5	0.002982743		0.0049391 5	0.0118549 4	0.0063477 8	
A5	0.002618152		0.0049988 2			
A6	0.010101583		0.0173176			
A6	0.010550946		0.0205849 8			
A7	0.005119681		0.0111474 1			
A7	0.005896693		0.0121417 1			0.0036648 9
C1	0.005574352		0.0124513 3	0.0119327 6	0.0054050 2	
C1	0.003596696		0.0076645			
C2	0.002975223		0.0079630 6			
C2	0.002263084		0.0066894 6			
C3	0.00763941		0.0188127 8			
C3	0.008801215		0.0180154 4			0.0031205 9
D1	0.008245872		0.0216661 6	0.0200185	0.0071710 1	
D1	0.007943324		0.0222109 8			
D7	0.005140484		0.0115975 7			
D7	0.004862387		0.0111468 2			
D4	0.007884282		0.0289231 8			
D4	0.007925832		0.0245663 2			0.0041401 8
E3	0.005092103		0.0123947	0.0138138 4	0.0045026	

E3	0.004821857		0.0115848 6			
E5	0.009099462		0.0186347 2			
E5	0.009517309		0.0202874 7			
E7	0.003878641		0.0099571 6			
E7	0.003326066		0.0100241 1			0.0025995 8
A5		0.603898222		0.5280746 6	0.0558449 2	0.0322420 8
A5		0.523754012				
A6		0.583313031				
A6		0.512555581				
A7		0.459271051				
A7		0.485656046				
C1		0.447691099		0.4205841 5	0.0581506 6	0.0335733
C1		0.469266948				
C2		0.373628121				
C2		0.338305936				
C3		0.406075557				
C3		0.488537247				
D1		0.380587598		0.3688155 1	0.0659341	0.0380670 7
D1		0.357630492				
D7		0.443238165				
D7		0.436212895				
D4		0.27259391				
D4		0.322629982				
E3		0.410829021		0.4176363 8	0.0563028 5	0.0325064 7
E3		0.416220637				
E5		0.488306881				
E5		0.469122486				
E7		0.389532662				
E7		0.33180658				

Male Akt Standardized to WT

Sample	Normalized/ Average WT	Average	Std Dev	Std Error
A5	0.4166319	1	0.53545442	0.30914475
A5	0.42166543			
A6	1.46079159			
A6	1.73640471			
A7	0.94031707			
A7	1.0241893			
C1	1.05030734			
C1	0.64652351			
C2	0.67170793			
C2	0.56427594			
C3	1.58691441			
C3	1.51965657			
D1	1.82760545	1.68862077	0.60489577	0.34923674
D1	1.87356264			
D7	0.97828937			
D7	0.94026764			
D4	2.43975678			
D4	2.07224275			
E3	1.04553008			
E3	0.9772175			
E5	1.57189449			
E5	1.71130889			
E7	0.83991668			
E7	0.84556385			
A5	1.14358493	1	0.10575194	0.06105591
A5	0.99181812			
A6	1.10460334			
A6	0.97061197			
A7	0.86970856			
A7	0.91967308			
C1	0.84777994			
C1	0.88863751			
C2	0.70752898			
C2	0.64064036			
C3	0.76897376			

C3	0.92512913			
D1	0.72070794	0.69841546	0.12485753	0.07208653
D1	0.67723472			
D7	0.83934754			
D7	0.82604399			
D4	0.51620335			
D4	0.61095525			
E3	0.77797527	0.79086616	0.10661912	0.06155658
E3	0.78818521			
E5	0.92469289			
E5	0.88836395			
E7	0.73764695			
E7	0.62833271			

Female Akt Plate							
Sample	Primary	Secondary	Capillary	P1 CHEMI Total Area	P2 CHEMI Total Area	pAkt	Akt
A2	pAkt	RTU	P1:2	17139		12727.6	
A2	pAkt	RTU	P1:3	39059.9		13852.3	
A3	pAkt	RTU	P1:4	25402.9		9007.1	
A3	pAkt	RTU	P1:5	9320.9		7879.6	
A4	pAkt	RTU	P1:6	18413.7		17192.1	
A4	pAkt	RTU	P1:7	28472.5		20318.1	
C10	pAkt	RTU	P1:8	23163.8		16231.2	
C10	pAkt	RTU	P1:9	27511.2		15858.5	
C14	pAkt	RTU	P1:10	18490.7		12585.7	
C14	pAkt	RTU	P1:11	13809.8		12371	
C12	pAkt	RTU	P1:12	22864.2		11908.6	
C12	pAkt	RTU	P1:13	20741		18943.3	
D10	pAkt	RTU	P1:14	32010.6		31402.4	
D10	pAkt	RTU	P1:15	34960		29110.3	
D11	pAkt	RTU	P1:16	31132.2		27665.4	
D11	pAkt	RTU	P1:17	36958.6		33262.9	
D12	pAkt	RTU	P1:18	24376.5		24376.5	
D12	pAkt	RTU	P1:19	19412.7		18518.7	
E8	pAkt	RTU	P1:20	163754.6		21937.9	
E8	pAkt	RTU	P1:21	24698.1		23874.5	

E11	pAkt	RTU	P1:22	37062.8		32920.3	
E11	pAkt	RTU	P1:23	45319.9		35283.7	
E13	pAkt	RTU	P1:24	22145.4		21468.3	
E13	pAkt	RTU	P1:25	22457.5		22457.5	
A2	Akt	RTU	P2:2		3082243.6		3059365.6
A2	Akt	RTU	P2:3		3254501.9		3254501.9
A3	Akt	RTU	P2:4		2756169.8		2756169.8
A3	Akt	RTU	P2:5		2520199.3		2520199.3
A4	Akt	RTU	P2:6		2402311.7		2402311.7
A4	Akt	RTU	P2:7		2651561.9		2651561.9
C10	Akt	RTU	P2:8		3070606.4		3020449.7
C10	Akt	RTU	P2:9		2851737.4		2851737.4
C14	Akt	RTU	P2:10		2875187.1		2875187.1
C14	Akt	RTU	P2:11		2781575.7		2756804.4
C12	Akt	RTU	P2:12		2574956.6		2560362.2
C12	Akt	RTU	P2:13		2680700.6		2669139.5
D10	Akt	RTU	P2:14		2765746.6		2765746.6
D10	Akt	RTU	P2:15		2569541.4		2569541.4
D11	Akt	RTU	P2:16		2018750		2014002
D11	Akt	RTU	P2:17		2097539.5		2062412.7
D12	Akt	RTU	P2:18		1845421		1845421
D12	Akt	RTU	P2:19		1994008.9		1994008.9
E8	Akt	RTU	P2:20		2461194		2461194
E8	Akt	RTU	P2:21		2421618.3		2421618.3
E11	Akt	RTU	P2:22		2729010.3		2729010.3
E11	Akt	RTU	P2:23		2710087.4		2710087.4
E13	Akt	RTU	P2:24		2416959.8		2416959.8
E13	Akt	RTU	P2:25		2302849.1		2302849.1

Female Akt Plate Calculations						
Sample	pAkt Normalized	Akt Normalized	pAkt/Akt	Average	StdDev	Std Error
A2	0.003464683		0.0041602 1	0.0049383 8	0.0019741	0.0011397 5
A2	0.003770847		0.0042563 5			
A3	0.002661358		0.0032679 8			

A3	0.002328211		0.0031265 8			
A4	0.00476774		0.0071564 8			
A4	0.005634648		0.0076626 9			
C10	0.004500001		0.0053737 7	0.0052579 8	0.0010222 8	0.0005902 1
C10	0.004396672		0.005561			
C14	0.003873861		0.0043773 5			
C14	0.003807777		0.0044874 4			
C12	0.003169319		0.0046511 4			
C12	0.005041513		0.0070971 6			
D10	0.007811874		0.0113540 4	0.0125073 4	0.0023749 5	0.0013711 8
D10	0.007241676		0.0113289 9			
D11	0.008524129		0.0137365 3			
D11	0.010248803		0.0161281 5			
D12	0.006613696		0.0132091 8			
D12	0.005024391		0.0092871 7			
E8	0.00593098		0.0089135 2	0.0104148 9	0.0017234 4	0.0009950 3
E8	0.006454545		0.0098589			
E11	0.00830608		0.0120630 9			
E11	0.008902387		0.0130194			
E13	0.005700379		0.0088823 6			
E13	0.005963037		0.0097520 5			
A2		0.832814649		0.7798872 2	0.0792274 6	0.0457419 9
A2		0.885934279				
A3		0.814374599				

A3		0.744651616				
A4		0.666212867				
A4		0.735335325				
C10		0.837401157		0.7922184 7	0.0809952 2	0.0467626 1
C10		0.790626706				
C14		0.884978585				
C14		0.848540554				
C12		0.68140709				
C12		0.710356753				
D10		0.688025916		0.6041567 3	0.0695781 1	0.0401709 4
D10		0.639216578				
D11		0.62054452				
D11		0.63546059				
D12		0.500689356				
D12		0.541003398				
E8		0.665391465		0.6576074 5	0.0286070 2	0.0165162 7
E8		0.654692051				
E11		0.688553216				
E11		0.683778802				
E13		0.641764242				
E13		0.611464952				

Female Akt Standardized to WT				
Sample	Normalized/ Average WT	Average	Std Dev	Std Error
A2	0.8424236	1	0.39974719	0.23079415
A2	0.86189179			
A3	0.66175069			
A3	0.63311801			
A4	1.44915539			
A4	1.55166052			
C10	1.08816413	1.06471637	0.20700725	0.11951569
C10	1.12607667			
C14	0.88639368			

C14	0.90868684			
C12	0.9418347			
C12	1.43714223			
D10	2.29914224	2.53268074	0.48091603	0.277657
D10	2.29406885			
D11	2.78158568			
D11	3.26587773			
D12	2.67479977			
D12	1.88061021			
E8	1.80494757	2.1089676	0.34898931	0.20148907
E8	1.99638354			
E11	2.44272173			
E11	2.63636908			
E13	1.79863738			
E13	1.97474632			
A2	1.06786549	1	0.10158835	0.05865206
A2	1.13597743			
A3	1.04422098			
A3	0.95481961			
A4	0.85424257			
A4	0.94287392			
C10	1.07374648	1.01581158	0.10385504	0.05996074
C10	1.01377056			
C14	1.134752			
C14	1.08802982			
C12	0.87372516			
C12	0.91084548			
D10	0.88221206	0.77467191	0.0892156	0.05150865
D10	0.81962694			
D11	0.79568494			
D11	0.81481087			
D12	0.64200226			
D12	0.6936944			
E8	0.85318934	0.8432084	0.03668097	0.02117777
E8	0.83947016			
E11	0.88288819			
E11	0.87676626			
E13	0.82289365			

E13	0.78404279			
-----	------------	--	--	--

Figure 3.4, 3.9

Male mTOR Plate							
Sample	Primary	Secondary	Capillary	P1 CHEMI Total Area	P2 CHEMI Total Area	pMTOR	mTOR
A5	P- mTOR	RTU	P1:2	286580.3		280573	
A5	P- mTOR	RTU	P1:3	276496.1		271051. 5	
A6	P- mTOR	RTU	P1:4	145051.7		140504. 4	
A6	P- mTOR	RTU	P1:5	142546.2		135114. 1	
A7	P- mTOR	RTU	P1:6	238133.7		234046. 9	
A7	P- mTOR	RTU	P1:7	271565.6		267818. 5	
C1	P- mTOR	RTU	P1:8	119663		102183. 1	
C1	P- mTOR	RTU	P1:9	110521.1		102638. 7	
C2	P- mTOR	RTU	P1:10	236143.6		230672. 5	
C2	P- mTOR	RTU	P1:11	269311.8		267329. 3	
C3	P- mTOR	RTU	P1:12	144429.3		140315. 5	
C3	P- mTOR	RTU	P1:13	133921.7		133178. 8	
D1	P- mTOR	RTU	P1:14	87461.4		85077	
D1	P- mTOR	RTU	P1:15	86893.7		84672.5	
D7	P- mTOR	RTU	P1:16	113991.2		109277. 8	
D7	P- mTOR	RTU	P1:17	107901.8		103953. 5	
D4	P- mTOR	RTU	P1:18	23365.8		22622.4	
D4	P- mTOR	RTU	P1:19	26427.4		25391.9	

E3	P-mTOR	RTU	P1:20	118541.6		112701.4	
E3	P-mTOR	RTU	P1:21	113015.6		111260.9	
E5	P-mTOR	RTU	P1:22	63897.9		60916	
E5	P-mTOR	RTU	P1:23	67896.2		62187.9	
E7	P-mTOR	RTU	P1:24	25593.7		19220.2	
E7	P-mTOR	RTU	P1:25	19455.5		17663.2	
A5	mTOR	RTU	P2:2		2928829.7		1602394.5
A5	mTOR	RTU	P2:3		2965357.3		1596804.3
A6	mTOR	RTU	P2:4		2576354.3		1283061.8
A6	mTOR	RTU	P2:5		2474132.4		1275449.8
A7	mTOR	RTU	P2:6		1900360.3		1217546.3
A7	mTOR	RTU	P2:7		2135271		1268677.4
C1	mTOR	RTU	P2:8		1997145.3		881284.5
C1	mTOR	RTU	P2:9		1909656.9		857599.9
C2	mTOR	RTU	P2:10		3932645.5		2008477.4
C2	mTOR	RTU	P2:11		4080914		2051614.2
C3	mTOR	RTU	P2:12		2272527.8		1014496.7
C3	mTOR	RTU	P2:13		2524104.2		1034855.4
D1	mTOR	RTU	P2:14		1886190.3		501361.9
D1	mTOR	RTU	P2:15		1868245.5		490530.5
D7	mTOR	RTU	P2:16		2816645		986157.3
D7	mTOR	RTU	P2:17		2769097.9		934893.4
D4	mTOR	RTU	P2:18		518989		161732.4
D4	mTOR	RTU	P2:19		523055.4		154795.3
E3	mTOR	RTU	P2:20		1847945.4		584874.8
E3	mTOR	RTU	P2:21		1949528.6		584317.7

E5	mTOR	RTU	P2:22		1965526.5		357673.9
E5	mTOR	RTU	P2:23		1955942.3		342830.5
E7	mTOR	RTU	P2:24		1673128.2		273418.1
E7	mTOR	RTU	P2:25		1113721.4		274912.9

Male mTOR Plate Calculations						
Sample	pMTOR Normalized	MTOR Normalized	pMTOR/MTOR	Average	StdDev	Std Error
A5	0.09407235		0.17509608 3	0.1606021 3	0.0434586	
A5	0.09087992		0.16974622 4			
A6	0.04524368		0.10950711 8			
A6	0.04350795		0.10593447 1			
A7	0.07522226		0.19222833 7			
A7	0.08607639		0.21110055 2			0.0250908 3
C1	0.0322971		0.11594791 5	0.1246307	0.0092883	
C1	0.0324411		0.11968133 4			
C2	0.08727138		0.11484943 8			
C2	0.10113991		0.13030193 5			
C3	0.03645901		0.13831045 5			
C3	0.03460464		0.12869314 9			0.0053626
D1	0.02393963		0.16969179 3	0.1447035 7	0.0285379 1	
D1	0.02382581		0.17261413 9			
D7	0.02962549		0.11081173 4			
D7	0.02818206		0.11119289 1			
D4	0.00703024		0.13987549 8			

D4	0.0078909		0.16403534 2			0.0164763 7
E3	0.0332174		0.19269320 5	0.1448930 1	0.0606684 7	
E3	0.03279283		0.19041165 4			
E5	0.01697467		0.17031156			
E5	0.0173291		0.18139547 1			
E7	0.004746		0.07029600 5			
E7	0.00436153		0.06425016 8			0.0350269 6
A5		0.5372613		0.4492633 1	0.0678708 5	0.0391852 5
A5		0.53538698				
A6		0.41315743				
A6		0.4107063				
A7		0.39131721				
A7		0.40775066				
C1		0.27854832		0.4363631 6	0.2570097 4	0.1483846 4
C1		0.27106231				
C2		0.75987642				
C2		0.77619657				
C3		0.2636027				
C3		0.26889263				
D1		0.14107711		0.1497122 8	0.0948959 8	0.0547882 2
D1		0.13802928				
D7		0.26734974				
D7		0.25345197				
D4		0.05026069				
D4		0.04810489				
E3		0.17238492		0.1125340 4	0.0482071 3	0.0278324
E3		0.17222072				
E5		0.09966835				
E5		0.09553214				
E7		0.06751449				
E7		0.0678836				

Male mTOR Standardized to WT				
Sample	Normalized/ Average WT	Average	Std Dev	Std Error
A5	1.09024757	1	0.27059791	0.15622978
A5	1.05693631			
A6	0.68185346			
A6	0.65960813			
A7	1.1969227			
A7	1.31443183			
C1	0.72195751			
C1	0.7452039			
C2	0.71511777			
C2	0.81133379			
C3	0.86119938			
C3	0.80131657			
D1	1.0565974	0.90100652	0.17769321	0.10259122
D1	1.07479358			
D7	0.68997673			
D7	0.69235004			
D4	0.87094422			
D4	1.02137712			
E3	1.19981724			
E3	1.18561101			
E5	1.06045642			
E5	1.12947113			
E7	0.43770281			
E7	0.400058			
A5	1.19587174	1	0.15107142	0.08722113
A5	1.19169975			
A6	0.91963314			
A6	0.91417724			
A7	0.87101974			
A7	0.90759839			
C1	0.62001128			
C1	0.60334843			

C2	1.69138321			
C2	1.72770966			
C3	0.58674434			
C3	0.59851899			
D1	0.31401876	0.3332395	0.21122575	0.12195124
D1	0.30723471			
D7	0.59508474			
D7	0.56415016			
D4	0.11187357			
D4	0.10707504			
E3	0.38370575	0.2504857	0.10730263	0.0619512
E3	0.38334026			
E5	0.22184841			
E5	0.21264175			
E7	0.15027822			
E7	0.15109981			

Female mTOR Plate							
Sample	Primary	Secondary	Capillary	P1 CHEMI Total Area	P2 CHEMI Total Area	pmTOR	mTOR
A2	pmTOR	RTU	P1:2	69491.1		22704.7	
A2	pmTOR	RTU	P1:3	45758.6		28234.5	
A3	pmTOR	RTU	P1:4	28277.6		24238.8	
A3	pmTOR	RTU	P1:5	30600.2		24297.1	
A4	pmTOR	RTU	P1:6	67294.7		62451.5	
A4	pmTOR	RTU	P1:7	63922.6		62779.4	
C10	pmTOR	RTU	P1:8	43279.9		41693.2	
C10	pmTOR	RTU	P1:9	45253.5		41029.1	
C14	pmTOR	RTU	P1:10	39124		37953.7	
C14	pmTOR	RTU	P1:11	40852.8		39704.8	

C12	pmTOR	RTU	P1:12	37864		37701.9	
C12	pmTOR	RTU	P1:13	39642.8		33558.7	
D10	pmTOR	RTU	P1:14	65660.2		62730	
D10	pmTOR	RTU	P1:15	69002		63781	
D11	pmTOR	RTU	P1:16	26975.7		25923.8	
D11	pmTOR	RTU	P1:17	26812.9		24356	
D12	pmTOR	RTU	P1:18	35704.8		32316.1	
D12	pmTOR	RTU	P1:19	30928.9		30028.5	
E8	pmTOR	RTU	P1:20	33183.6		32468.1	
E8	pmTOR	RTU	P1:21	34811.1		28197.3	
E11	pmTOR	RTU	P1:22	34120.9		30701.5	
E11	pmTOR	RTU	P1:23	38382.7		33611.8	
E13	pmTOR	RTU	P1:24	44071.4		37477.5	
E13	pmTOR	RTU	P1:25	46380.8		40575.2	
A2	mTOR	RTU	P2:2		3235243.8		1362883.5
A2	mTOR	RTU	P2:3		3090902.4		1329482.2
A3	mTOR	RTU	P2:4		1776561.5		734741.7
A3	mTOR	RTU	P2:5		1717600.1		806386
A4	mTOR	RTU	P2:6		2765279.1		1320940.8
A4	mTOR	RTU	P2:7		2408105.5		1320272.5
C10	mTOR	RTU	P2:8		2942323.7		1284646.3
C10	mTOR	RTU	P2:9		3110823.5		1386268.7
C14	mTOR	RTU	P2:10		1879671.9		748152.9
C14	mTOR	RTU	P2:11		1445954.2		770248.7
C12	mTOR	RTU	P2:12		1460452.1		844601.7
C12	mTOR	RTU	P2:13		1630768.1		864917.8

D10	mTOR	RTU	P2:14		2082192.6		728311.9
D10	mTOR	RTU	P2:15		1778228.4		786953.4
D11	mTOR	RTU	P2:16		1208690.7		243030.8
D11	mTOR	RTU	P2:17		1208280		227902.5
D12	mTOR	RTU	P2:18		1117558.7		243092.1
D12	mTOR	RTU	P2:19		1262899		303567.5
E8	mTOR	RTU	P2:20		1384729.3		471904.2
E8	mTOR	RTU	P2:21		1326811.3		397483.1
E11	mTOR	RTU	P2:22		2009752.6		574287.6
E11	mTOR	RTU	P2:23		1763115.4		540410.6
E13	mTOR	RTU	P2:24		1552775.7		395854.7
E13	mTOR	RTU	P2:25		1428371.2		390178.8

Female mTOR Plate Calculations						
Sample	pMTOR Normalized	MTOR Normalized	pMTOR/MTOR	Average	StdDev	Std Error
A2	0.00618063		0.01665931	0.03264089	0.01287179	0.00743153
A2	0.00768594		0.02123722			
A3	0.00716192		0.03298955			
A3	0.00717914		0.03013086			
A4	0.01731915		0.04727805			
A4	0.01741008		0.04755034			
C10	0.01155918		0.032455	0.04129471	0.00923624	0.00533255
C10	0.01137507		0.02959679			
C14	0.0116821		0.05072987			
C14	0.01222108		0.05154803			
C12	0.01003387		0.04463867			
C12	0.00893121		0.03879987			
D10	0.01560514		0.08613068	0.10209568	0.01845491	0.01065495
D10	0.01586659		0.081048			
D11	0.00798752		0.10666878			
D11	0.00750445		0.10687026			
D12	0.00876782		0.13293768			
D12	0.00814717		0.09891869			

E8	0.00877785		0.06880231	0.0756775 1	0.0195326 8	0.0112772
E8	0.00762323		0.07093962			
E11	0.00774626		0.05346015			
E11	0.00848055		0.06219678			
E13	0.00995123		0.09467489			
E13	0.01077375		0.1039913			
A2		0.37100154		0.3201230 3	0.0719750 3	0.0415548
A2		0.3619091				
A3		0.21709656				
A3		0.23826554				
A4		0.36632538				
A4		0.36614005				
C10		0.35616031		0.2771371 8	0.0727758 1	0.0420171 3
C10		0.3843345				
C14		0.23028042				
C14		0.23708148				
C12		0.22477975				
C12		0.23018662				
D10		0.18117982		0.1117276 7	0.0598738 5	0.0345681 8
D10		0.19576787				
D11		0.07488147				
D11		0.07022021				
D12		0.0659544				
D12		0.08236224				
E8		0.12758077		0.1208335 9	0.0178234 3	0.0102903 6
E8		0.10746079				
E11		0.14489779				
E11		0.13635033				
E13		0.10510948				
E13		0.10360239				

Female mTOR Standardized to WT				
Sample	Normalized/	Average	Std Dev	Std Error

	Average WT			
A2	0.5103817	1	0.39434549	0.22767547
A2	0.65063232			
A3	1.0106819			
A3	0.92310164			
A4	1.44843023			
A4	1.4567722			
C10	0.99430522	1.26512208	0.28296543	0.16337017
C10	0.90673971			
C14	1.5541818			
C14	1.57924714			
C12	1.36756931			
C12	1.18868931			
D10	2.63873601	3.12784658	0.56539238	0.32642944
D10	2.48302087			
D11	3.26795003			
D11	3.2741226			
D12	4.07273506			
D12	3.03051492			
E8	2.10785675	2.31848818	0.5984115	0.34549304
E8	2.17333622			
E11	1.63782772			
E11	1.90548693			
E13	2.90049999			
E13	3.18592144			
A2	1.15893424	1	0.22483553	0.12980885
A2	1.13053129			
A3	0.67816601			
A3	0.74429365			
A4	1.14432688			
A4	1.14374793			
C10	1.11257322	0.86572085	0.22733699	0.13125307
C10	1.20058372			
C14	0.71934975			
C14	0.74059488			
C12	0.70216678			
C12	0.71905674			

D10	0.56596933	0.34901478	0.18703387	0.10798406
D10	0.61153949			
D11	0.23391466			
D11	0.21935383			
D12	0.20602828			
D12	0.2572831			
E8	0.39853669	0.37745986	0.05567681	0.03214502
E8	0.33568592			
E11	0.45263159			
E11	0.42593103			
E13	0.3283409			
E13	0.32363303			

Figure 3.5, 3.10

Male P70S6K Plate 64 kDa Peak							
Sample	Primary	Secondary	Capillary	P1 CHEMI Total Area	P2 CHEMI Total Area	pP70S6K	P70S6K
A5	P-P70S6K	RTU	P1:2	119503.5		87129.7	
A5	P-P70S6K	RTU	P1:3	127297.5		95556.2	
A6	P-P70S6K	RTU	P1:4	119347.2		77791.9	
A6	P-P70S6K	RTU	P1:5	75499		33100.5	
A7	P-P70S6K	RTU	P1:6	66585.8		34067.5	
A7	P-P70S6K	RTU	P1:7	77375.5		51226.4	
C1	P-P70S6K	RTU	P1:8	4675.7			

C1	P- P70S6 K	RTU	P1:9	66602.2		34170.1	
C2	P- P70S6 K	RTU	P1:10	64388.7		29543.8	
C2	P- P70S6 K	RTU	P1:11	34356.5		27004.2	
C3	P- P70S6 K	RTU	P1:12	143402.8		67394	
C3	P- P70S6 K	RTU	P1:13	76073.7		51103.7	
D1	P- P70S6 K	RTU	P1:14	52787.9		8910.5	
D1	P- P70S6 K	RTU	P1:15	38482.2		5216.9	
D7	P- P70S6 K	RTU	P1:16	55312.7		10287.5	
D7	P- P70S6 K	RTU	P1:17	24683.1		7016.3	
D4	P- P70S6 K	RTU	P1:18	58716.4		5658.8	
D4	P- P70S6 K	RTU	P1:19	53507.4		4031.6	
E3	P- P70S6 K	RTU	P1:20	52063.8		8239.2	
E3	P- P70S6 K	RTU	P1:21	39077.4		6494.4	
E5	P- P70S6 K	RTU	P1:22	28977.5		3778.1	

E5	P- P70S6 K	RTU	P1:23	31531.7		4959.6	
E7	P- P70S6 K	RTU	P1:24	37645.3		6200.4	
E7	P- P70S6 K	RTU	P1:25	44872		9481.9	
A5	P70S6 K	RTU	P2:2		510545.7		497064. 5
A5	P70S6 K	RTU	P2:3		491524.7		477108. 3
A6	P70S6 K	RTU	P2:4		494205.2		492386. 6
A6	P70S6 K	RTU	P2:5		480219.1		478608
A7	P70S6 K	RTU	P2:6		411096.8		398297. 5
A7	P70S6 K	RTU	P2:7		472324.9		438214. 2
C1	P70S6 K	RTU	P2:8		7124.3		998.7
C1	P70S6 K	RTU	P2:9		248425.8		247535. 1
C2	P70S6 K	RTU	P2:10		388454.5		373816
C2	P70S6 K	RTU	P2:11		326775.2		311408. 5
C3	P70S6 K	RTU	P2:12		420904		418265. 2
C3	P70S6 K	RTU	P2:13		459105		457909. 1
D1	P70S6 K	RTU	P2:14		228795.5		228795. 5
D1	P70S6 K	RTU	P2:15		217702.9		216205. 3
D7	P70S6 K	RTU	P2:16		250191.6		249048. 7
D7	P70S6 K	RTU	P2:17		248476.5		248476. 5
D4	P70S6 K	RTU	P2:18		175988.2		175988. 2

D4	P70S6 K	RTU	P2:19		175272.8		175175. 5
E3	P70S6 K	RTU	P2:20		202864.1		201316. 8
E3	P70S6 K	RTU	P2:21		223104.7		222962. 7
E5	P70S6 K	RTU	P2:22		136373.7		133679. 2
E5	P70S6 K	RTU	P2:23		133520.3		129433. 4
E7	P70S6 K	RTU	P2:24		189091.4		182378. 5
E7	P70S6 K	RTU	P2:25		193244.5		191345. 6

Male P70S6K Calculations 64 kDa Peak						
Sample	pP70 Normalized	P70 Normalized	pP70/P70	Average	StdDev	Std Error
A5	0.029213415		0.1752885 2	0.1341918	0.0519982 6	
A5	0.032038707		0.2002819 9			
A6	0.025049691		0.1579894 7			
A6	0.010658658		0.0691599 4			
A7	0.010949234		0.0855328			
A7	0.016464074		0.1168980 8			0.0300212 1
C1	0		0	0.0960867 5	0.0562894 6	
C1	0.010800172		0.1380414 3			
C2	0.011177441		0.079033			
C2	0.010216622		0.0867163 2			
C3	0.017511383		0.1611274 4			
C3	0.013278578		0.1116022 8			0.0324987 4
D1	0.002507306		0.0389452 6	0.0312980 3	0.0075995 9	

D1	0.001467972		0.0241293 8			
D7	0.002788967		0.0413071 8			
D7	0.001902137		0.0282372 8			
D4	0.001758554		0.0321544 3			
D4	0.001252878		0.0230146 3			0.0043876 3
E3	0.002428407		0.0409265 4	0.0366976 2	0.0080191 8	
E3	0.001914147		0.0291277 4			
E5	0.001052794		0.0282624 4			
E5	0.001382028		0.0383177 8			
E7	0.00153105		0.0339974 3			
E7	0.002341343		0.0495537 9			0.0046298 8
A5		0.166659033		0.1513582 3	0.0143056 6	0.0082593 8
A5		0.159967988				
A6		0.15855291				
A6		0.154116077				
A7		0.128012108				
A7		0.140841264				
C1		0.00031566		0.0942433 3	0.0503606 9	0.0290757 6
C1		0.078238625				
C2		0.141427514				
C2		0.117816599				
C3		0.108680331				
C3		0.118981241				
D1		0.064380256		0.0615378 9	0.0059252 1	0.0034209 2
D1		0.060837528				
D7		0.067517733				
D7		0.067362609				
D4		0.05469089				

D4		0.054438331				
E3		0.059335741		0.04844206	0.01190346	0.00687247
E3		0.065715613				
E5		0.037250651				
E5		0.036067529				
E7		0.045034297				
E7		0.047248522				

Male P70S6K 64 kDa Peak Standardized to WT				
Sample	Normalized/ Average WT	Average	Std Dev	Std Error
A5	1.30625357	1	0.3874921	0.22371867
A5	1.49250542			
A6	1.17734074			
A6	0.51538126			
A7	0.63739214			
A7	0.87112687			
C1				
C1	1.02868754			
C2	0.58895551			
C2	0.64621178			
C3	1.20072491			
C3	0.83166244			
D1	0.29022085	0.23323353	0.05663232	0.03269668
D1	0.17981263			
D7	0.30782195			
D7	0.21042476			
D4	0.23961545			
D4	0.17150552			
E3	0.3049854			
E3	0.21706052			
E5	0.21061225			
E5	0.28554484			
E7	0.25334952			
E7	0.36927585			
A5	1.10109	1	0.09451525	0.0545684

A5	1.05688332			
A6	1.04753412			
A6	1.01822066			
A7	0.84575585			
A7	0.93051606			
C1	0.00208552	0.62265084	0.33272515	0.19209895
C1	0.51691028			
C2	0.93438932			
C2	0.77839573			
C3	0.71803384			
C3	0.78609033			
D1	0.42535022	0.40657116	0.03914693	0.02260149
D1	0.40194397			
D7	0.44607904			
D7	0.44505415			
D4	0.3613341			
D4	0.35966548			
E3	0.3920219	0.32004906	0.07864429	0.0454053
E3	0.43417271			
E5	0.24610919			
E5	0.23829249			
E7	0.29753451			
E7	0.31216355			

Male P70S6K Plate 88 kDa Peak							
Sample	Primary	Secondary	Capillary	P1 CHEMI Total Area	P2 CHEMI Total Area	pP70S6K- 88 kDa	P70S6K
A5	P- P70S6 K	RTU	P1:2	119503.5		13205.3	
A5	P- P70S6 K	RTU	P1:3	127297.5		10099.1	
A6	P- P70S6 K	RTU	P1:4	119347.2			
A6	P- P70S6 K	RTU	P1:5	75499		3770.9	

A7	P- P70S6 K	RTU	P1:6	66585.8		4467.1	
A7	P- P70S6 K	RTU	P1:7	77375.5		10981	
C1	P- P70S6 K	RTU	P1:8	4675.7		2437.8	
C1	P- P70S6 K	RTU	P1:9	66602.2		13779.7	
C2	P- P70S6 K	RTU	P1:10	64388.7		3582.1	
C2	P- P70S6 K	RTU	P1:11	34356.5		2745.1	
C3	P- P70S6 K	RTU	P1:12	143402.8			
C3	P- P70S6 K	RTU	P1:13	76073.7		4921.6	
D1	P- P70S6 K	RTU	P1:14	52787.9		22852.7	
D1	P- P70S6 K	RTU	P1:15	38482.2		27111.8	
D7	P- P70S6 K	RTU	P1:16	55312.7		14716.8	
D7	P- P70S6 K	RTU	P1:17	24683.1		9729.4	
D4	P- P70S6 K	RTU	P1:18	58716.4		41392.4	
D4	P- P70S6 K	RTU	P1:19	53507.4		40632.6	

E3	P- P70S6 K	RTU	P1:20	52063.8		14987.3	
E3	P- P70S6 K	RTU	P1:21	39077.4		17963.2	
E5	P- P70S6 K	RTU	P1:22	28977.5		20734.3	
E5	P- P70S6 K	RTU	P1:23	31531.7		22501.3	
E7	P- P70S6 K	RTU	P1:24	37645.3		19504.4	
E7	P- P70S6 K	RTU	P1:25	44872		20020.4	
A5	P70S6 K	RTU	P2:2		510545.7		497064. 5
A5	P70S6 K	RTU	P2:3		491524.7		477108. 3
A6	P70S6 K	RTU	P2:4		494205.2		492386. 6
A6	P70S6 K	RTU	P2:5		480219.1		478608
A7	P70S6 K	RTU	P2:6		411096.8		398297. 5
A7	P70S6 K	RTU	P2:7		472324.9		438214. 2
C1	P70S6 K	RTU	P2:8		7124.3		998.7
C1	P70S6 K	RTU	P2:9		248425.8		247535. 1
C2	P70S6 K	RTU	P2:10		388454.5		373816
C2	P70S6 K	RTU	P2:11		326775.2		311408. 5
C3	P70S6 K	RTU	P2:12		420904		418265. 2
C3	P70S6 K	RTU	P2:13		459105		457909. 1
D1	P70S6 K	RTU	P2:14		228795.5		228795. 5

D1	P70S6 K	RTU	P2:15		217702.9		216205. 3
D7	P70S6 K	RTU	P2:16		250191.6		249048. 7
D7	P70S6 K	RTU	P2:17		248476.5		248476. 5
D4	P70S6 K	RTU	P2:18		175988.2		175988. 2
D4	P70S6 K	RTU	P2:19		175272.8		175175. 5
E3	P70S6 K	RTU	P2:20		202864.1		201316. 8
E3	P70S6 K	RTU	P2:21		223104.7		222962. 7
E5	P70S6 K	RTU	P2:22		136373.7		133679. 2
E5	P70S6 K	RTU	P2:23		133520.3		129433. 4
E7	P70S6 K	RTU	P2:24		189091.4		182378. 5
E7	P70S6 K	RTU	P2:25		193244.5		191345. 6

Male P70S6K Calculations 88 kDa Peak						
Sample	pP70 Normalized	P70 Normalized	pP70/P70	Average	StdDev	Std Error
A5	0.004427559		0.0265665 7	0.0183773 6	0.0083814 6	
A5	0.003386092		0.0211673 1			
A6	0					
A6	0.001214264		0.0078788 9			
A7	0.001435718		0.0112154 9			
A7	0.003529274		0.0250585 2			0.0048390 4
C1	0.000770517		2.4409732 7	0.4209644 2	0.9897947 4	
C1	0.004355361		0.0556676 6			
C2	0.001355232		0.0095825 2			

C2	0.001038566		0.0088151 1			
C3	0		0			
C3	0.001278809		0.0107479 8			0.5714582 6
D1	0.00643047		0.0998826 5	0.1317804 8	0.0844408 7	
D1	0.007628929		0.1253984 1			
D7	0.003989762		0.0590920 6			
D7	0.002637665		0.0391562 2			
D4	0.01286329		0.2351998 6			
D4	0.012627171		0.2319536 7			0.0487519 6
E3	0.004417329		0.0744463 5	0.1159226 6	0.0401714 4	
E3	0.00529444		0.0805659 4			
E5	0.005777759		0.1551049 1			
E5	0.006270146		0.1738446 2			
E7	0.004816176		0.1069446 2			
E7	0.004943591		0.1046295 3			0.0231929 9
A5		0.166659033		0.1513582 3	0.0143056 6	0.0082593 8
A5		0.159967988				
A6		0.15855291				
A6		0.154116077				
A7		0.128012108				
A7		0.140841264				
C1		0.00031566		0.0942433 3	0.0503606 9	0.0290757 6
C1		0.078238625				
C2		0.141427514				
C2		0.117816599				
C3		0.108680331				

C3		0.118981241				
D1		0.064380256		0.06153789	0.00592521	0.00342092
D1		0.060837528				
D7		0.067517733				
D7		0.067362609				
D4		0.05469089				
D4		0.054438331				
E3		0.059335741		0.04844206	0.01190346	0.00687247
E3		0.065715613				
E5		0.037250651				
E5		0.036067529				
E7		0.045034297				
E7		0.047248522				

Male P70S6K 88 kDa Peak Standardized to WT				
Sample	Normalized/ Average WT	Average	Std Dev	Std Error
A5	1.44561447	1	0.4560752	0.26331514
A5	1.15181482			
A6				
A6	0.42872817			
A7	0.61028832			
A7	1.36355421			
C1	132.825049			
C1	3.02914411			
C2	0.52143092			
C2	0.47967233			
C3				
C3	0.58484934			
D1	5.43509329	7.17080703	4.59483206	2.65282753
D1	6.82352802			
D7	3.21548192			
D7	2.13067741			
D4	12.7983512			
D4	12.6217104			

E3	4.0509823	6.30790733	2.18592063	1.26204186
E3	4.38397888			
E5	8.4400011			
E5	9.45971851			
E7	5.8193693			
E7	5.69339392			
A5	1.10109	1	0.09451525	0.0545684
A5	1.05688332			
A6	1.04753412			
A6	1.01822066			
A7	0.84575585			
A7	0.93051606			
C1	0.00208552	0.62265084	0.33272515	0.19209895
C1	0.51691028			
C2	0.93438932			
C2	0.77839573			
C3	0.71803384			
C3	0.78609033			
D1	0.42535022	0.40657116	0.03914693	0.02260149
D1	0.40194397			
D7	0.44607904			
D7	0.44505415			
D4	0.3613341			
D4	0.35966548			
E3	0.3920219	0.32004906	0.07864429	0.0454053
E3	0.43417271			
E5	0.24610919			
E5	0.23829249			
E7	0.29753451			
E7	0.31216355			

Male P70S6K Calculations 88 kDa Peak – CLEAN OUTLIERS REMOVED						
Sample	pP70 Normalized	P70 Normalized	pP70/P70	Average	StdDev	Std Error
A5	0.00442755 9		0.0265665 7	0.0183773 6	0.0083814 6	
A5	0.00338609 2		0.0211673 1			

A6						
A6	0.00121426 4		0.0078788 9			
A7	0.00143571 8		0.0112154 9			
A7	0.00352927 4		0.0250585 2			0.0048390 4
C1				0.0212033 2	0.0229899 7	
C1	0.00435536 1		0.0556676 6			
C2	0.00135523 2		0.0095825 2			
C2	0.00103856 6		0.0088151 1			
C3						
C3	0.00127880 9		0.0107479 8			0.0132732 6
D1	0.00643047		0.0998826 5	0.1317804 8	0.0844408 7	
D1	0.00762892 9		0.1253984 1			
D7	0.00398976 2		0.0590920 6			
D7	0.00263766 5		0.0391562 2			
D4	0.01286329		0.2351998 6			
D4	0.01262717 1		0.2319536 7			0.0487519 6
E3	0.00441732 9		0.0744463 5	0.1159226 6	0.0401714 4	
E3	0.00529444		0.0805659 4			
E5	0.00577775 9		0.1551049 1			
E5	0.00627014 6		0.1738446 2			
E7	0.00481617 6		0.1069446 2			
E7	0.00494359 1		0.1046295 3			0.0231929 9
A5		0.166659033		0.1513582 3	0.0143056 6	0.0082593 8

A5		0.159967988				
A6		0.15855291				
A6		0.154116077				
A7		0.128012108				
A7		0.140841264				
C1		0.00031566		0.0942433 3	0.0503606 9	0.0290757 6
C1		0.078238625				
C2		0.141427514				
C2		0.117816599				
C3		0.108680331				
C3		0.118981241				
D1		0.064380256		0.0615378 9	0.0059252 1	0.0034209 2
D1		0.060837528				
D7		0.067517733				
D7		0.067362609				
D4		0.05469089				
D4		0.054438331				
E3		0.059335741		0.0484420 6	0.0119034 6	0.0068724 7
E3		0.065715613				
E5		0.037250651				
E5		0.036067529				
E7		0.045034297				
E7		0.047248522				

Male P70S6K 88 kDa Peak Standardized to WT – CLEANED OUTLIERS REMOVED				
Sample	Normalized/ Average WT	Average	Std Dev	Std Error
A5	1.44561447	1	0.4560752	0.26331514
A5	1.15181482			
A6				
A6	0.42872817			
A7	0.61028832			
A7	1.36355421			
C1		1.15377418	1.25099416	0.72226181

C1	3.02914411			
C2	0.52143092			
C2	0.47967233			
C3				
C3	0.58484934			
D1	5.43509329	7.17080703	4.59483206	2.65282753
D1	6.82352802			
D7	3.21548192			
D7	2.13067741			
D4	12.7983512			
D4	12.6217104			
E3	4.0509823	6.30790733	2.18592063	1.26204186
E3	4.38397888			
E5	8.4400011			
E5	9.45971851			
E7	5.8193693			
E7	5.69339392			
A5	1.10109	1	0.09451525	0.0545684
A5	1.05688332			
A6	1.04753412			
A6	1.01822066			
A7	0.84575585			
A7	0.93051606			
C1	0.00208552	0.62265084	0.33272515	0.19209895
C1	0.51691028			
C2	0.93438932			
C2	0.77839573			
C3	0.71803384			
C3	0.78609033			
D1	0.42535022	0.40657116	0.03914693	0.02260149
D1	0.40194397			
D7	0.44607904			
D7	0.44505415			
D4	0.3613341			
D4	0.35966548			
E3	0.3920219	0.32004906	0.07864429	0.0454053
E3	0.43417271			
E5	0.24610919			

E5	0.23829249			
E7	0.29753451			
E7	0.31216355			

Female P70S6K Plate							
Sample	Primary	Secondary	Capillary	P1 CHEMI Total Area	P2 CHEMI Total Area	pP70S6 K	P70S6K
A2	pP70S6 K	RTU	P1:2	29922.6		7135.5	
A2	pP70S6 K	RTU	P1:3	26360.3		10060.6	
A3	pP70S6 K	RTU	P1:4	50897.9		12137.2	
A3	pP70S6 K	RTU	P1:5	22119.7		13138.3	
A4	pP70S6 K	RTU	P1:6	21922.4		6163.9	
A4	pP70S6 K	RTU	P1:7	18220.2		6168.6	
C10	pP70S6 K	RTU	P1:8	23616.6		5595	
C10	pP70S6 K	RTU	P1:9	39983.3		7423.5	
C14	pP70S6 K	RTU	P1:10	26748.3		5583.3	
C14	pP70S6 K	RTU	P1:11	17945.2		7197.9	
C12	pP70S6 K	RTU	P1:12	40083.8		7261.7	
C12	pP70S6 K	RTU	P1:13	36323.6		6588.3	
D10	pP70S6 K	RTU	P1:14	60073.8		53165	
D10	pP70S6 K	RTU	P1:15	69504.6		48051.8	
D11	pP70S6 K	RTU	P1:16	60584.6		40206.5	
D11	pP70S6 K	RTU	P1:17	51861.8		33216.4	
D12	pP70S6 K	RTU	P1:18	22651.2		8153.9	
D12	pP70S6 K	RTU	P1:19	20834.7		6821.1	

E8	pP70S6 K	RTU	P1:20	35960.3		20052.1	
E8	pP70S6 K	RTU	P1:21	31168		19647.1	
E11	pP70S6 K	RTU	P1:22	27442.9		20213.4	
E11	pP70S6 K	RTU	P1:23	21646.6		12158.5	
E13	pP70S6 K	RTU	P1:24	42638		21110.7	
E13	pP70S6 K	RTU	P1:25	47959.3		24875.8	
A2	P70S6K	RTU	P2:2		409267.5		394831. 5
A2	P70S6K	RTU	P2:3		413822.2		393552. 8
A3	P70S6K	RTU	P2:4		305478.5		299896. 7
A3	P70S6K	RTU	P2:5		290839.4		288391. 2
A4	P70S6K	RTU	P2:6		232046.3		219201. 6
A4	P70S6K	RTU	P2:7		252411.5		238359. 7
C10	P70S6K	RTU	P2:8		347023.4		327419. 2
C10	P70S6K	RTU	P2:9		323586.9		313316. 5
C14	P70S6K	RTU	P2:10		272268.4		260782. 5
C14	P70S6K	RTU	P2:11		178206.6		167933. 1
C12	P70S6K	RTU	P2:12		213333.7		210020. 8
C12	P70S6K	RTU	P2:13		219885.6		208614. 3
D10	P70S6K	RTU	P2:14		103621		102518. 3
D10	P70S6K	RTU	P2:15		93372.8		93372.8
D11	P70S6K	RTU	P2:16		138571.7		134788. 2
D11	P70S6K	RTU	P2:17		151999.2		139412. 1
D12	P70S6K	RTU	P2:18		99910.3		99602.3

D12	P70S6K	RTU	P2:19		107643.6		102412.7
E8	P70S6K	RTU	P2:20		131831.4		129509.5
E8	P70S6K	RTU	P2:21		147083.5		146534.7
E11	P70S6K	RTU	P2:22		192166.4		192166.4
E11	P70S6K	RTU	P2:23		188560		184694.8
E13	P70S6K	RTU	P2:24		164754.1		163596.5
E13	P70S6K	RTU	P2:25		147921.5		147921.5

Female P70S6K Calculations						
Sample	pP70 Normalized	P70 Normalized	pP70/P70	Average	StdDev	Std Error
A2	0.001942412		0.01807227	0.03061057	0.01031412	0.00595486
A2	0.002738677		0.02556353			
A3	0.003586219		0.04047127			
A3	0.003882017		0.04555722			
A4	0.001709382		0.02811978			
A4	0.001710686		0.02587937			
C10	0.001551179		0.01708819	0.02853506	0.00955269	0.00551525
C10	0.00205812		0.02369329			
C14	0.001718532		0.0214098			
C14	0.002215504		0.04286171			
C12	0.001932607		0.0345761			
C12	0.00175339		0.03158125			
D10	0.013225687		0.51859034	0.28637275	0.19929978	0.11506578
D10	0.011953692		0.5146231			

D11	0.012388232		0.2982939 2			
D11	0.010234476		0.2382605 2			
D12	0.002212271		0.0818645 8			
D12	0.001850663		0.0666040 4			
E8	0.005421148		0.1548311 1	0.1261894 4	0.0367078 4	0.0211932 8
E8	0.005311655		0.1340781 4			
E11	0.005100018		0.1051869 6			
E11	0.003067696		0.0658302 2			
E13	0.005605427		0.1290412 7			
E13	0.006605157		0.1681689 3			
A2		0.107480275		0.0858879 1	0.0197323 8	0.0113924 9
A2		0.10713219				
A3		0.088611469				
A3		0.085211901				
A4		0.060789333				
A4		0.066102288				
C10		0.090774965		0.0701687 3	0.0176930 2	0.0102150 7
C10		0.086865078				
C14		0.08026849				
C14		0.051689574				
C12		0.055894304				
C12		0.055519982				
D10		0.025503149		0.0313376 8	0.0086009 8	0.0049657 8
D10		0.023228052				
D11		0.041530286				
D11		0.04295498				
D12		0.027023542				
D12		0.027786044				

E8		0.035013297		0.04207179	0.00504325	0.00291172
E8		0.039616113				
E11		0.048485267				
E11		0.046600117				
E13		0.043439028				
E13		0.039276917				

Female P70S6K Standardized to WT				
Sample	Normalized/ Average WT	Average	Std Dev	Std Error
A2	0.59039295	1	0.33694637	0.19453608
A2	0.83512104			
A3	1.32213368			
A3	1.48828368			
A4	0.91862955			
A4	0.8454391			
C10	0.55824456	0.93219608	0.31207157	0.1801746
C10	0.77402323			
C14	0.69942487			
C14	1.40022572			
C12	1.12954762			
C12	1.03171048			
D10	16.9415433	9.35535428	6.51081516	3.75902089
D10	16.8119398			
D11	9.74480031			
D11	7.78360236			
D12	2.67438891			
D12	2.17585098			
E8	5.05809269	4.12241357	1.19918818	0.69235162
E8	4.3801252			
E11	3.43629519			
E11	2.15057147			
E13	4.21557844			
E13	5.49381844			
A2	1.25140169	1	0.22974571	0.13264375
A2	1.24734891			

A3	1.03171063			
A3	0.99212918			
A4	0.70777521			
A4	0.76963438			
C10	1.0569004	0.81698033	0.20600126	0.11893489
C10	1.01137726			
C14	0.93457264			
C14	0.60182597			
C12	0.65078198			
C12	0.64642372			
D10	0.29693526	0.36486713	0.10014196	0.05781699
D10	0.27044612			
D11	0.48354054			
D11	0.50012836			
D12	0.31463732			
D12	0.3235152			
E8	0.4076627	0.48984531	0.05871895	0.0339014
E8	0.46125366			
E11	0.56451795			
E11	0.542569			
E13	0.50576418			
E13	0.45730438			

Figure 3.6, 3.11

Male IRS-1 Plate							
Sample	Primary	Secondary	Capillary	P1 CHEMI Total Area	P2 CHEMI Total Area	pIRS-1	IRS-1
A5	P-IRS1	RTU	P1:2	11776.7		3445. 5	
A5	P-IRS1	RTU	P1:3	15002.6		58.9	
A6	P-IRS1	RTU	P1:4	13678.2		3231. 8	
A6	P-IRS1	RTU	P1:5	15302.4		1575. 7	
A7	P-IRS1	RTU	P1:6	4864.6		502	
A7	P-IRS1	RTU	P1:7	1094.8			

C1	P-IRS1	RTU	P1:8	511			
C1	P-IRS1	RTU	P1:9	5438.3			
C2	P-IRS1	RTU	P1:10	11258.9			
C2	P-IRS1	RTU	P1:11	15716.8		3277.9	
C3	P-IRS1	RTU	P1:12	14741.2			
C3	P-IRS1	RTU	P1:13	6406.2		2477	
D1	P-IRS1	RTU	P1:14	10713		1885.1	
D1	P-IRS1	RTU	P1:15	6827.6		952.6	
D7	P-IRS1	RTU	P1:16	2612.6			
D7	P-IRS1	RTU	P1:17	1708.6			
D4	P-IRS1	RTU	P1:18	556.4			
D4	P-IRS1	RTU	P1:19	1807.7		288.3	
E3	P-IRS1	RTU	P1:20	3691.7			
E3	P-IRS1	RTU	P1:21	17939.6			
E5	P-IRS1	RTU	P1:22	13672.1		1015	
E5	P-IRS1	RTU	P1:23	2517.2			
E7	P-IRS1	RTU	P1:24	28496.8		2472.9	
E7	P-IRS1	RTU	P1:25	9407.2		2159.5	
A5	IRS1	RTU	P2:2		459101.9		452322.4
A5	IRS1	RTU	P2:3		447955.7		435408.9
A6	IRS1	RTU	P2:4		345154.2		330886.5
A6	IRS1	RTU	P2:5		421151.5		411630.2
A7	IRS1	RTU	P2:6		97464.4		94045.8
A7	IRS1	RTU	P2:7		95782.7		93391.6
C1	IRS1	RTU	P2:8		88705.8		74379.6
C1	IRS1	RTU	P2:9		79318.7		64700
C2	IRS1	RTU	P2:10		216996		212046.2
C2	IRS1	RTU	P2:11		261504.1		232638.4
C3	IRS1	RTU	P2:12		234301.2		220294.9

C3	IRS1	RTU	P2:13		261199.8		235372.2
D1	IRS1	RTU	P2:14		143793.2		143793.2
D1	IRS1	RTU	P2:15		148735.3		142471.6
D7	IRS1	RTU	P2:16		69758.3		67892
D7	IRS1	RTU	P2:17		73993.1		73606
D4	IRS1	RTU	P2:18		7370.6		7370.6
D4	IRS1	RTU	P2:19		9434.4		8072.4
E3	IRS1	RTU	P2:20		166548.1		153222.5
E3	IRS1	RTU	P2:21		165133.9		157875
E5	IRS1	RTU	P2:22		118067.5		107277
E5	IRS1	RTU	P2:23		117431		111293.9
E7	IRS1	RTU	P2:24		174403.9		166166.5
E7	IRS1	RTU	P2:25		201033.1		130740.1

Male IRS-1 Plate Calculations						
Sample	pIRS Normalized	IRS Normalized	pIRS/IRS	Average	StdDev	Std Error
A5	0.00115523		0.00761735	0.0053371	0.00367971	
A5	1.97484E-05		0.00013528			
A6	0.001040669		0.0097671			
A6	0.00050739		0.00382795			
A7	0.000161342		0.00533782			
A7	0					0.00212448
C1	0		0	0.00410231	0.00645456	
C1	0		0			
C2	0		0			
C2	0.001240143		0.01409011			

C3	0		0			
C3	0.00064361 4		0.0105237 6			0.0037265 4
D1	0.00053044 4		0.0131098	0.0092517 2	0.0139894	
D1	0.00026805		0.0066862 4			
D7	0		0			
D7	0		0			
D4	0		0			
D4	8.95934E-05		0.0357142 9			0.0080767 8
E3	0		0	0.0068101 8	0.0078173 2	
E3	0		0			
E5	0.00028283 7		0.0094614 9			
E5	0		0			
E7	0.00061062 7		0.0148820 6			
E7	0.00053324		0.0165175			0.0045133 3
A5		0.15165761		0.0994972 4	0.0559468 2	0.0323009 1
A5		0.145986741				
A6		0.106548426				
A6		0.132548623				
A7		0.030226153				
A7		0.030015894				
C1		0.023509222		0.0550995 4	0.0281230 9	0.0162368 7
C1		0.020449783				
C2		0.080224407				
C2		0.088015148				
C3		0.057240532				
C3		0.061158157				
D1		0.040461648		0.0206185	0.0169829 4	0.0098051
D1		0.040089766				
D7		0.018405693				
D7		0.019954773				

D4		0.002290521				
D4		0.002508616				
E3		0.045160516		0.03765218	0.00747987	0.0043185
E3		0.046531785				
E5		0.029893492				
E5		0.03101283				
E7		0.041031106				
E7		0.032283348				

Male IRS-1 Standardized to WT				
Sample	Normalized/ Average WT	Average	Std Dev	Std Error
A5	1.42724595	1	0.68945787	0.39805869
A5	0.02534619			
A6	1.83003791			
A6	0.71723416			
A7	1.0001358			
A7				
C1				
C1				
C2				
C2	2.64003058			
C3				
C3	1.97181197			
D1	2.45635258	3.46694708	2.85682147	1.64938664
D1	1.25278612			
D7				
D7				
D4				
D4	6.69170255			
E3		2.55201337	0.69201285	0.39953381
E3				
E5	1.77277689			
E5				
E7	2.78841713			
E7	3.09484608			

A5	1.52423934	1	0.56229516	0.32464126
A5	1.46724411			
A6	1.07086815			
A6	1.3321839			
A7	0.30378885			
A7	0.30167564			
C1	0.23628014			
C1	0.20553115			
C2	0.8062978			
C2	0.88459888			
C3	0.57529768			
C3	0.61467189			
D1	0.40666101	0.20722688	0.1706875	0.09854648
D1	0.40292339			
D7	0.18498697			
D7	0.20055604			
D4	0.02302095			
D4	0.02521292			
E3	0.45388712			
E3	0.4676691			
E5	0.30044544			
E5	0.31169537			
E7	0.41238436			
E7	0.32446475			

Female IRS1 Plate							
Sample	Primary	Secondary	Capillary	P1 CHEMI Total Area	P2 CHEMI Total Area	pIRS-1	IRS-1
A2	P- IRS1	RTU	P1:2	102597.6		13291. 1	
A2	P- IRS1	RTU	P1:3	52240.6		18050	
A3	P- IRS1	RTU	P1:4	19770.6		7055.3	
A3	P- IRS1	RTU	P1:5	14829.1		6304.9	
A4	P- IRS1	RTU	P1:6	22873.2		10153. 6	

A4	P-IRS1	RTU	P1:7	13755.6		5673.6	
C10	P-IRS1	RTU	P1:8	25478		8725.5	
C10	P-IRS1	RTU	P1:9	19182.4		8933.2	
C14	P-IRS1	RTU	P1:10	13940		6584.8	
C14	P-IRS1	RTU	P1:11	9663.1		6123.3	
C12	P-IRS1	RTU	P1:12	18914.1		7780.6	
C12	P-IRS1	RTU	P1:13	18370.3		7280.1	
D10	P-IRS1	RTU	P1:14	9287.7		3554.6	
D10	P-IRS1	RTU	P1:15	11541		3091.6	
D11	P-IRS1	RTU	P1:16	6366.1		2291.8	
D11	P-IRS1	RTU	P1:17	11345.1		3276.7	
D12	P-IRS1	RTU	P1:18	7303.3			
D12	P-IRS1	RTU	P1:19	6319.6		2431.3	
E8	P-IRS1	RTU	P1:20	41387.7		1019.4	
E8	P-IRS1	RTU	P1:21	4100.6			
E11	P-IRS1	RTU	P1:22	9269.4		1558.5	
E11	P-IRS1	RTU	P1:23	8250.2		1951.7	
E13	P-IRS1	RTU	P1:24	5848.6		3239.2	
E13	P-IRS1	RTU	P1:25	4647.7		3105.3	
A2	IRS1	RTU	P2:2		496511.8		490732.8
A2	IRS1	RTU	P2:3		541333.5		535418.3
A3	IRS1	RTU	P2:4		289179.3		279169.1

A3	IRS1	RTU	P2:5		288021.7		283803.8
A4	IRS1	RTU	P2:6		365911.1		340931.9
A4	IRS1	RTU	P2:7		323085		302826
C10	IRS1	RTU	P2:8		322275.7		317356
C10	IRS1	RTU	P2:9		307639.6		305077.5
C14	IRS1	RTU	P2:10		269143.2		250545.2
C14	IRS1	RTU	P2:11		261719.8		253401.4
C12	IRS1	RTU	P2:12		345834.3		327467.4
C12	IRS1	RTU	P2:13		318147.3		291252.8
D10	IRS1	RTU	P2:14		253730.6		242863.9
D10	IRS1	RTU	P2:15		272916.8		233625.5
D11	IRS1	RTU	P2:16		208405.6		168632.5
D11	IRS1	RTU	P2:17		177591.5		171840.9
D12	IRS1	RTU	P2:18		169373.2		146547.3
D12	IRS1	RTU	P2:19		132508.5		132508.5
E8	IRS1	RTU	P2:20		191264.6		186092.6
E8	IRS1	RTU	P2:21		205476.4		195799.3
E11	IRS1	RTU	P2:22		242061.9		240933.3
E11	IRS1	RTU	P2:23		303812.4		249346.8
E13	IRS1	RTU	P2:24		277629.5		202415
E13	IRS1	RTU	P2:25		204806.7		197376.3

Female IRS1 Calculations							
Sample	pIRS Normalized	IRS Normalized		pIRS/IRS	Average	StdDev	Std Error

A2	0.00361807 8		0.0270841 9	0.0261336 3	0.0053379 5	0.0030818 7
A2	0.00491353 6		0.0337119 6			
A3	0.00208465 3		0.0252725			
A3	0.00186293		0.0222157			
A4	0.00281581 2		0.0297819			
A4	0.00157341 2		0.0187355 1			
C10	0.00241909 1		0.0274943 6	0.0259963 6	0.0021202 8	0.0012241 5
C10	0.00247667 5		0.0292817 4			
C14	0.00202679 2		0.0262818 8			
C14	0.00188474 3		0.0241644 3			
C12	0.00207070 5		0.0237599 2			
C12	0.00193750 4		0.0249958 1			
D10	0.00088426 6		0.0146361 8	0.0157752 6	0.0027384 7	0.0015810 6
D10	0.00076908 7		0.0132331 4			
D11	0.00070613 8		0.0135905			
D11	0.00100960 1		0.0190682 2			
D12						
D12	0.00065964 7		0.0183482 6			
E8	0.00027559 8		0.0054779 2	0.0103018 8	0.0051498 7	0.0029732 8
E8						
E11	0.00039322 3		0.0064686			
E11	0.00049243 1		0.0078272 5			
E13	0.00086009		0.0160027 7			

E13	0.00082453 6		0.0157328 9			
A2		0.133586344		0.1040347 2	0.0282034 1	0.0162832 5
A2		0.145750545				
A3		0.082487017				
A3		0.083856447				
A4		0.094547772				
A4		0.083980184				
C10		0.087985005		0.0820573 8	0.0050792 6	0.0029325 1
C10		0.084580866				
C14		0.077117464				
C14		0.077996598				
C12		0.087151188				
C12		0.077513144				
D10		0.060416474		0.0498586	0.0098895 7	0.0057097 5
D10		0.058118267				
D11		0.051958227				
D11		0.052946784				
D12		0.039760398				
D12		0.035951469				
E8		0.050310714		0.0555170 6	0.0050806 1	0.0029332 9
E8		0.052934951				
E11		0.060789583				
E11		0.062912383				
E13		0.053746326				
E13		0.052408423				

Female IRS-1 Standardized to WT				
Sample	Normalized/ Average WT	Average	Std Dev	Std Error
A2	1.03637318	1	0.2042559	0.1179272
A2	1.289984			
A3	0.96704897			
A3	0.85008103			

A4	1.13960078			
A4	0.71691205			
C10	1.0520683	0.99474744	0.08113232	0.04684177
C10	1.12046219			
C14	1.00567309			
C14	0.92464889			
C12	0.90917052			
C12	0.95646165			
D10	0.56005167	0.60363841	0.10478731	0.06049898
D10	0.50636465			
D11	0.52003882			
D11	0.72964308			
D12				
D12	0.7020938			
E8	0.20961186	0.39420035	0.19705898	0.11377206
E8				
E11	0.24752			
E11	0.2995088			
E13	0.6123439			
E13	0.60201718			
A2	1.28405542	1	0.27109613	0.15651742
A2	1.40097986			
A3	0.79287971			
A3	0.80604291			
A4	0.90880981			
A4	0.80723229			
C10	0.84572734	0.78874994	0.04882274	0.02818782
C10	0.81300616			
C14	0.74126662			
C14	0.74971701			
C12	0.83771254			
C12	0.74506996			
D10	0.58073377	0.47924966	0.0950603	0.05488309
D10	0.558643			
D11	0.49943162			
D11	0.5089338			
D12	0.38218394			
D12	0.34557184			

E8	0.48359543	0.53363977	0.04883567	0.02819529
E8	0.50882005			
E11	0.58432016			
E11	0.60472489			
E13	0.51661913			
E13	0.50375898			

REFERENCES

- Akhtar, A., & Sah, S. P. (2020). Insulin signaling pathway and related molecules: Role in neurodegeneration and Alzheimer's disease. *Neurochem Int*, *135*, 104707. doi:10.1016/j.neuint.2020.104707
- An, W. L., Cowburn, R. F., Li, L., Braak, H., Alafuzoff, I., Iqbal, K., . . . Pei, J. J. (2003). Up-regulation of phosphorylated/activated p70 S6 kinase and its relationship to neurofibrillary pathology in Alzheimer's disease. *Am J Pathol*, *163*(2), 591-607. doi:10.1016/S0002-9440(10)63687-5
- Angelova, P. R., & Abramov, A. Y. (2018). Role of mitochondrial ROS in the brain: from physiology to neurodegeneration. *FEBS Lett*, *592*(5), 692-702. doi:10.1002/1873-3468.12964
- Antico-Arciuch, V. G., Dima, M., Liao, X. H., Refetoff, S., & Di Cristofano, A. (2010). Cross-talk between PI3K and estrogen in the mouse thyroid predisposes to the development of follicular carcinomas with a higher incidence in females. *Oncogene*, *29*(42), 5678-5686. doi:10.1038/onc.2010.308
- Balestrino, R., & Schapira, A. H. V. (2020). Parkinson disease. *Eur J Neurol*, *27*(1), 27-42. doi:10.1111/ene.14108
- Barodia, S. K., Creed, R. B., & Goldberg, M. S. (2017). Parkin and PINK1 functions in oxidative stress and neurodegeneration. *Brain Res Bull*, *133*, 51-59. doi:10.1016/j.brainresbull.2016.12.004
- Bartolome, A., Garcia-Aguilar, A., Asahara, S. I., Kido, Y., Guillen, C., Pajvani, U. B., & Benito, M. (2017). MTORC1 Regulates both General Autophagy and Mitophagy Induction after Oxidative Phosphorylation Uncoupling. *Mol Cell Biol*, *37*(23). doi:10.1128/MCB.00441-17
- Bazinet, R. P., & Laye, S. (2014). Polyunsaturated fatty acids and their metabolites in brain function and disease. *Nat Rev Neurosci*, *15*(12), 771-785. doi:10.1038/nrn3820
- Beal, M. F. (2003). Mitochondria, oxidative damage, and inflammation in Parkinson's disease. *Ann N Y Acad Sci*, *991*, 120-131. doi:10.1111/j.1749-6632.2003.tb07470.x
- Bendor, J. T., Logan, T. P., & Edwards, R. H. (2013). The function of alpha-synuclein. *Neuron*, *79*(6), 1044-1066. doi:10.1016/j.neuron.2013.09.004
- Braak, H., Del Tredici, K., Rub, U., de Vos, R. A., Jansen Steur, E. N., & Braak, E. (2003). Staging of brain pathology related to sporadic Parkinson's disease. *Neurobiol Aging*, *24*(2), 197-211. doi:10.1016/s0197-4580(02)00065-9
- Bretscher, M. S. (1972). Asymmetrical lipid bilayer structure for biological membranes. *Nat New Biol*, *236*(61), 11-12. doi:10.1038/newbio236011a0
- Burman, J. L., Pickles, S., Wang, C., Sekine, S., Vargas, J. N. S., Zhang, Z., . . . Youle, R. J. (2017). Mitochondrial fission facilitates the selective mitophagy of protein aggregates. *J Cell Biol*, *216*(10), 3231-3247. doi:10.1083/jcb.201612106
- Burre, J. (2015). The Synaptic Function of alpha-Synuclein. *J Parkinsons Dis*, *5*(4), 699-713. doi:10.3233/JPD-150642
- Butterfield, D. A., Bader Lange, M. L., & Sultana, R. (2010). Involvements of the lipid peroxidation product, HNE, in the pathogenesis and progression of Alzheimer's disease. *Biochim Biophys Acta*, *1801*(8), 924-929. doi:10.1016/j.bbalip.2010.02.005

- Butterfield, D. A., & Halliwell, B. (2019). Oxidative stress, dysfunctional glucose metabolism and Alzheimer disease. *Nat Rev Neurosci*, 20(3), 148-160. doi:10.1038/s41583-019-0132-6
- Calabrese, V., Lodi, R., Tonon, C., D'Agata, V., Sapienza, M., Scapagnini, G., . . . Butterfield, D. A. (2005). Oxidative stress, mitochondrial dysfunction and cellular stress response in Friedreich's ataxia. *J Neurol Sci*, 233(1-2), 145-162. doi:10.1016/j.jns.2005.03.012
- Castegna, A., Lauderback, C. M., Mohammad-Abdul, H., & Butterfield, D. A. (2004). Modulation of phospholipid asymmetry in synaptosomal membranes by the lipid peroxidation products, 4-hydroxynonenal and acrolein: implications for Alzheimer's disease. *Brain Res*, 1004(1-2), 193-197. doi:10.1016/j.brainres.2004.01.036
- Cerri, S., Mus, L., & Blandini, F. (2019). Parkinson's Disease in Women and Men: What's the Difference? *J Parkinsons Dis*, 9(3), 501-515. doi:10.3233/JPD-191683
- Chadha, R., & Meador-Woodruff, J. H. (2020). Downregulated AKT-mTOR signaling pathway proteins in dorsolateral prefrontal cortex in Schizophrenia. *Neuropsychopharmacology*, 45(6), 1059-1067. doi:10.1038/s41386-020-0614-2
- Chaudhuri, K. R., Healy, D. G., Schapira, A. H., & National Institute for Clinical, E. (2006). Non-motor symptoms of Parkinson's disease: diagnosis and management. *Lancet Neurol*, 5(3), 235-245. doi:10.1016/S1474-4422(06)70373-8
- Chen, H., & Ritz, B. (2018). The Search for Environmental Causes of Parkinson's Disease: Moving Forward. *J Parkinsons Dis*, 8(s1), S9-S17. doi:10.3233/JPD-181493
- Chen, L., Deng, H., Cui, H., Fang, J., Zuo, Z., Deng, J., . . . Zhao, L. (2018). Inflammatory responses and inflammation-associated diseases in organs. *Oncotarget*, 9(6), 7204-7218. doi:10.18632/oncotarget.23208
- Chinta, S. J., & Andersen, J. K. (2005). Dopaminergic neurons. *Int J Biochem Cell Biol*, 37(5), 942-946. doi:10.1016/j.biocel.2004.09.009
- Ciccarone, F., Castelli, S., & Ciriolo, M. R. (2019). Oxidative Stress-Driven Autophagy acROSS Onset and Therapeutic Outcome in Hepatocellular Carcinoma. *Oxid Med Cell Longev*, 2019, 6050123. doi:10.1155/2019/6050123
- Codolo, G., Plotegher, N., Pozzobon, T., Brucale, M., Tessari, I., Bubacco, L., & de Bernard, M. (2013). Triggering of inflammasome by aggregated alpha-synuclein, an inflammatory response in synucleinopathies. *PLoS One*, 8(1), e55375. doi:10.1371/journal.pone.0055375
- Copp, J., Manning, G., & Hunter, T. (2009). TORC-specific phosphorylation of mammalian target of rapamycin (mTOR): phospho-Ser2481 is a marker for intact mTOR signaling complex 2. *Cancer Res*, 69(5), 1821-1827. doi:10.1158/0008-5472.CAN-08-3014
- Dawson, T. M., Ko, H. S., & Dawson, V. L. (2010). Genetic animal models of Parkinson's disease. *Neuron*, 66(5), 646-661. doi:10.1016/j.neuron.2010.04.034
- Edouard, S., Colson, P., Melenotte, C., Di Pinto, F., Thomas, L., La Scola, B., . . . Drancourt, M. (2021). Evaluating the serological status of COVID-19 patients using an indirect immunofluorescent assay, France. *Eur J Clin Microbiol Infect Dis*, 40(2), 361-371. doi:10.1007/s10096-020-04104-2
- Engelman, J. A., Luo, J., & Cantley, L. C. (2006). The evolution of phosphatidylinositol 3-kinases as regulators of growth and metabolism. *Nat Rev Genet*, 7(8), 606-619. doi:10.1038/nrg1879

- Fields, C. R., Bengoa-Vergniory, N., & Wade-Martins, R. (2019). Targeting Alpha-Synuclein as a Therapy for Parkinson's Disease. *Frontiers in Molecular Neuroscience, 12*. doi:10.3389/fnmol.2019.00299
- Frank, M., Duvezin-Caubet, S., Koob, S., Occhipinti, A., Jagasia, R., Petcherski, A., . . . Reichert, A. S. (2012). Mitophagy is triggered by mild oxidative stress in a mitochondrial fission dependent manner. *Biochim Biophys Acta, 1823*(12), 2297-2310. doi:10.1016/j.bbamcr.2012.08.007
- Gabbouj, S., Ryhanen, S., Marttinen, M., Wittrahm, R., Takalo, M., Kemppainen, S., . . . Natunen, T. (2019). Altered Insulin Signaling in Alzheimer's Disease Brain - Special Emphasis on PI3K-Akt Pathway. *Front Neurosci, 13*, 629. doi:10.3389/fnins.2019.00629
- Gilgun-Sherki, Y., Melamed, E., & Offen, D. (2001). Oxidative stress induced-neurodegenerative diseases: the need for antioxidants that penetrate the blood brain barrier. *Neuropharmacology, 40*(8), 959-975. doi:10.1016/s0028-3908(01)00019-3
- Glick, D., Barth, S., & Macleod, K. F. (2010). Autophagy: cellular and molecular mechanisms. *J Pathol, 221*(1), 3-12. doi:10.1002/path.2697
- Gogtay, N., Vyas, N. S., Testa, R., Wood, S. J., & Pantelis, C. (2011). Age of onset of schizophrenia: perspectives from structural neuroimaging studies. *Schizophr Bull, 37*(3), 504-513. doi:10.1093/schbul/sbr030
- Gomez-Benito, M., Granada, N., Garcia-Sanz, P., Michel, A., Dumoulin, M., & Moratalla, R. (2020). Modeling Parkinson's Disease With the Alpha-Synuclein Protein. *Front Pharmacol, 11*, 356. doi:10.3389/fphar.2020.00356
- Gorman, A. M. (2008). Neuronal cell death in neurodegenerative diseases: recurring themes around protein handling. *J Cell Mol Med, 12*(6A), 2263-2280. doi:10.1111/j.1582-4934.2008.00402.x
- Grover, S., Sahoo, S., & Goyal, M. K. (2017). Schizophrenia with Comorbid Idiopathic Parkinson's Disease: A Difficult Clinical Management Scenario. *Indian J Psychol Med, 39*(6), 823-827. doi:10.4103/IJPSYM.IJPSYM_68_17
- Guo, C., Sun, L., Chen, X., & Zhang, D. (2013). Oxidative stress, mitochondrial damage and neurodegenerative diseases. *Neural Regen Res, 8*(21), 2003-2014. doi:10.3969/j.issn.1673-5374.2013.21.009
- Hassan, A., Sharma Kandel, R., Mishra, R., Gautam, J., Alaref, A., & Jahan, N. (2020). Diabetes Mellitus and Parkinson's Disease: Shared Pathophysiological Links and Possible Therapeutic Implications. *Cureus, 12*(8), e9853. doi:10.7759/cureus.9853
- Hemmings, B. A., & Restuccia, D. F. (2012). PI3K-PKB/Akt pathway. *Cold Spring Harb Perspect Biol, 4*(9), a011189. doi:10.1101/cshperspect.a011189
- Hernandez, D. G., Reed, X., & Singleton, A. B. (2016). Genetics in Parkinson disease: Mendelian versus non-Mendelian inheritance. *J Neurochem, 139 Suppl 1*, 59-74. doi:10.1111/jnc.13593
- Hijaz, B. A., & Volpicelli-Daley, L. A. (2020). Initiation and propagation of α -synuclein aggregation in the nervous system. *Molecular Neurodegeneration, 15*(1), 19. doi:10.1186/s13024-020-00368-6
- Hong, C. T., Chen, K. Y., Wang, W., Chiu, J. Y., Wu, D., Chao, T. Y., . . . Bamodu, O. A. (2020). Insulin Resistance Promotes Parkinson's Disease through Aberrant Expression of alpha-Synuclein, Mitochondrial Dysfunction, and Deregulation of the Polo-Like Kinase 2 Signaling. *Cells, 9*(3). doi:10.3390/cells9030740

- Huang, Z., Ren, S., Jiang, Y., & Wang, T. (2016). PINK1 and Parkin cooperatively protect neurons against constitutively active TRP channel-induced retinal degeneration in *Drosophila*. *Cell Death Dis*, 7, e2179. doi:10.1038/cddis.2016.82
- Jiang, P., & Dickson, D. W. (2018). Parkinson's disease: experimental models and reality. *Acta Neuropathol*, 135(1), 13-32. doi:10.1007/s00401-017-1788-5
- Jin, S. M., & Youle, R. J. (2013). The accumulation of misfolded proteins in the mitochondrial matrix is sensed by PINK1 to induce PARK2/Parkin-mediated mitophagy of polarized mitochondria. *Autophagy*, 9(11), 1750-1757. doi:10.4161/auto.26122
- Juan, C. A., Perez de la Lastra, J. M., Plou, F. J., & Perez-Lebena, E. (2021). The Chemistry of Reactive Oxygen Species (ROS) Revisited: Outlining Their Role in Biological Macromolecules (DNA, Lipids and Proteins) and Induced Pathologies. *Int J Mol Sci*, 22(9). doi:10.3390/ijms22094642
- Khan, K. H., Yap, T. A., Yan, L., & Cunningham, D. (2013). Targeting the PI3K-AKT-mTOR signaling network in cancer. *Chin J Cancer*, 32(5), 253-265. doi:10.5732/cjc.013.10057
- Kurutas, E. B. (2016). The importance of antioxidants which play the role in cellular response against oxidative/nitrosative stress: current state. *Nutr J*, 15(1), 71. doi:10.1186/s12937-016-0186-5
- Laidoudi, Y., Sereme, Y., Medkour, H., Watier-Grillot, S., Scandola, P., Ginesta, J., . . . Davoust, B. (2021). SARS-CoV-2 antibodies seroprevalence in dogs from France using ELISA and an automated western blotting assay. *One Health*, 13, 100293. doi:10.1016/j.onehlt.2021.100293
- Lemarie, A., & Grimm, S. (2011). Mitochondrial respiratory chain complexes: apoptosis sensors mutated in cancer? *Oncogene*, 30(38), 3985-4003. doi:10.1038/onc.2011.167
- Liu, J., Wang, X., Lu, Y., Duan, C., Gao, G., Lu, L., & Yang, H. (2017). Pink1 interacts with alpha-synuclein and abrogates alpha-synuclein-induced neurotoxicity by activating autophagy. *Cell Death Dis*, 8(9), e3056. doi:10.1038/cddis.2017.427
- Lizama, B. N., & Chu, C. T. (2021). Neuronal autophagy and mitophagy in Parkinson's disease. *Mol Aspects Med*, 82, 100972. doi:10.1016/j.mam.2021.100972
- MacMahon Copas, A. N., McComish, S. F., Fletcher, J. M., & Caldwell, M. A. (2021). The Pathogenesis of Parkinson's Disease: A Complex Interplay Between Astrocytes, Microglia, and T Lymphocytes? *Front Neurol*, 12, 666737. doi:10.3389/fneur.2021.666737
- Malpartida, A. B., Williamson, M., Narendra, D. P., Wade-Martins, R., & Ryan, B. J. (2021). Mitochondrial Dysfunction and Mitophagy in Parkinson's Disease: From Mechanism to Therapy. *Trends Biochem Sci*, 46(4), 329-343. doi:10.1016/j.tibs.2020.11.007
- Miller, I. N., & Cronin-Golomb, A. (2010). Gender differences in Parkinson's disease: clinical characteristics and cognition. *Mov Disord*, 25(16), 2695-2703. doi:10.1002/mds.23388
- Monzio Compagnoni, G., Di Fonzo, A., Corti, S., Comi, G. P., Bresolin, N., & Masliah, E. (2020). The Role of Mitochondria in Neurodegenerative Diseases: the Lesson from Alzheimer's Disease and Parkinson's Disease. *Mol Neurobiol*, 57(7), 2959-2980. doi:10.1007/s12035-020-01926-1
- Moser, B. A., Dennis, P. B., Pullen, N., Pearson, R. B., Williamson, N. A., Wettenhall, R. E., . . . Thomas, G. (1997). Dual requirement for a newly identified phosphorylation site in p70s6k. *Mol Cell Biol*, 17(9), 5648-5655. doi:10.1128/MCB.17.9.5648

- Nakano, N., Matsuda, S., Ichimura, M., Minami, A., Ogino, M., Murai, T., & Kitagishi, Y. (2017). PI3K/AKT signaling mediated by G protein-coupled receptors is involved in neurodegenerative Parkinson's disease (Review). *Int J Mol Med*, *39*(2), 253-260. doi:10.3892/ijmm.2016.2833
- Nelson, P. T., Soma, L. A., & Lavi, E. (2002). Microglia in diseases of the central nervous system. *Ann Med*, *34*(7-8), 491-500. doi:10.1080/078538902321117698
- Nguyen, U., Squaglia, N., Boge, A., & Fung, P. A. (2011). The Simple Western™: a gel-free, blot-free, hands-free Western blotting reinvention. *Nature Methods*, *8*(11), v-vi. doi:10.1038/nmeth.f.353
- Nicholson, K. M., & Anderson, N. G. (2002). The protein kinase B/Akt signalling pathway in human malignancy. *Cell Signal*, *14*(5), 381-395. doi:10.1016/s0898-6568(01)00271-6
- Nowak, J. Z. (2013). Oxidative stress, polyunsaturated fatty acids-derived oxidation products and bisretinoids as potential inducers of CNS diseases: focus on age-related macular degeneration. *Pharmacol Rep*, *65*(2), 288-304. doi:10.1016/s1734-1140(13)71005-3
- Okatsu, K., Oka, T., Iguchi, M., Imamura, K., Kosako, H., Tani, N., . . . Matsuda, N. (2012). PINK1 autophosphorylation upon membrane potential dissipation is essential for Parkin recruitment to damaged mitochondria. *Nat Commun*, *3*, 1016. doi:10.1038/ncomms2016
- Pajares, M., A, I. R., Manda, G., Bosca, L., & Cuadrado, A. (2020). Inflammation in Parkinson's Disease: Mechanisms and Therapeutic Implications. *Cells*, *9*(7). doi:10.3390/cells9071687
- Pearce, L. R., Alton, G. R., Richter, D. T., Kath, J. C., Lingardo, L., Chapman, J., . . . Alessi, D. R. (2010). Characterization of PF-4708671, a novel and highly specific inhibitor of p70 ribosomal S6 kinase (S6K1). *Biochem J*, *431*(2), 245-255. doi:10.1042/BJ20101024
- Perluigi, M., Di Domenico, F., & Butterfield, D. A. (2015). mTOR signaling in aging and neurodegeneration: At the crossroad between metabolism dysfunction and impairment of autophagy. *Neurobiol Dis*, *84*, 39-49. doi:10.1016/j.nbd.2015.03.014
- Picconi, B., Piccoli, G., & Calabresi, P. (2012). Synaptic dysfunction in Parkinson's disease. *Adv Exp Med Biol*, *970*, 553-572. doi:10.1007/978-3-7091-0932-8_24
- Pizzino, G., Irrera, N., Cucinotta, M., Pallio, G., Mannino, F., Arcoraci, V., . . . Bitto, A. (2017). Oxidative Stress: Harms and Benefits for Human Health. *Oxid Med Cell Longev*, *2017*, 8416763. doi:10.1155/2017/8416763
- Przedborski, S., Vila, M., & Jackson-Lewis, V. (2003). Neurodegeneration: what is it and where are we? *J Clin Invest*, *111*(1), 3-10. doi:10.1172/JCI17522
- Quinn, P. M. J., Moreira, P. I., Ambrosio, A. F., & Alves, C. H. (2020). PINK1/PARKIN signalling in neurodegeneration and neuroinflammation. *Acta Neuropathol Commun*, *8*(1), 189. doi:10.1186/s40478-020-01062-w
- Rapoport, S. I. (2008). Arachidonic acid and the brain. *J Nutr*, *138*(12), 2515-2520. doi:10.1093/jn/138.12.2515
- Reeve, A., Simcox, E., & Turnbull, D. (2014). Ageing and Parkinson's disease: why is advancing age the biggest risk factor? *Ageing Res Rev*, *14*, 19-30. doi:10.1016/j.arr.2014.01.004
- Ren, X. (2019). STUDIES OF OXIDATIVE DAMAGE, BRAIN PROTEOME, AND NEUROCHEMICAL METABOLITES IN COGNITIVE AND NEURODEGENERATIVE DISORDERS: (1) CHEMOTHERAPY-INDUCED COGNITIVE IMPAIRMENT; (2) PARKINSON DISEASE RAT MODEL. *Theses and*

- Dissertations--Chemistry University of Kentucky*. Retrieved from https://uknowledge.uky.edu/chemistry_etds/116
- Ren, X., & Butterfield, D. A. (2021). Fidelity of the PINK1 knockout rat to oxidative stress and other characteristics of Parkinson disease. *Free Radic Biol Med*, *163*, 88-101. doi:10.1016/j.freeradbiomed.2020.12.004
- Ren, X., Hinchie, A., Swomley, A., Powell, D. K., & Butterfield, D. A. (2019). Profiles of brain oxidative damage, ventricular alterations, and neurochemical metabolites in the striatum of PINK1 knockout rats as functions of age and gender: Relevance to Parkinson disease. *Free Radic Biol Med*, *143*, 146-152. doi:10.1016/j.freeradbiomed.2019.08.008
- Rhea, E. M., & Banks, W. A. (2019). Role of the Blood-Brain Barrier in Central Nervous System Insulin Resistance. *Front Neurosci*, *13*, 521. doi:10.3389/fnins.2019.00521
- Sarkar, S. (2013). Regulation of autophagy by mTOR-dependent and mTOR-independent pathways: autophagy dysfunction in neurodegenerative diseases and therapeutic application of autophagy enhancers. *Biochem Soc Trans*, *41*(5), 1103-1130. doi:10.1042/BST20130134
- Sato, H., Arawaka, S., Hara, S., Fukushima, S., Koga, K., Koyama, S., & Kato, T. (2011). Authentically phosphorylated alpha-synuclein at Ser129 accelerates neurodegeneration in a rat model of familial Parkinson's disease. *J Neurosci*, *31*(46), 16884-16894. doi:10.1523/JNEUROSCI.3967-11.2011
- Saxton, R. A., & Sabatini, D. M. (2017). mTOR Signaling in Growth, Metabolism, and Disease. *Cell*, *168*(6), 960-976. doi:10.1016/j.cell.2017.02.004
- Sengupta, P. (2013). The Laboratory Rat: Relating Its Age With Human's. *Int J Prev Med*, *4*(6), 624-630. Retrieved from <https://www.ncbi.nlm.nih.gov/pubmed/23930179>
- Sheppard, P. A. S., Puri, T. A., & Galea, L. A. M. (2021). Sex Differences and Estradiol Effects in MAPK and Akt Cell Signaling across Subregions of the Hippocampus. *Neuroendocrinology*. doi:10.1159/000519072
- Shin, Y. S., Ryall, J. G., Britto, J. M., Lau, C. L., Devenish, R. J., Nagley, P., & Beart, P. M. (2019). Inhibition of bioenergetics provides novel insights into recruitment of PINK1-dependent neuronal mitophagy. *J Neurochem*, *149*(2), 269-283. doi:10.1111/jnc.14667
- Solleiro-Villavicencio, H., & Rivas-Arancibia, S. (2018). Effect of Chronic Oxidative Stress on Neuroinflammatory Response Mediated by CD4(+)T Cells in Neurodegenerative Diseases. *Front Cell Neurosci*, *12*, 114. doi:10.3389/fncel.2018.00114
- Song, J., & Kim, J. (2016). Degeneration of Dopaminergic Neurons Due to Metabolic Alterations and Parkinson's Disease. *Front Aging Neurosci*, *8*, 65. doi:10.3389/fnagi.2016.00065
- Sponagel, J., Yu, K., Ippolito, J., Deneen, B., & Rubin, J. (2018). HGG-10. THE PI3K/mTOR PATHWAY CONTRIBUTES TO SEX DIFFERENCES IN GLIOBLASTOMA. *Neuro-Oncology*, *20*(Suppl 2), i90-i91. doi:10.1093/neuonc/noy059.282
- Steinlechner, S., Stahlberg, J., Volkel, B., Djarmati, A., Hagenah, J., Hiller, A., . . . Lencer, R. (2007). Co-occurrence of affective and schizophrenia spectrum disorders with PINK1 mutations. *J Neurol Neurosurg Psychiatry*, *78*(5), 532-535. doi:10.1136/jnnp.2006.105676
- Sumi, T., & Harada, K. (2020). Mechanism underlying hippocampal long-term potentiation and depression based on competition between endocytosis and exocytosis of AMPA receptors. *Sci Rep*, *10*(1), 14711. doi:10.1038/s41598-020-71528-3

- Switon, K., Kotulska, K., Janusz-Kaminska, A., Zmorzynska, J., & Jaworski, J. (2017). Molecular neurobiology of mTOR. *Neuroscience*, *341*, 112-153. doi:10.1016/j.neuroscience.2016.11.017
- Takei, N., & Nawa, H. (2014). mTOR signaling and its roles in normal and abnormal brain development. *Front Mol Neurosci*, *7*, 28. doi:10.3389/fnmol.2014.00028
- Tanokashira, D., Fukuokaya, W., & Taguchi, A. (2019). Involvement of insulin receptor substrates in cognitive impairment and Alzheimer's disease. *Neural Regen Res*, *14*(8), 1330-1334. doi:10.4103/1673-5374.253535
- Tibar, H., El Bayad, K., Bouhouche, A., Ait Ben Haddou, E. H., Benomar, A., Yahyaoui, M., . . . Regragui, W. (2018). Non-Motor Symptoms of Parkinson's Disease and Their Impact on Quality of Life in a Cohort of Moroccan Patients. *Front Neurol*, *9*, 170. doi:10.3389/fneur.2018.00170
- Triplett, J. C., Zhang, Z., Sultana, R., Cai, J., Klein, J. B., Bueler, H., & Butterfield, D. A. (2015). Quantitative expression proteomics and phosphoproteomics profile of brain from PINK1 knockout mice: insights into mechanisms of familial Parkinson's disease. *J Neurochem*, *133*(5), 750-765. doi:10.1111/jnc.13039
- Unoki, M., & Nakamura, Y. (2001). Growth-suppressive effects of BPOZ and EGR2, two genes involved in the PTEN signaling pathway. *Oncogene*, *20*(33), 4457-4465. doi:10.1038/sj.onc.1204608
- Uttara, B., Singh, A. V., Zamboni, P., & Mahajan, R. T. (2009). Oxidative stress and neurodegenerative diseases: a review of upstream and downstream antioxidant therapeutic options. *Curr Neuropharmacol*, *7*(1), 65-74. doi:10.2174/157015909787602823
- Volpicelli, F., Perrone-Capano, C., Bellenchi, G. C., Colucci-D'Amato, L., & di Porzio, U. (2020). Molecular Regulation in Dopaminergic Neuron Development. Cues to Unveil Molecular Pathogenesis and Pharmacological Targets of Neurodegeneration. *Int J Mol Sci*, *21*(11). doi:10.3390/ijms21113995
- Wang, Y., & Zhang, H. (2019). Regulation of Autophagy by mTOR Signaling Pathway. *Adv Exp Med Biol*, *1206*, 67-83. doi:10.1007/978-981-15-0602-4_3
- Xu, F., Na, L., Li, Y., & Chen, L. (2020). Roles of the PI3K/AKT/mTOR signalling pathways in neurodegenerative diseases and tumours. *Cell Biosci*, *10*(1), 54. doi:10.1186/s13578-020-00416-0
- Xu, W., Ocak, U., Gao, L., Tu, S., Lenahan, C. J., Zhang, J., & Shao, A. (2021). Selective autophagy as a therapeutic target for neurological diseases. *Cell Mol Life Sci*, *78*(4), 1369-1392. doi:10.1007/s00018-020-03667-9
- Yang, J., Nie, J., Ma, X., Wei, Y., Peng, Y., & Wei, X. (2019). Targeting PI3K in cancer: mechanisms and advances in clinical trials. *Mol Cancer*, *18*(1), 26. doi:10.1186/s12943-019-0954-x
- Yang, L., Wang, H., Liu, L., & Xie, A. (2018). The Role of Insulin/IGF-1/PI3K/Akt/GSK3beta Signaling in Parkinson's Disease Dementia. *Front Neurosci*, *12*, 73. doi:10.3389/fnins.2018.00073
- Yoneyama, Y., Inamitsu, T., Chida, K., Iemura, S. I., Natsume, T., Maeda, T., . . . Takahashi, S. I. (2018). Serine Phosphorylation by mTORC1 Promotes IRS-1 Degradation through SCFbeta-TRCP E3 Ubiquitin Ligase. *iScience*, *5*, 1-18. doi:10.1016/j.isci.2018.06.006

- Zarogoulidis, P., Lampaki, S., Turner, J. F., Huang, H., Kakolyris, S., Syrigos, K., & Zarogoulidis, K. (2014). mTOR pathway: A current, up-to-date mini-review (Review). *Oncol Lett*, 8(6), 2367-2370. doi:10.3892/ol.2014.2608
- Zhao, Y., Qian, Y., Sun, Z., Shen, X., Cai, Y., Li, L., & Wang, Z. (2021). Role of PI3K in the Progression and Regression of Atherosclerosis. *Front Pharmacol*, 12, 632378. doi:10.3389/fphar.2021.632378
- Zhu, Z., Yang, C., Iyaswamy, A., Krishnamoorthi, S., Sreenivasmurthy, S. G., Liu, J., . . . Li, M. (2019). Balancing mTOR Signaling and Autophagy in the Treatment of Parkinson's Disease. *Int J Mol Sci*, 20(3). doi:10.3390/ijms20030728
- Zou, Z., Tao, T., Li, H., & Zhu, X. (2020). mTOR signaling pathway and mTOR inhibitors in cancer: progress and challenges. *Cell Biosci*, 10, 31. doi:10.1186/s13578-020-00396-1

VITA

Martha Mortell was born and raised in Cork, Ireland. Martha received her B.S. in chemistry (biochemistry option) with a minor in mathematics from the University of Kentucky in 2020. Martha has research experience from Dr. Atwood's Environmental Chemistry Lab at the University of Kentucky, as a Nutrigenomics Research Intern at Alltech Inc., and in the Butterfield Neurochemistry Lab at the University of Kentucky. Martha placed 2nd in the University of Kentucky Undergraduate Chemistry Research Competition in spring of 2020 before starting her M.S. degree through the College of Medicine at the University of Kentucky in the fall of 2020.